Supercontinuum generation in microstructured fibers and novel optical measurement techniques

Goëry Genty

Dissertation for the degree of Doctor of Science in Technology to be presented with due permission of the Department of Electrical Engineering, Helsinki University of Technology, for public examination and debate in Auditorium S4 at the Helsinki University of Technology (Espoo, Finland) on the 12th of March 2004 at 12 o'clock noon.

Helsinki University of Technology
Metrology Research Institute
PL 3000
FIN-02015 HUT
Finland
Tel. +358 9 451 2268
Fax. +358 9 451 2222
E-mail: goery.genty@hut.fi

Abstract

Over the past few years microstructured fibers have shown potential for many practical applications and permitted significant progress in various domains such as nonlinear optics, medical science or telecommunications as the fabrication process allows for a great flexibility in the design of these fibers. In particular, small core microstructured fibers has proven to be the most efficient way for supercontinuum generation. Supercontinuum is one of the most spectacular outcome of nonlinear optics as it possesses the properties of a laser combined with an ultra-broad bandwidth spanning more than two octaves. The thesis provides a comprehensive review of the different physical mechanisms leading to the generation of these spectra in microstructured fibers.

Dispersion, which reflects the dependence of the refractive index of a material on the frequency of light plays a crucial role in the pulse propagation in optical fibers or components. A novel technique to characterize the anomalous dispersion of small core microstructured fibers using short optical pulses is demonstrated. The method presents several advantages over conventional techniques and relies on the spectral modulation resulting from the evolution of the input pulse into a soliton wave.

As the demand for capacity of optical networks increases, the requirements for the components employed in transmission systems becomes more stringent. In particular, the dispersion of fiber Bragg gratings or thin-film filters commonly employed in the links needs to be accurately evaluated as it may have a strong impact on the overall performance of the system. A novel method for improving the accuracy of dispersion measurements, based on the well-established phase-shift technique widely used in the characterization of optical components, is presented.

The performance of diode lasers can be greatly enhanced with the use of an external cavity configuration. The wavelength tunability of the diode is increased and its linewidth considerably reduced. The behavior of the linewidth of a grating cavity laser is both theoretically and experimentally explored as the oscillation frequency of the laser is varied. Surprisingly, large changes in the linewidth value are observed, which may have an impact in applications requiring lasers with a stable and narrow linewidth.

The fabrication of integrated silica-based optical components performing active functionalities is an exciting prospect for obvious reasons. Poling of silica glass is a very promising technique for the development of this type of component as it allows for the introduction of an effective second-order nonlinearity essential for performing active functions. A new technique based on the inscription of Bragg gratings for measuring the second-order nonlinearity induced by negative thermal poling is demonstrated.

Keywords: Supercontinuum, microstructured fibers, dispersion measurements, linewidth, external cavity laser, poling.

Preface

The work presented in this thesis has been carried out at the Metrology Research Institute, Helsinki University of Technology, within the Fiber-Optics Group during the years 1999-2003.

I would like to thank the head of the Department of Electrical and Communications Engineering, Professor Pekka Wallin and Professor Erkki Ikonen the head of the laboratory.

I would also like to thank my supervisor Docent Hanne Ludvigsen for giving me the opportunity to work with various aspects of Optics. I would also like to thank her for her professional and tireless guidance in writing publications.

I would also like to express all my gratitude to Professor Matti Kaivola for useful discussions, help in the writing of the publications and advice in many different aspects during all those years.

I also acknowledge my co-authors, Mikko Lehtonen, Tapio Niemi, Carl-Johan Marckmann, Aki Gröhn Hannu Talvitie, J. Broeng and K.P. Hansen.

People from Crystal Fibre A/S are thanked for the generous loan of the microstructured fibers used in this work and for providing useful information about the fibers properties.

Professor Martin Kristensen is acknowledged for kindly inviting me to Research Center COM in Denmark for a three-month stay and interesting work on thermal poling of planar waveguides.

To all the present or past members of the Fiber-Optics Group, and in particular to Tapio Niemi and Mikko Lehtonen, I would like to express my best thanks for providing help and allowing for interesting and useful discussions about various subjects. Silica is also acknowledged for being such a nice material and therefore having made this work possible.

Funding of the work has been provided by Graduate School on Electronics, Telecommunications and Automation (GETA), Academy of Finland, National Technology Agency (TEKES), NKT Research, Nordisk Forskerutdanningsakademi (NorFA), Jenny and Antti Wihurin Rahasto, Vaisala Oy rahasto and Nokia Oy scholarship.

Finally, I would like to thank all my family for support and also for asking every second week when I would graduate.

To my grand parents

Espoo, March 2004

Goëry Genty

List of publications

[I]   G. Genty, M. Lehtonen, H. Ludvigsen, J. Broeng, and M. Kaivola, "Spectral broadening of femtosecond pulses into continuum radiation in microstructured fibers", *Opt. Express* **10**, 1083-1098 (2002).

[II]   M. Lehtonen, G. Genty, H. Ludvigsen, and M. Kaivola, "Supercontinuum generation in a highly birefringent microstructured fiber", *Appl. Phys. Lett.* **82**, 2197-2199 (2003).

[III]   G. Genty, H. Ludvigsen, K. P. Hansen, and M. Kaivola, "Measurement of anomalous dispersion in microstructured fibers using spectral modulation", *Opt. Express*, submitted.

[IV]   G. Genty, T. Niemi, and H. Ludvigsen, "New method to improve the accuracy of group-delay measurements using the phase-shift technique", *Opt. Commun.* **204**, 119-126 (2002).

[V]   G. Genty, A. Gröhn, H. Talvitie, M. Kaivola, and H. Ludvigsen, "Analysis of the linewidth of a grating-feedback GaAlAs laser", *IEEE J. Quantum Electron.* **36**, 1193-1198 (2000).

[VI]   G. Genty, M. Kaivola, and H. Ludvigsen, "Measurements of linewidth variations within external cavity modes of a grating-cavity laser", *Opt. Commun.* **203**, 295-300 (2002).

[VII] C. J. Marckmann, Y. Ren, G. Genty, and M. Kristensen, "Strength and symmetry of the third-order nonlinearity during poling of glass waveguides", *IEEE Photonics Technol. Lett.* **14**, 1294-1296 (2002).

Author's contribution

The scientific results presented in this thesis have been carried out at the Metrology Research Institute within the Fiber-Optics Group during the years 1999-2003. The thesis is composed of a short introduction and seven publications referred to as I-VII. All the experiments and simulations presented in this thesis have been performed by the author unless specified otherwise. The publications are the results of group work. The author has performed the experiments and developed the theory of supercontinuum generation presented in papers I-II. He has also initiated the new method for dispersion measurement presented in paper III. For paper IV, he developed the theoretical model and contributed to the measurements. The author has performed the calculations and simulations shown in paper VI and performed the experiments presented in paper V. During a three-month stay at Research Centre COM, Technical University of Denmark, he wrote the waveguides and gratings onto the glass samples utilized in paper VII and performed the poling experiments. He has written papers I,III-VI and contributed to the writing of paper II. Part of the results of this thesis have been also presented in several international conferences.

1. Introduction

The history of photonic crystal fibers (PCFs) started as early as in the seventies [1]. However, its impact remained rather marginal until the nineties when the maturity of the technology enabled the fabrication of almost perfect structures. The great flexibility in the design of PCFs led to tremendous progress in various areas of the field of optics, ranging from frequency metrology to medial science and the future prospects have aroused the interest of many research groups [2-22].

Photonic crystal fibers can be classified in two categories: microstructured fibers (MFs) which guide light as standard optical fibers [2-4,7,9,10,13,17,21-24] and photonic bandgap fibers (PBFs) [17,25-29] where the light is confined through the bandgap effect. Microstructured fibers could play an important role in optical telecommunications [30-35]. Indeed, various optical functions [36-39] ranging from optical switching [37-39] to wavelength conversion [40-44], soliton squeezing [45,46] and tunable filters [47-52] can be performed using MFs. In particular, the large nonlinearities of these fibers [53,54] permit these functions to be achieved with a shorter length than when using conventional fibers. Microstructured fibers also find applications in laser and amplifier technology [55-72]. Large core, high numerical aperture and endlessly single-mode MFs can provide high-power delivery [73,74] and erbium/ytterbium-doped MFs were recently demonstrated to be efficient for constructing high-power fiber lasers or amplifiers [57,58,70-72]. Poling of MFs has also been achieved and led to an enhanced second-order susceptibility [75]. Due to their intrinsic very low nonlinearities and in combination with anomalous dispersion in their transmission band, PBFs allow for high power soliton transmission [76]. Furthermore, the possibility of filling gases into the core of PBFs [77] opens up new prospects for sensor technology [78,79], harmonic generation, particle guidance [80] and cold atom guiding.

One of the very first applications of MFs has been supercontinuum (SC) generation. Supercontinuum is a broadband coherent light source [81] that finds numerous applications in the fields of telecommunication [82-92], optical metrology [93-107], spectroscopy [108-112] and medical imaging [113-115]. In particular, the ultra-broad spectrum of a supercontinuum has allowed for submicron resolution in optical coherence tomography [115-117]. In metrology, a direct link between the repetition rate of a mode-locked laser and optical frequencies has been established and potential accuracy of 10^{-18} may be achieved in the definition of the second, thus replacing the currently used cesium atom clocks [94,100-106]. In dense-wavelength-division-multiplexing telecommunication systems, a SC can be sliced into hundreds of channels yielding transmission bandwidths of the order of a few terahertz [89,118,119]. A supercontinuum can also be utilized for characterization of fiber-optic components or can be used in any application where broadband sources are required [120-124]. The first generation of supercontinuum dates back to 1970, when high power picosecond pulses were focused into a glass sample [125]. Continua were subsequently generated in various gases and liquids [126-130]. The development of ultra-fast lasers producing trains of short pulses with a wavelength near the minimum dispersion wavelength of optical fibers allowed to generate SC in conventional and speciality fibers [90,131-140]. The use of optical fibers for SC generation presents advantages over that of bulk media. In particular, the mode can be confined into a small area, thus enhancing the strength of the nonlinear processes that are responsible for SC formation. Microstructured fibers have allowed to go one step further in SC generation. Indeed, the possibility of tailoring the dispersion profile of these fibers combined with the tight confinement of the propagating mode, which enhances drastically the nonlinear effects, led to the generation of a SC spanning from 400 nm to beyond 1600 nm [141]. Since the first demonstration of SC generation in MFs in 1999 [142], comprehensive studies have been conducted to identify the properties and the various processes leading to these ultra-broad spectra in MFs, making presently SC research one of the hottest topic in the optics field [141,143-180].

Microstructured fibers exhibit a whole range of unique properties. In particular, they can allow for single-mode guidance from *UV* to near infrared wavelengths [181] and their zero-dispersion wavelength may be pushed far into the visible region of the spectrum [182]. As dispersion may have a strong impact on the use of a particular MF, it is very important to be able to characterize accurately the dispersion properties of these fibers. Such a task may become difficult or unpractical in the case of small core MFs using standard dispersion measurement techniques. Indeed, the length of fiber required and the coupling of light into this type of fiber may prevent the use of conventional techniques, thus calling for the need of developing new techniques that are particularly suitable for the characterization of MFs.

Dispersion is one of the major parameters for optical communication systems since it sets the limits of the networks capacity [183]. Optical components performing the various functions needed for the data exchange within the network contribute to the total dispersion experienced by the different channels in dense-wavelength-division-multiplexing systems. As the traffic increases constantly channels spacing must be decreased and, therefore the effect of the dispersion of the components becomes more dramatic. For efficient utilization of components and optimization of the system performances, the dispersion should therefore be assessed as accurately as possible. The resolution of existing methods, however, may not be sufficient in some cases, and development or modification of existing dispersion measurement techniques to obtain better accuracy is highly desirable.

The performance of communication systems also strongly depends on the light source employed. Diode lasers are widely used in optical data transmission [183,184]. However, the rapid fluctuations of their phase which contribute to the laser lineshape can introduce errors in coherent communication systems. The inherent broad linewidth of semiconductor lasers, which typically exceeds tens of MHz for a 1 mW output power, can therefore be detrimental for their use in any application requiring a high degree of coherence. A simple and very successful means to enhance the performance of diode lasers consists in adding an external reflector element to form an external cavity laser [185,186]. The optical feedback thus provided to the diode laser strongly affects its properties [187]. Various external cavity schemes have been explored since the beginning of the eighties [185,188-190]. External cavity lasers have recently regained interest as communication systems demands more and more tunability combined with a narrow linewidth. Using a grating as an external reflector has proven to be an efficient way to extend the tuning range of diode lasers over tens of nanometers while reducing their linewidth by more than an order of magnitude [191-195]. The linewidth of external cavity lasers can be as low as a few kHz and any variations from this value may have an impact on the application where it is used. Consequently, accurate characterization of the linewidth of this type of laser is crucial.

Several in-line components used in optical telecommunications, such as optical modulators, wavelength converters or Bragg gratings, are presently made of other materials than silica. To reduce significant losses and other undesired effects occuring when light is transmitted from silica fibers to other materials, it is of prime importance to realize all-silica optical links, which calls for the development of integrated silica-based active components [196]. The operation principle of these components primarily relies on the second-order nonlinearity of the employed material which is extremely low for silica glass. To modify the intrinsic properties of the glass and thereby induce a suitable second-order nonlinearity, poling seems to be a very promising technique and has attracted an increasing interest since the high second-order nonlinearity achieved in 1991 in bulk silica by thermal poling [197]. Nevertheless, the physical mechanisms leading to an effective second-order nonlinearity during poling experiments is yet to be fully clarified and efficient characterization methods which gives insight into the poling effects are of high interest.

2. Photonic crystal fibers

The first demonstration of a photonic crystal fiber (PCF) dates back to 1970 [1]. The technology of PCFs has matured tremendously during the last decade. In particular, precise control of the fiber drawing process has enabled to produce a great variety of complex structures.

2.1 Modal, dispersive and nonlinear properties

Photonic crystal fibers exhibit some unique features compared to those of standard optical fibers [2,3,7,9-11,18,20,182,198]. In particular, the introduction of air-holes allows new degrees of freedom to manipulate the modal, dispersive and nonlinear properties of the fiber. For instance, PCFs can be designed to guide light in a single transverse mode in the near-*UV* to near-infrared wavelength range with variable core sizes [20,181,182,198,199]. Besides, the arrangement and size of air-holes allow for tailoring of the waveguide dispersion of PCFs. Thus, the zero-dispersion wavelength can be pushed into the visible region of the optical spectrum [182,200-202]. It is also possible to manufacture PCFs that exhibit very low dispersion values over a broad wavelength range [203-209].
Furthermore, mechanically robust PCFs can be fabricated with extremely small core down to 1 μm [182], thus enhancing considerably the nonlinear optical processes along the fiber [20,53]. Large core single-mode PCFs can also be manufactured for reducing the nonlinear effects [20,33,198,199,210-212]. Moreover, high amounts of birefringence can be introduced in the core to maintain the polarization of light traveling along the fiber [213-218]. Propagation losses of PCFs are however an order of magnitude larger than in conventional optical fibers due various phenomena [219-229]. Presently, this limits their use in practice as a transmission medium.

2.2 Classes of photonic crystal fibers

Photonic crystal fibers can be classified in two categories depending on the nature of the core as is shown in Fig. 1. Microstructured fibers (MFs) possess a solid core made of materials such as silica [5,15,18,22] or non-silica glasses [230-232] whereas photonic bandgap fibers (PBFs) exhibit a hollow core [17,25-27,233] or a core made of a dielectric whose refractive index is lower than that of silica. In the case of MFs, the air-holes around the core allow for lowering the refractive index of the cladding. Therefore light can be guided inside the core according to the principle of total internal reflection as in standard optical fibers [17]. In PBFs, the periodicity of the air-hole lattice enables to trap the light in the core by a two-dimensional photonic bandgap. Bandgaps result from the multiple interference and scattering at the Bragg condition [17]. As a consequence, only light with a given wavelength range can be guided in the hollow or dielectric core. Figure 2 illustrates the guiding principles of these two types of fiber. Photonic bandgap fibers are beyond the scope of this thesis and only the properties and applications of microstructured fibers will be discussed in the following paragraphs.
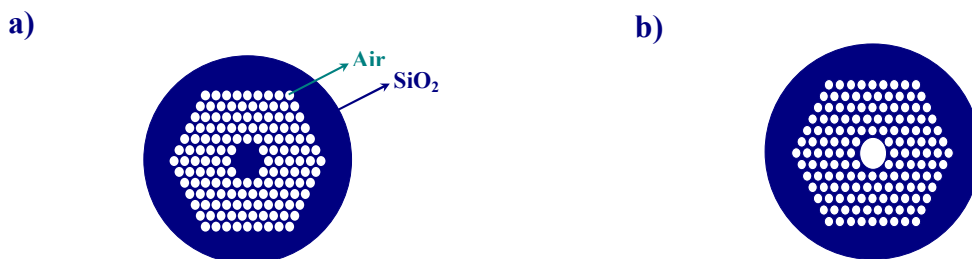
a)

b)

Figure 1. a) Schematic cross-section of a MF.   **b) Schematic cross-section of a PBF.**
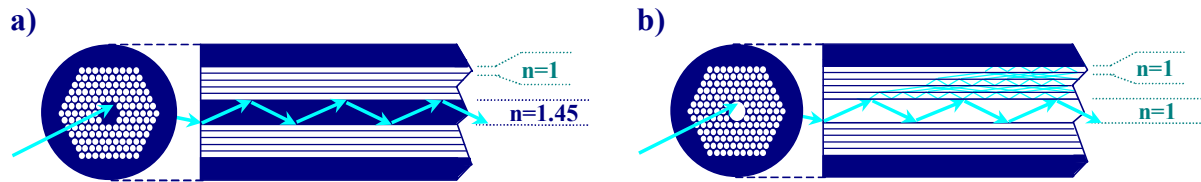
Figure 3. a) Guidance principle in a MF.   **b) Guidance principle in a PBF.**

2.3 Fabrication of photonic crystal fibers

Photonic crystal fibers are fabricated in a two-stage process [7,20,22,234]. In the first stage, a preform is formed by stacking capillary tubes and rods made of silica (or whichever glass). This permits a high level of flexibility to control the index profile of the cladding region. In particular, the positioning and/or removal of capillary tubes allows customizing the air/silica structure. In the second stage, the preform is drawn into a very thin fiber using a precision mechanism that feeds it into a hot furnace at a proper speed. The structure of the preform is maintained during the drawing process through careful control of the feeding speed and heating temperature. In this way, very complex designs of structure can be manufactured, e.g., large air-filling fraction [20,235], highly birefringent [213-218], elliptical holes [236] or triangular core [212] PCFs can be produced. The fibers are then coated with a protective jacket.
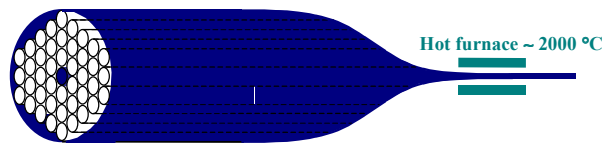
Figure 3. Capillary tubes and a silica rod are stacked to form a preform which is subsequently drawn into a thin PCF through a hot furnace.

2.4 Microstructured fibers

The fundamental properties of MFs, i.e, mode guidance, dispersion, and nonlinearities are briefly reviewed in the next paragraphs.

2.4.1 Modeling

Various parameters can affect drastically the properties of MFs. These parameters include the material used for the fabrication of the fiber, the size, pitch and shape of air-holes, as well as the number of holes surrounding the core. A proper choice of parameters allows for designing a particular structure for an intended application. For this reason, it is essential to be able to model the properties of MFs accurately for a given set of parameters.

Several attempts have been made to model the properties of MFs [17,22,210,235,237-274]. These methods include beam propagation [246,251,254,265], effective-index [248,255] and plane-wave expansion modeling [237,268], localized function [210,235,256,263,275] and multipole expansion technique [244,258,269-271], finite-difference time domain and finite-difference frequency domain methods [264,273,274] or finite-element techniques [239,250,257]. All the methods exhibit some advantages and disadvantages [17]. Yet a fast and efficient technique that can model any arbitrary structure has to be found. The main features of each technique are summarized in Table 1.

Table 1. **Comparison of the different methods to model MFs. MFD: mode field distribution, β: propagation constant, and A_{eff}: effective area.**

Method	Modeled properties	Model accuracy	Limitations	Computational effort
Beam propagation	MFD	Reliable		High
Effective-index	MFD, β	Inaccurate at longer λ	Pol. analysis impossible	Low
Plane-wave expansion	MFD, β, A_{eff}	Fair	Assumes infinite cladding	Intensive
Localized function expansion	MFD, β, A_{eff}	Accurate		High
Multipole expansion	MFD, β, A_{eff}	Accurate	Symmetric structures	
Finite-difference time domain	MFD, β , A_{eff}	Reliable	Summation over all excited modes	Very intensive
Finite-difference frequency domain	MFD, β , A_{eff}	Reliable	Summation over all excited modes	High

2.4.2 Modal properties

As for conventional fibers, the modal properties of MFs can be analyzed using the normalized frequency parameter *V* defined as [243,248,255,276,277]

$$V = \frac{2\pi a}{\lambda}\sqrt{n_a^2 - n_{cl}^2} \, , \tag{1}$$

where *a* is the core radius of the fiber, n_a and n_{cl} the refractive index of the core and cladding respectively. A conventional fiber guides a single-mode when *V*<2.405. It can be seen from Eq. (1) that when either λ decreases or *a* increases, *V* increases and eventually exceeds the critical value for single-mode guidance. In MFs, the refractive index of the cladding is actually an effective refractive index resulting from the introduction of air-holes around the core. It depends on the air-filling fraction of the fiber (defined as the ratio of the hole diameter *d* to the pitch of the lattice Λ and on the wavelength. The wavelength dependence of n_{cl} results in a constant *V* value even at short wavelengths. Choosing a proper value for the air-filling fraction, this constant value can be smaller than 2.405 over a very broad wavelength range and the fiber is then endlessly single-mode [2,3,7,10,11,20,181,278]. Single-mode guidance can be achieved even with a very large core [20,181,198,199,212].

In the short wavelength limit, i.e. when λ is small compared to the characteristic distances of the fiber, i.e., the hole diameter *d* and the pitch Λ, the fundamental mode is well-confined in the core. For very short wavelengths, however, the mode starts leaking to the silica bridges between the air-holes.

When the wavelength is of the order of the characteristics distances, the mode also leaks into the cladding. Figure 4 shows examples of the spatial intensity pattern of the fundamental mode propagating at several wavelengths calculated using an eigenmode expansion method [279-281].
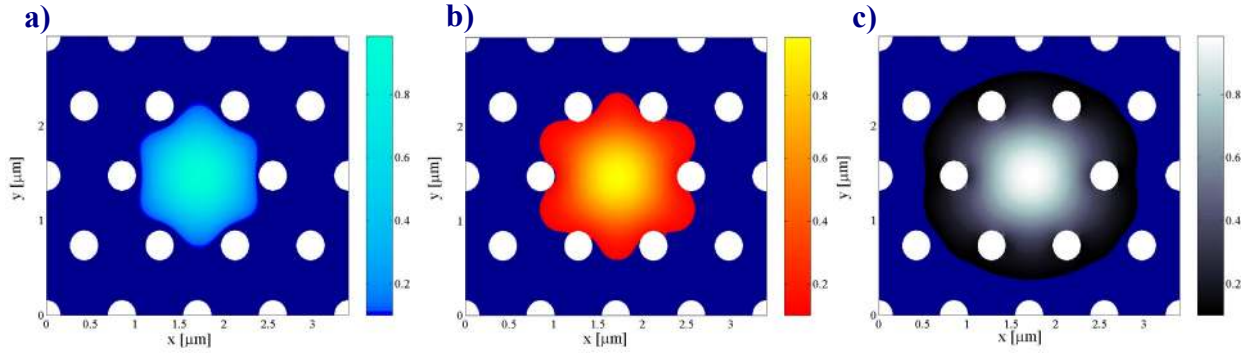
Figure 4. **Contour plot of the fundamental mode propagating in a MF with λ equal to a) 400 nm, b) 800 nm, and c) 1500 nm. The air-filling fraction of the MF is $d/\Lambda \approx 0.35$.**

2.4.3 Dispersion

The strong wavelength dependence of the effective refractive index of the cladding of MFs leads to a new range of dispersion properties that cannot be achieved with conventional fibers. The dispersion profile of MFs strongly depends on the air-filling fraction and core size. For instance, increasing the air-filling fraction and reducing the size of the core allows for a drastic increase of the waveguide dispersion, thus enabling to push the zero-dispersion wavelength of MFs well below 800 nm [182]. The dispersion is then anomalous at visible wavelengths and soliton propagation becomes possible for this range of wavelengths. The zero-dispersion wavelength is primarily determined by the core size of the fiber and the air-filling fraction of the fiber controls the higher-order dispersion. Altering the size and pitch of air-holes allows a shift of the zero-dispersion wavelength of the fiber to any value from 500 nm to beyond 1500 nm. Large air-filling fraction can also produce high anomalous or normal dispersion values, which can be used for dispersion compensation purposes. Values as high as -2000 ps/nm·km have been reported [202,282,283]. Furthermore, by choosing the appropriate air-hole size and pitch, it is possible to fabricate MFs that exhibit very low and flat dispersion over a relatively broad wavelength range [21,203-209]. Figure 5 illustrates different MFs structures along with the corresponding dispersion profile. The dispersion was calculated by double differentiation of the propagation constant obtained using an eigenmode expansion method [279,280]. To summarize, a proper choice of size of air-holes and pitch enables to engineer a great variety of dispersion profiles which cannot be obtained in conventional fibers.
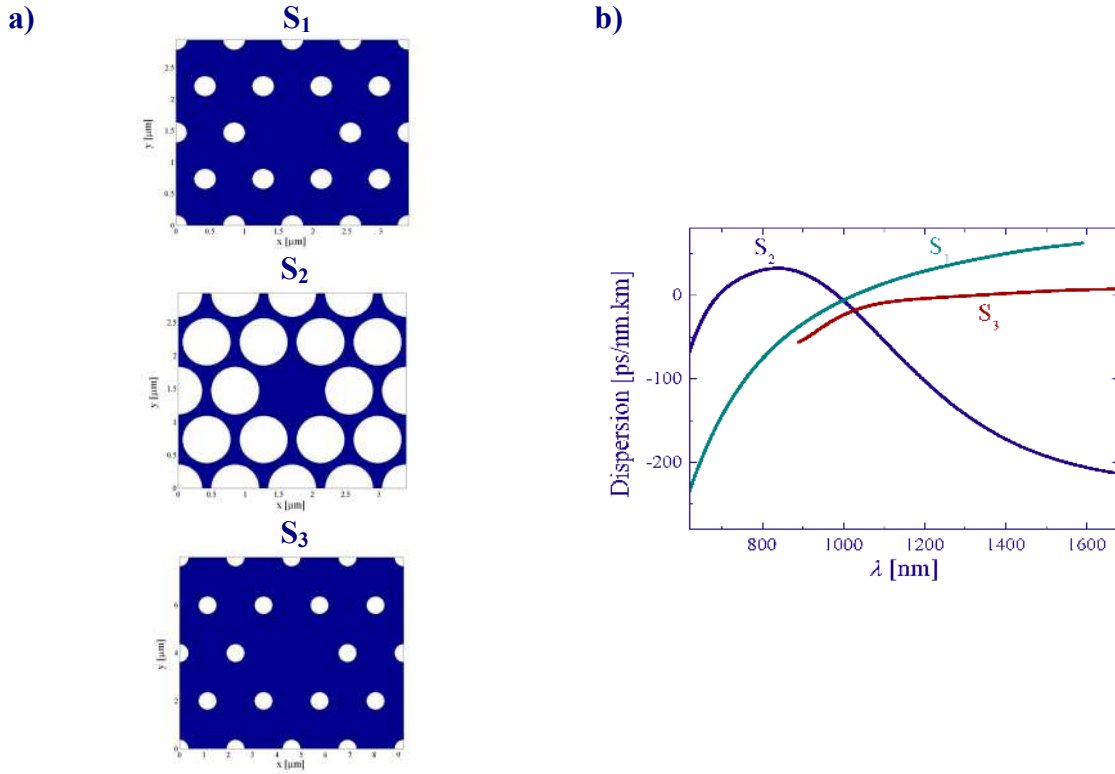
Figure 5. a) Examples of MFs structures. S₁: Λ=0.85 μm and d=0.3 μm, S₂: Λ=0.85 μm and d=0.7 μm, S₃: Λ=2.3 μm and d=0.69 μm.

b) Dispersion profiles corresponding to structures S₁₋₃.

2.4.4 Nonlinearities

Nonlinear effects in optical fibers are inversely proportional to the area of the propagating mode inside the fiber [284]. As is the case with the dispersion profile, nonlinearities of MFs can be tailored by varying the size of the core [9,20,53]. Large core MFs allows a single-mode to propagate with a large area. This mode consequently experiences very low nonlinearities. On the other hand, it is possible to produce very small core MFs and therefore enhance the nonlinear optical processes. Fibers with a core diameter ranging from 1 to 50 μm have been demonstrated. Contrary to conventional optical fibers, MFs offer the possibility of scaling of the nonlinearities experienced by the propagating mode [20]. The confinement of the propagating mode inside the core of the fiber depends on the wavelength of the light. For wavelengths much shorter than the core diameter, the mode is well confined into the core. When the wavelength is of the order of the core diameter, the mode tends to leak outside the first ring of air-holes, thus increasing the effective area of the propagating mode [53,285-288]. The wavelength-dependence of the area of the propagating mode translates into a wavelength-dependence of the strength of the nonlinearities. Figure 6 shows the dependence of the effective mode area on the wavelength for a 1 μm core MF calculated using a plane wave technique.

Figure 6. Effective mode area as a function of wavelength for a 1 μm core MF. Λ=1.22 μm.

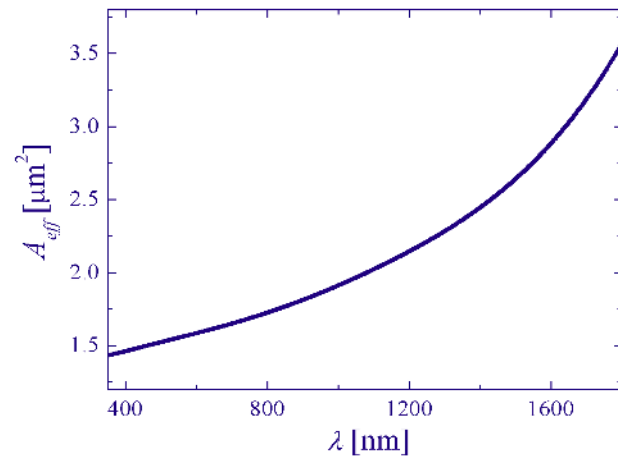# 3. Supercontinuum generation in microstructured fibers

3.1 Introduction to supercontinuum

The optical spectrum of a laser pulse train consists of many spectral peaks separated by the repetition rate of the laser. The frequency of the peaks are related to the repetition rate of the pulse train by

$$\omega = \omega_{off} + m \cdot \omega_r , \qquad (2)$$

where ω_r is the repetition rate of the laser, ω_{off} is an offset frequency and m an integer number. In a simple picture, when intense pulses interact with a cubic nonlinear medium, new frequency peaks appear in the optical spectrum of the pulses. The frequencies of these new peaks correspond to the various mixing products of the input frequency peaks

$$\omega_{ijk} = \omega_i + \omega_j - \omega_k , \qquad (3)$$

where ω_{ijk} is the frequency of the new peak and ω_i, ω_j and ω_k correspond to the frequency of the ith, j^{th} and k^{th} peak already present in the spectrum, respectively. Therefore, the cascaded nonlinear processes broaden the optical spectrum of the pump pulses while preserving its comb-like structure [289]. Broad coherent spectra, extending over tens of nanometers and resulting from the broadening of the spectrum of optical pulses in a nonlinear medium, are commonly referred to as supercontinua (SC). Broad incoherent spectra resulting from nonlinear interaction of CW waves in a nonlinear medium are also sometimes referred to as SC [149]. However, such continua are beyond the scope of this thesis and are not discussed here.

Continua were first generated by focusing high power ps pulses into glass samples [125]. The use of various gases (H_2O, D_2O, ethylene glycol…) [126-128,290,291] and liquids (water,...) [129,130,292] as a nonlinear medium was subsequently demonstrated. The development of tunable mode-locked lasers emitting short pulses led naturally to the use of optical fibers as the nonlinear medium. Indeed, in optical fibers, light can be confined into a very small area, which increases the strength of the nonlinear processes and results in much lower powers needed for SC generation. Several special fiber designs have thereafter been proposed to enhance the bandwidth of SC [90,121,131-133,135-137,139,140]. Table 2 summarizes the history and characteristics of SC generation in various nonlinear media.

Table 2. History of SC generation. MMF: multimode fiber, DSF: dispersion-shifted fiber.

Year	Nonlinear medium	Laser type	Pulse width	Pulse intensity/ Peak power	SC -20 dB bandwidth	Ref.
1970	Borosilicate	Nd:Glass	5 ps	1 GW/cm^2	300 nm	[125]
1977	Water	YAlG:Nd	30 ps	45 MW	600 nm	[292]
1983	Ethylene glycol	Rh6G	80 fs	3 GW	130 nm	[291]
1987	MMF	Nd:YAG	25 ps	1.5 GW/cm^2	60 nm	[293]
1995	DSF	Er^{3+} fiber laser	1 ps	1.2 kW	300 nm	[121]
1999	MF	Ti:Sapphire	100 fs	8 kW	1200 nm	[141]

Due to their unique range of properties, microstructured fibers have allowed one step further in SC generation and SC spanning from 400 nm to beyond 1600 nm have been demonstrated (see Table 2). The possibility of tailoring the dispersion profile of MFs opens new prospects for controlling the properties of SC. The first demonstration of SC generation in MFs dates back to 1999 [141] and, since then, the various processes leading to these ultra-broad spectra in MFs have been the subject of extensive research [21,141,143-148,151,153-155,160,162,163,166-168,172,178,180,294-297]. It was found that the mechanisms leading to SC generation depends on both the parameters of the input pulses (temporal width, peak power) and the parameters of the MF (dispersion profile, effective modal area, birefringence) [294]. These mechanisms include self-phase modulation (SPM), cross-phase modulation (XPM), four-wave mixing (FWM) and stimulated Raman scattering (SRS). Figure 7a illustrates the far-field intensity pattern of a SC generated in a MF using 100 fs pulses with a wavelength of 740 nm. Figure 7b shows the pattern observed when this bright white light is dispersed by a grating which

spatially separates the various frequency components present in the optical spectrum. All the visible frequencies of the spectrum from near *UV* to red are observed.
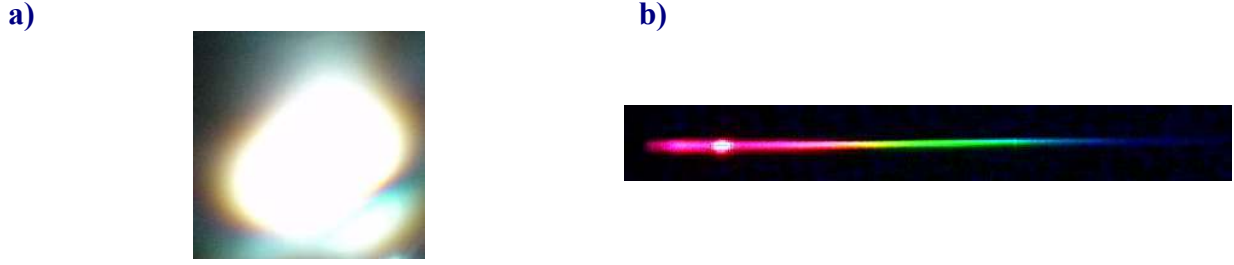
a)

b)

Figure 7. a)   Far-field intensity pattern of the SC   b)   Pattern observed when the SC light is generated in the MF described in I-II.   dispersed by a grating.

3.2 Nonlinear effects in optical fibers

An electromagnetic field propagating in a medium induces a polarization of the electric dipoles. The evolution of the electromagnetic field in the medium can be described by a propagation equation derived from the general wave equation [284]

$$\nabla^2 E - \frac{1}{c^2}\frac{\partial^2 E}{\partial t^2} = -\mu_0 \frac{\partial^2 P}{\partial t^2}, \tag{4}$$

where E is the electric field, P the induced polarization, μ_0 the vacuum permeability and c the speed of light in vacuum. For intense radiation such as laser pulses, the response of the medium becomes nonlinear and the induced polarization consists of a linear and a nonlinear part. In the scalar approximation, the linear and nonlinear induced polarization are related to the electromagnetic field as [284]

$$P_L = \varepsilon_0 \chi^{(1)} E, \tag{5}$$

$$P_{NL} = \varepsilon_0 \sum_{j \geq 2} \chi^{(j)} E^j, \tag{6}$$

where ε_0 is the vacuum permittivity and $\chi^{(j)}$ is the jth order susceptibility of the medium.

The inversion symmetry of silica glass at the molecular level results in negligible even-order susceptibilities [284]. Moreover, susceptibilities of order higher than 3 are not significant for silica glass. Therefore, the relevant nonlinear effects in optical fibers are induced by $\chi^{(3)}$. Optical nonlinear processes can be divided in two categories. Elastic processes correspond to photon-photon interactions and no energy exchange occurs between the electric field and the medium. Such effects include self-phase modulation [284,298] , cross-phase modulation [284], four-wave mixing [284] and third-harmonic generation [299], the two latter requiring phase-matching to be efficient [284,299]. The phase-matching condition for third harmonic generation is more stringent and is seldom satisfied in fibers. This process is not discussed in the following. Inelastic processes correspond to photon-phonon interactions, which leads to energy exchange between the electric field and the nonlinear medium. Such effects include Raman and Brillouin scattering [284]. Stimulated Brillouin scattering is negligible for short pulses and is not considered here.

Treating the nonlinear part of the induced polarization as a perturbation in Eq. (4), and assuming that the electric field is of the form

$$E(z,T) = A(z,T)\ e^{i(\beta z - \omega_0 T)}, \tag{7}$$

where β is the propagation constant of the propagating mode at the center frequency of the field ω_0, one can derive the well-known nonlinear Schrödinger equation (NSE). The function $A(z,T)$ is commonly referred to as the slowly varying envelope of the electric field. The NSE models accurately the propagation of light along optical fibers for pulses as short as 30 fs [300]. In a frame of reference moving at the group velocity of the pulse, the NSE can be written as [284]

$$\frac{\partial A}{\partial z} + \frac{\alpha}{2}A - \sum_{k \geq 2} i^{k+1} \frac{\beta_k}{k!} \frac{\partial^k A}{\partial T^k} = i\gamma \left(1 + \frac{i}{\omega_0} \frac{\partial}{\partial T} \right) \left[A(z,T) \int_0^\infty R(T') \left| A(z, T - T') \right|^2 dT' \right], \quad (8)$$

where α is the fiber loss and β_k are the coefficients of the Taylor-series expansion of the propagation constant β around ω_0. The nonlinear coefficient γ of the fiber accounts for the intensity dependence of the refractive index. The response function of the nonlinearity is defined as $R(T) = (1-f_R)\delta(T) + f_R h_R(T)$, with f_R being the value of the fractional contribution of the delayed response h_R and taken to be 0.18 for silica fibers [300,301]. The second term on the right-hand side of Eq. (8) accounts for the dispersion of the nonlinear coefficient.

- Self-phase modulation

Self-phase modulation originates from the intensity-dependence of the refractive index of silica [298]

$$n = n_L + n_2 |A|^2, \quad (9)$$

where n_L is the linear part of the refractive index, $|A|^2$ is the optical intensity and n_2 is the nonlinear-index coefficient related to $\chi^{(3)}$ as [284]

$$n_2 = \frac{3}{8n_L} Re(\chi^{(3)}), \quad (10)$$

with Re standing for the real part and the optical field being assumed to be linearly polarized. A typical value of n_2 for silica material is 3.2×10^{-20} m^2/W [298]. Self-phase modulation refers to the self-induced nonlinear phase shift that an optical pulse experiences as it propagates along the fiber

$$\phi_{NL}^{SPM} = \frac{2\pi L}{\lambda} n_2 |A|^2, \quad (11)$$

where L is the length of the fiber. Due to its time-dependence, this nonlinear phase-shift translates into broadening of the optical spectrum as the pulse travels inside the fiber. The temporal shape of the pulse remains unaffected. A useful quantity is the so-called nonlinear length L_{NL} that corresponds to the effective propagation distance at which the maximum phase-shift is equal to 1. It is defined as

$$L_{NL} = \frac{1}{\gamma P_p}, \quad (12)$$

where P_p is the peak power of the optical pulse and γ the nonlinear coefficient related to n_2 as [284]

$$\gamma = \frac{n_2 \omega}{c A_{eff}}, \quad (13)$$

with A_{eff} being the effective area of the propagating mode inside the fiber and ω the carrier frequency of the optical field. The nonlinear coefficient γ represents the strength of nonlinear effects. Small core MFs exhibit nonlinear effects an order of magnitude higher than conventional fibers.

- Cross-phase modulation

When two optical fields with different wavelengths co-propagate in a nonlinear medium, the refractive index seen by one of the fields not only depends on its own intensity but also on the intensity of the other field [302]. Consequently, the optical field with a center wavelength λ_i experiences a nonlinear phase-shift induced by the co-propagating optical field at wavelength λ_j such that [284]

$$\phi_{NL}^{XPM} = \frac{4\pi L}{\lambda_i} n_2 |A_j|^2, \quad (14)$$

where $|A_j|^2$ represents the intensity of the co-propagating field and L is the interaction length between the two fields. This nonlinear phase-shift is commonly referred to as cross-phase modulation and requires the optical fields to overlap temporally. Equation (14) shows that XPM is twice as effective as SPM.

- Four-wave mixing

Four-wave mixing is a nonlinear recombination process of photons of different energies through the third-order susceptibility $\chi^{(3)}$: two pump photons at frequencies ω_1 and ω_2 are annihilated with the simultaneous creation of two new photons at frequencies ω_3 and ω_4 [284,299]

$$\omega_1 + \omega_2 = \omega_3 + \omega_4 . \qquad (15)$$

The conservation of momentum results in a phase-matching condition to be fulfilled for the process to be efficient [284,299]

$$\Delta\phi = \left(\frac{n_1\omega_1 + n_2\omega_2 - n_3\omega_3 - n_4\omega_4}{c} + (1 - f_R)\gamma_1(\omega_1)P_{p1} + (1 - f_R)\gamma_2(\omega_2)P_{p2} \right) L = 0 , \quad (16)$$

where n_j, γ_j, and P_{pj} are the linear refractive index, nonlinear coefficient of silica, and peak power of the optical field at the frequency ω_j. Here, L is the fiber length.

A special case referred to as degenerate FWM occurs for $\omega_1 = \omega_2 = \omega_p$. The new generated photons are called Stokes and anti-Stokes photons. This case is of practical interest because when only an intense pump wave propagates along the fiber, Stokes and anti-Stokes waves build up from noise and are subsequently amplified through FWM. The frequency of the generated Stokes and anti-Stokes waves are such that the energy conservation described by Eq. (15) is fulfilled. In terms of propagation constant, the phase-matching condition for degenerate FWM can be expressed as

$$\sum_{k \geq 1} \frac{\beta_{2k}}{(2k)!} (\omega_s - \omega_p)^{2k} + (1 - f_R)\gamma(\omega_p)P_p = 0 , \qquad (17)$$

where ω_p and ω_s represent the frequency of the pump and Stokes waves, respectively. Here, P_p is the peak power of the pump wave.

- Stimulated Raman scattering

Stimulated Raman scattering is a photon-phonon interaction. The energy from an intense pump beam is shifted to lower frequencies (Stokes waves) through scattering from vibrational modes of the material molecules [303]. Shifting of energy to higher frequencies (anti-Stokes waves) can also occur but is less efficient

$$2\omega_p \rightarrow \omega_{as} + \omega_{st} , \qquad (18)$$

with ω_p, ω_{as} and ω_{st} being the frequency of the pump, anti-Stokes, and Stokes photons, respectively. Stimulated Raman scattering yields gain for a probe wave co-propagating with a pump wave and whose wavelength is located within the Raman gain bandwidth. The normalized Raman gain spectrum of silica is shown in Fig. 8 as a function of frequency difference between the pump and probe waves [304]. The Raman gain of MFs is comparable to that of silica fibers [54]. The gain bandwidth is 40 THz with a peak located at 13.2 THz from the pump frequency.

In the time domain, SRS can be thought as the delayed nonlinear response of the material. In silica, this delayed response can be approximated by [300]

$$h_R(t) = \frac{\tau_1 + \tau_2}{\tau_1 \tau_2^2} e^{-\frac{t}{\tau_2}} sin\left(\frac{t}{\tau_1} \right) , \qquad (19)$$

where τ_1 and τ_2 are the relaxation parameters taken to be 12.2 fs and 32 fs, respectively .
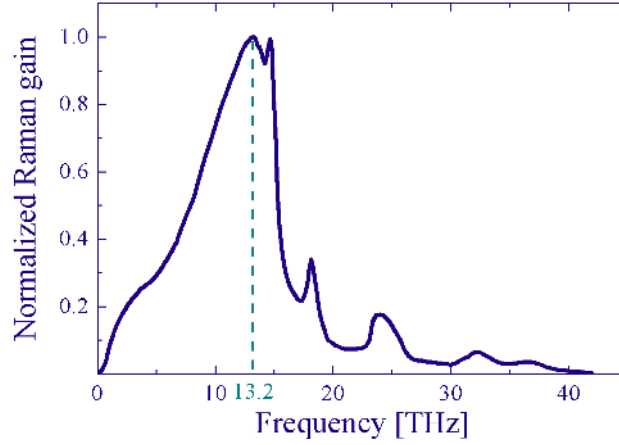
Figure 8. Normalized Raman gain of silica.

- Soliton propagation, soliton decay and soliton self-frequency shift

Neglecting the higher-order terms and attenuation, and using convenient transformations, Eq. (8) reduces to [284]

$$i\frac{\partial A}{\partial z} = \frac{1}{2}sgn(\beta_2)\frac{\partial^2 A}{\partial T^2} - N^2 A|A|^2 ,$$ (20)

where *sgn* refers to the sign function and *N* is defined as

$$N = \sqrt{\frac{L_D}{L_{NL}}} = \sqrt{\frac{\gamma P_P T_0^{\,2}}{|\beta_2|}} ,$$ (21)

with L_{NL} being the nonlinear length and L_D the dispersion length defined as

$$L_D = \frac{T_0^2}{|\beta_2|} ,$$ (22)

where T_0 is the temporal width of the pulse related to the full-width at half maximum T_{FWHM} by $T_0=T_{FWHM}/1.76$. A special case corresponds to negative values of β_2, i.e., when the dispersion is anomalous. In general, Eq. (20) can be solved by the inverse scattering method [305]. The solutions define a particular class of waves known as solitons [306-308]. Among the various types of solitons, a special role is played by solitary waves whose initial symmetric amplitude can be mathematically represented by [307,309]

$$A(T, z = 0) = N \cdot sech\left(\frac{T}{T_0}\right).$$ (23)

The integer value closest to *N* is referred to as the soliton order. The case *N*=1 corresponds to a fundamental soliton, i.e., a state in which the effects of SPM and dispersion are in balance and allows for the wave to maintain its shape as it propagates. The cases *N*≥2 corresponds to higher-order solitons. Such waves follow a periodic evolution during propagation with shape recovering at multiples of the soliton period defined as $\pi/2 \cdot L_D$ [284].

Higher-order solitons actually consist of *N* fundamental solitons, whose relative peak power and temporal width are given by [309,310]

$$P_k = \frac{(2N-2k+1)^2}{N^2} P_p ,$$ (24)

$$T_k = \frac{T_0}{2N-2k+1} ,$$ (25)

where *k* refers to the kth index of the constituent. The fundamental constituents travel together due to the degeneracy of their group-velocities [309]. Higher-order solitons periodically change their shape and

13

spectrum while propagating along the fiber due to interference between the different constituents. Only the degeneracy of the group-velocities binds the constituents of a higher-order soliton together. A small perturbation affecting their relative group-velocities will lead to their subsequent separation. Such process is often referred to as soliton decay or soliton breakup [309,311]. These perturbations include higher-order dispersion, the self-steepening effect and stimulated Raman scattering.

For a soliton whose temporal width is smaller than 100 fs, the bandwidth of its optical spectrum is 10 THz and, consequently, the spectrum overlaps with the Raman gain. In that case, SRS transfers continuously energy from the blue part of the pulse spectrum to the red part of the pulse spectrum. This energy transfer results in a shift of the center frequency of the soliton towards the infrared as the soliton propagates along the fiber. This process is commonly referred to as the soliton self-frequency shift (SSFS) [312]. The magnitude of the Raman-induced SSFS can be approximated by [313]

$$\Delta f = \frac{1.2904 \lambda_0^2 D(\lambda_0) \; h(T_0) L}{T_0^4} \, , \qquad (26)$$

where T_0 is the temporal width of the soliton and D is the value of the dispersion at the wavelength λ_0. Here, L is the fiber length and $h(T_0)$ represents the overlap integral of the soliton and Raman gain spectra [313]

$$h(T_0) = 496 T_0 \int_0^\infty \frac{\Omega^3 R(\Omega / 2\pi T_0)}{sinh^2(\pi \Omega / 2)} d\Omega \, , \qquad (27)$$

where $R(\Omega)$ denotes the Raman gain spectrum and Ω the frequency shift from the soliton center frequency. As the soliton propagates along the fiber, its amplitude decreases due to the various loss mechanisms. To counteract this effect, the soliton broadens, which results in slowing-down the frequency-shift rate. Also, variations of dispersion with wavelength and self-steepening contribute to this slowing-down. The soliton eventually reaches a state where its optical spectrum does not overlap with the Raman gain and its center frequency does not shift any further.

- Self-steepening

Self-steepening (SS) results from the dispersion of the third-order susceptibility, i.e., the red frequency components experience a lower nonlinearity than blue frequency components. In the time domain, SS can be thought as the intensity dependence of the group velocity: the peak of the pulse moves at a slower velocity than the wings which induces the trailing edge of the pulse to become steeper as the pulse propagates [284,314]. In combination with SPM, self-steepening results in a more pronounced broadening of the blue frequency components compared to the red ones. The process of SSFS is substantially reduced by SS since the nonlinearity decreases as the center wavelength of the soliton shifts towards the red.

- Nonlinear phase-matched radiation

The bandwidth of femtosecond solitons exceeds several THz and the variation of dispersion across the soliton bandwidth must be taken into account in the propagation equation [284]

$$i \frac{\partial A}{\partial z} + \sum_{k \geq 2}^{\infty} \frac{i^k}{k!} \frac{\beta_k}{|\beta_2|} \frac{1}{T_0^{k-2}} \frac{\partial^k A}{\partial T^k} + N^2 A |A|^2 = 0 \, . \qquad (28)$$

The terms $k>2$ can be treated as a perturbation for the soliton-like solution of Eq. (20). This perturbation makes the solution of Eq. (28) very unstable. In particular, linear waves having the same wave-vector as the soliton can co-exist with the soliton [315-317]. Provided the soliton spectrum overlaps with the frequency of this resonant wave, energy transfer between the linear and solitary waves is possible [315]. The amplification of the linear wave manifests itself in the optical spectrum as the appearance of a sharp spectral peak in the normal dispersion region of the fiber. The amplitude of the linear wave is proportional to the overlap between the soliton and the linear wave spectra [315]. The frequency of the linear wave ω_R is determined by the phase-matching condition [166,167,294,315]

$$\phi_S - \phi_R = \left[\beta(\omega_S) - \omega_S \beta_I(\omega_S) + \gamma(\omega_S)P_{PS}\right]L - \left[\beta(\omega_R) - \omega_R \beta_I(\omega_S)\right]L = 0 \,, \qquad (29)$$

where ϕ_s and ϕ_r represent the phase of the soliton and resonant wave expressed in a frame moving at the group velocity of the soliton $\beta_I(\omega_s)$. Here, P_{PS} is the peak power of the soliton. Expanding β in Taylor-series around ω_s, this phase-matching condition can be rewritten as

$$(1 - f_R)\gamma(\omega_S)P_{PS} - \sum_{k \geq 2} \frac{(\omega_R - \omega_S)^k}{k!}\beta_k(\omega_S) = 0 \,. \qquad (30)$$

As the center frequency of the soliton is tuned away from the zero-dispersion wavelength of the fiber deeper into the anomalous dispersion region, the frequency of the resonant wave correspondingly shifts away from the zero-dispersion wavelength deeper into the normal dispersion region of the fiber. Furthermore, the spectral overlap reduces and the amplitude of the resonant wave decreases. The center frequency of the resonant wave resulting from the perturbation of a soliton propagating along a MF can be calculated by solving Eq. (30). Figure 9 illustrates the phase-matching condition desribed by Eq. (30) for solitons with a center wavelength located at 700 nm and 900 nm. The dispersion profile of the fiber used for the calculation ressembles that of the MF utilized in the experiments performed in publications I and II.
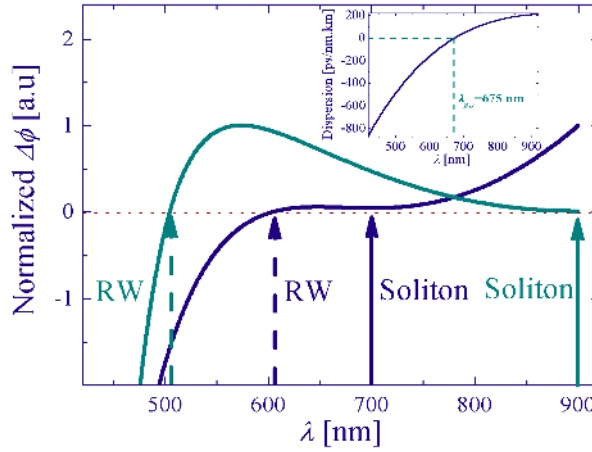

Figure 9. Phase-matching condition (see Eq. 30) for a resonant wave (dashed arrows) resulting from the perturbation of a soliton (solid arrows) with a center wavelength located at 700 nm (blue line) and 900 nm (green line). Inset: dispersion profile of the fiber used for the calculation. P_{PS}=5 kW, $\gamma_{700nm} \approx 200$ W^{-1}·km^{-1}, $\gamma_{900nm} \approx 150$ W^{-1}·km^{-1}.

3.3 Supercontinuum generation in microstructured fibers using fs pulses

Supercontinuum is the result of the interplay between the nonlinear effects described in the previous paragraph. Efficient SC generation requires the wavelength of the pump pulses to be in the vicinity of the zero-dispersion wavelength (λ_{ZD}) of the fiber since a high dispersion value tends to limit the magnitude of the nonlinear processes. Small core MFs typically exhibit λ_{ZD} in the range 600-1000 nm. This makes a mode-locked Ti:Sapphire laser a natural candidate for SC generation. Indeed, this type of laser produces intense femtosecond pulse trains at repetition rates varying from tens of MHz to one GHz with a wavelength tunable from 700 to 900 nm. It is also possible to manufacture MFs with λ_{ZD} in the near infrared region and, consequently, SC can be generated using other suitable laser sources such as ytterbium or erbium-doped fiber lasers.

The physics of SC generation in MFs using femtosecond pump pulses strongly depends on the relative detuning between the pump wavelength and the zero-dispersion of the fiber [I,167,171]. In particular, different mechanisms are observed depending on whether the pump wavelength is located in the anomalous or normal dispersion region of the fiber [I]. In the following, both cases are reviewed.

- Anomalous pumping

To clarify the role played by each nonlinear effect, Eq. (8) is solved in the Fourier domain using a standard split-step algorithm with the exact value of the propagation constant. This ensures the validity of the simulation for bandwidth exceeding several hundreds of nanometers [300]. The temporal width of the pump pulses is chosen to be 100 fs with a center wavelength at 750 nm. Figure 10 shows the dispersion profile of the MF used in the simulations and which is close to that of the fiber used in the experiments performed in the publications I-III. The MF has a core diameter of 1.5 μm yielding $\gamma \approx 150$ $W^{-1} \cdot km^{-1}$ at λ=750 nm and exhibits λ_{ZD} at 675 nm.
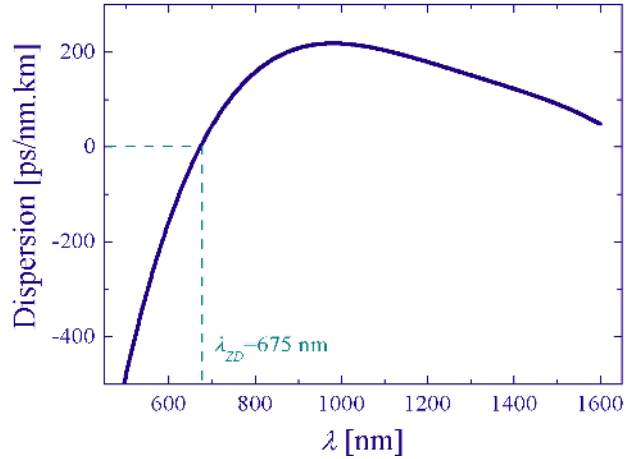

Figure 10. Dispersion of a MF with λ_{ZD}=675 nm.

Figure 11 illustrates the spectrum of the pulses at different fiber lengths when a) only the dispersion is included in the NSE, b) when the full propagation constant is implemented, c) when SRS is also added and d) when the SS is taken into account. When only the dispersion is included in the NSE, the pulse corresponds to a higher-order soliton and evolves periodically into a multi-peak structure along the MF. In the presence of higher-order dispersion (see Fig. 11b), the central part of the spectrum initially broadens in the first centimeters of the MF and does not spread any more with further propagation. The most noteworthy feature is the appearance of blue anti-Stokes frequency components in the spectrum [166,171,178,294]. Once they have been generated, these components are not affected by further propagation inside the MF. Adding the Raman term in the equation gives results qualitatively in better agreement with experimental observations, i.e., a strong spreading of the pulse spectrum towards the infrared. The inclusion of the self-steepening term results in an increased magnitude of the anti-Stokes components and reduces the spreading of the spectrum towards the infrared. New anti-Stokes components also appear in the spectrum for longer propagation lengths.

The onset of the supercontinuum formation can be explained as follows: the input pulse corresponding to a Nth order soliton is compressed in the first few centimeters of the fiber due to SPM, as can be seen from Fig. 12a which shows the temporal evolution of the pulse with all the terms included in the NSE (i.e., corresponding to the spectra of Fig. 11d). The perturbation of this N^{th} order soliton by SRS and higher-order dispersion leads to the breaking up of the Nth order soliton into multiple fundamental solitons whose amplitudes and widths are given by Eqs. (24) and (25) [166,167,294]. The splitting of the input pulse into multiple solitons is clearly observed in Fig. 12b-c. The red part of the spectra of the multiple solitons overlap with the Raman gain spectrum while their blue part overlaps with the resonant linear waves. As a consequence, the resonant waves are amplified and emerge as anti-Stokes components while the red components get amplified by SRS, which shifts the center frequency of the solitons further to the red. The multiple solitons having different widths, they experience different frequency shifts and appear in the spectrum as distinct Stokes peaks as is seen in Fig. 11c-d. Since the solitons experience different frequency shifts, they correspondingly experience different group delays and thus appear in the time trace as distinct pulses, the soliton experiencing the largest frequency shift being the originally narrowest soliton and corresponding to the most delayed pulse in Fig. 12c. The

16

magnitude of the frequency shifts is proportional to the fiber length (see Eq. (26)). Consequently, the longer the fiber, the more the spectrum spreads towards the infrared [I,177,311]. As they propagate along the MF, the various solitons experience losses and dispersion, which results in their temporal broadening. Therefore, their spectrum eventually does not overlap any more with the Raman gain spectrum and the frequency shift ceases. Furthermore, the SS reduces the strength of the nonlinearities as the solitons shifts their center frequency, which results in the decrease of the magnitude of the SSFS with propagation [I,157,318].
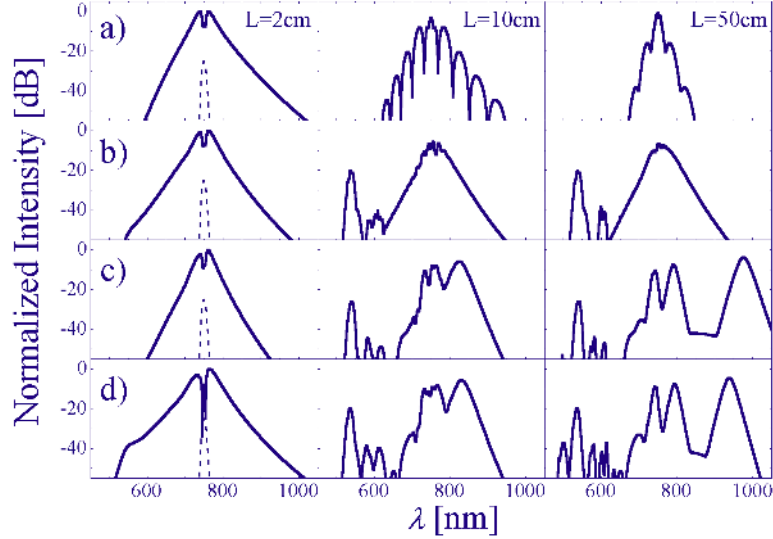

Figure 11. Simulation of the spectrum at the output of the MF after 2, 10, and 50 cm: a) only β_2, b) full β, c) full β + SRS, and d) full β + SRS + SS. The dashed lines represent the spectrum of the input pulses. P_p=3 kW (P_{av}=26 mW) , T_{FWHM}=100 fs and λ_p=750 nm.
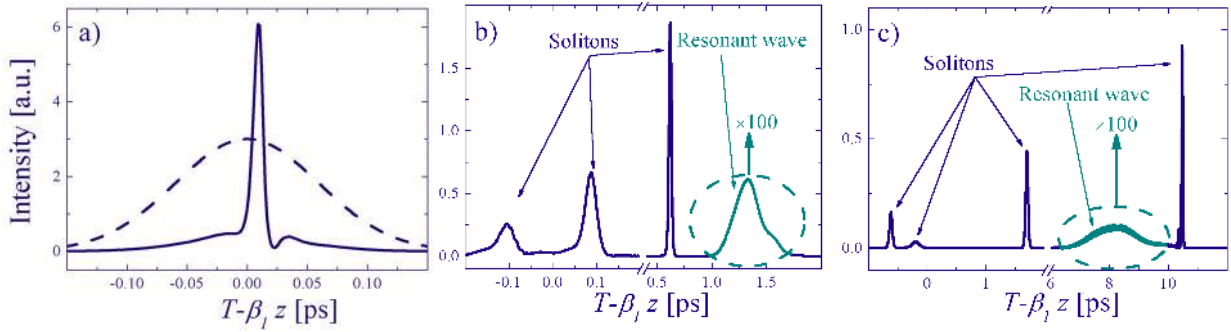
Figure 12. Simulated temporal profile of the pulse after a) 2 cm, b) 10 cm, and c) 50 cm. The dashed curve in Fig. 12a represents the input pulse.

More insight can be gained by plotting the spectrogram of the pulse as it propagates along the MF. Figure 13 presents the spectrograms calculated using the full NSE, i.e., corresponding to Figs. 11d and 12. The white solid line represents the group delay of the fiber for the corresponding length of propagation. From Fig. 13a it can be seen that the pulse is first compressed. The pulse subsequently splits into four solitons accompanied by the generation of resonant waves. The trajectory of the solitons originally coincide with the group delay of the fiber. However, as they experience the SSFS their trajectory tends to deviate from the group delay of the fiber. This is due to SRS which shifts their center frequency. The resonant waves follow the group delay of the fiber and temporally broaden as they propagate inside the MF. This fact shows evidence of the linear nature of these waves. It is interesting to notice that the resonant wave is originally lagging behind the soliton that generated it. This phase difference is due to the nonlinear induced phase-shift experience by the soliton. With further propagation the center frequency of the soliton is shifted and the soliton is therefore temporally delayed whereas the center frequency of the linear wave remains constant. The linear wave catches up the

soliton and overtakes it. As the linear wave sweeps through the soliton, an additional anti-Stokes frequency component is generated (see Fig. 13c and 11d). This additional anti-Stokes components results from the XPM induced by the soliton on the resonant wave. This phenomenon can only occur when the soliton and resonant wave overlap in the time domain. The resulting anti-Stokes component is coupled with the soliton via XPM and shifts its center frequency as the soliton experiences the SSFS: they form a pair (see Fig. 13c-d). It is this XPM-coupling that is responsible for the blue broadening of the spectrum with further propagation. If the fiber is long enough the resonant wave generated by the first soliton will also sweep through the second soliton and generate an additional anti-Stokes component. Therefore multiple XPM interactions due to the SSFS can occur between the solitons and the resonant waves leading to a significant extension of the SC to the blue.
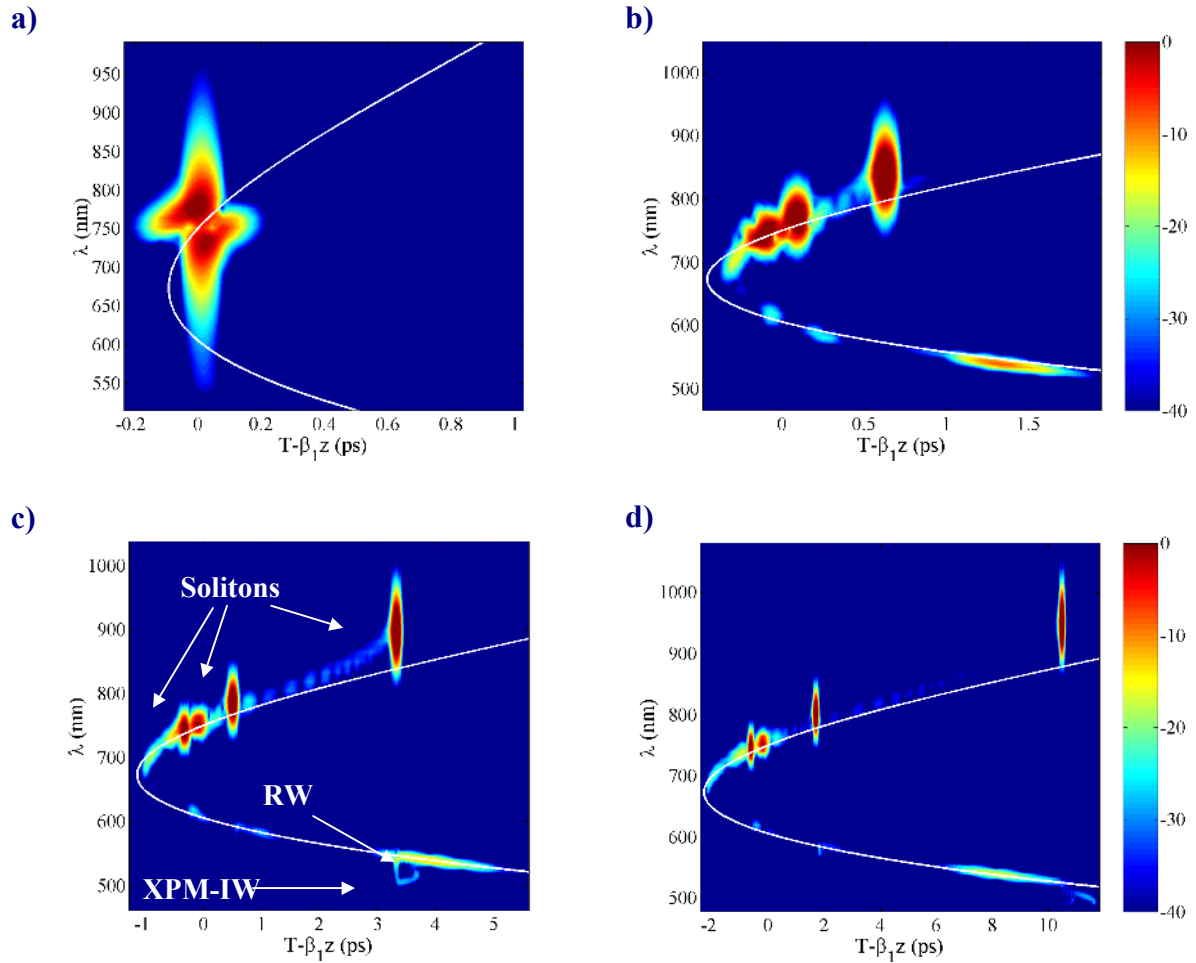
Figure 13. Simulated spectrogram of the pulses after a) 2 cm, b) 10 cm, c) 25 cm, and d) 50 cm of propagation inside the MF. The white line represents the group delay of the fiber. The scale is in dB units. P_p=3 kW (P_{av}=26 mW), T_{FWHM}=100 fs and λ_p=750 nm. RW: resonant wave, XPM-IW: cross-phase modulation induced wave.

Effect of increasing the pump power

An increase of the input pump power results in an enhanced *N*-value. The number of split fundamental solitons therefore increases and more Stokes peaks are observed in the spectrum. Furthermore, the temporal width of the fundamental solitons is reduced (see Eq. (25)) and the magnitude of the SSFS is consequently enhanced. The overlap between the solitons and the resonant waves is also larger which results in the increase of the magnitude of the anti-Stokes components. The XPM induced anti-Stokes components shifts also further to the blue since the solitons shifts further to the red. This can be observed in Fig. 14 which illustrates the effect of increasing the input pump power. Further increase in

18

the input power eventually leads to a flat spectrum due to the high number of fundamental solitons, with a gap located around λ_{ZD} [II]. This sequence of events was experimentally confirmed as is shown in Fig. 15 [I]. The gap results from the phase-matching condition (see Eqs. (29) and (30)) required for the generation of the resonant wave, the nearest anti-Stokes components from λ_{ZD} resulting from the soliton with lowest amplitude.
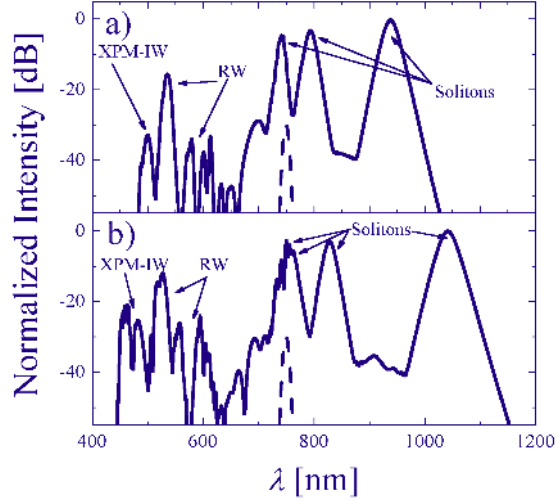
Figure 14. **Simulated spectrum of the pulses after 50 cm of propagation inside the MF with an input peak power of a) 3 kW (P_{av}=26 mW) and b) 4.5 kW (P_{av}=38 mW). T_{FWHM}=100 fs and λ_p=750 nm. RW: resonant wave, XPM-IW: cross-phase modulation induced wave. The dashed curves represent the spectrum of the input pulses.**

Figure 15. **Experimentally recorded spectra of pulses after 500 cm of propagation inside a MF (see Fig. 10 for the dispersion profile) for an average input power of a) 16 mW, b) 32 mW, c) 45 mW, and d) 55 mW. λ_p=804 nm and T_{FWHM}=100 fs. The dashed curve represents the spectrum of the input pulses.**

Effect of varying the pulse width

Keeping the energy constant while increasing the pulse width results in increasing the number of Stokes peaks and a reduced bandwidth for the generated SC as is illustrated in Fig. 16. Indeed, the *N*-value increases proportionally to $\sqrt{T_0}$ leading to the splitting of the input pulse into an increased number of fundamental solitons. These solitons have, nevertheless, broader temporal widths, which results in a decrease of the magnitude of the SSFS. This also means that the overlap between the spectra of the solitons and the resonant wave is reduced and, consequently, the magnitude of the anti-Stokes

components is decreased as is clearly observed in Fig. 16. At high input power values, the SC generated using broader pulses is flatter and exhibit the same bandwidth as the SC generated using narrower pulses due to a higher number of fundamental solitons [II]. The SSFS ceases beyond 1400 nm because of very high OH absorption losses around this wavelength, therefore limiting the bandwidth of the SC generated using narrower pulses [II].
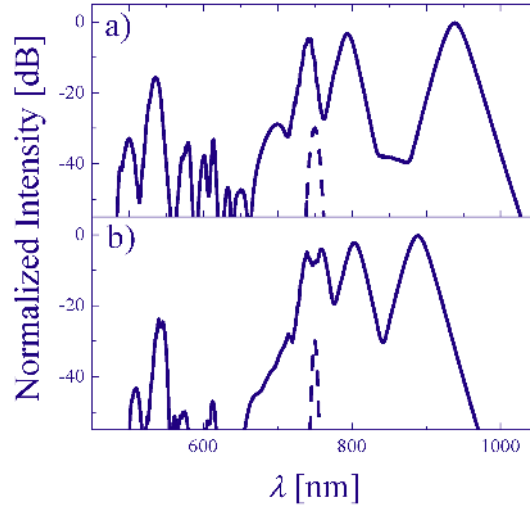
Figure 16. Simulated spectrum of the pulses after 50 cm of propagation inside the MF with a temporal width of a) 100 fs and P_p=3 kW (P_{av}=26 mW) b) 200 fs and P_p=3 kW (P_{av}=26 mW). λ_p=750 nm and λ_{ZD}=675 nm. The dashed curves represent the spectrum of the input pulses.

Effect of detuning the pump wavelength

When the pump wavelength is tuned closer to λ_{ZD} the N-value increases and so does the number of Stokes peaks observed in the spectrum at the output of the MF as is shown in Fig. 17. The wavelengths of the phase-matched resonant waves lie closer to λ_{ZD} leading to a reduction of the gap observed in the spectrum [I,II]. The overlap between the solitons and the resonant waves is also increased and, therefore, the magnitude of the anti-Stokes components is enhanced. Initially the solitons lose a lot of energy due to the large overlap with the linear waves, thus resulting in a decrease of the magnitude of the SSFS. The bandwidth of the SC is reduced though the SC is flatter, as was observed experimentally (see Fig. 18) [II].
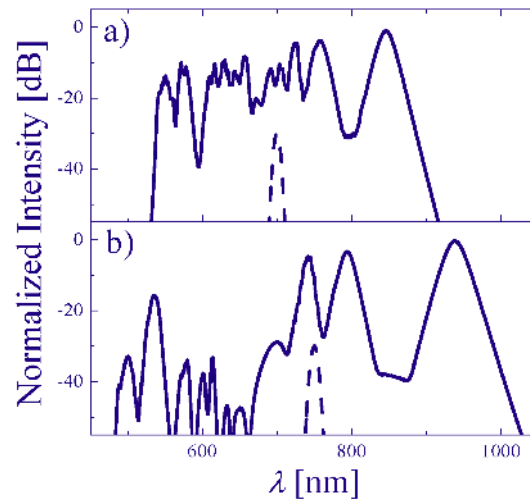
Figure 17. Simulated spectrum of the pulses after 50 cm of propagation inside the MF with a pump wavelength of a) 700 nm and b) 750 nm. P_p=3 kW (P_{av}=26 mW) and T_{FWHM}=100 fs. λ_{ZD}=675 nm. The dashed curves represent the spectrum of the input pulses.
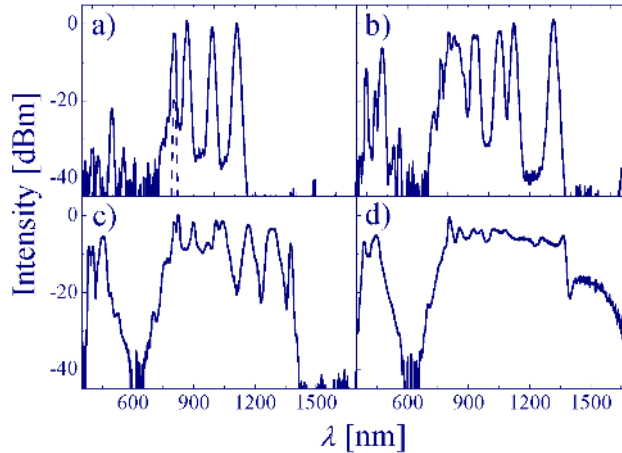
20
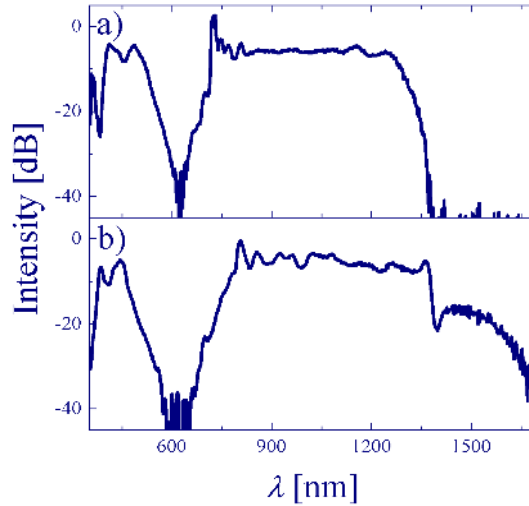
Figure 18. Experimentally recorded spectra of the pulses after 5 m of propagation inside a MF (see Fig. 10 for the dispersion profile) with a pump wavelength located at a) 722 nm and b) 804 nm. P_{av}=55 mW and T_{FWHM}=100 fs.

Limitations of the bandwidth

The bandwidth of the SC generated in MFs is limited by several factors. On the long wavelength side the Raman-shifted solitons suffer from very high losses when their center wavelength reaches 1400 nm because of the strong water absorption peak at this wavelength [I]. The magnitude of the OH losses is enanced for reduced core diameter and, therefore, may strongly affects the SSFS. Indeed, the losses lead to a subsequent large broadening of the temporal width of the solitons which prevents further SSFS. Figure 19 shows the effect of OH losses on the magnitude of the SSFS in a 1-m long small core MF. A plateau is observed when the input power is high enough so that the solitons are able to shift up to 1400 nm. Increasing the input power does not lead to any further shift. To overcome this limit it is necessary to use a very short piece of MF. However, in this case, the input power must be substancially increased to obtain the same bandwidth as in a longer fiber. When the wavelength of the light is of the order of the size of the pitch of the MF, the light is not well confined inside the core any more thus increasing considerably the leakage losses. Such losses strongly contributes to limiting the bandwidth of the SC on the long wavelength side when using small core MFs.
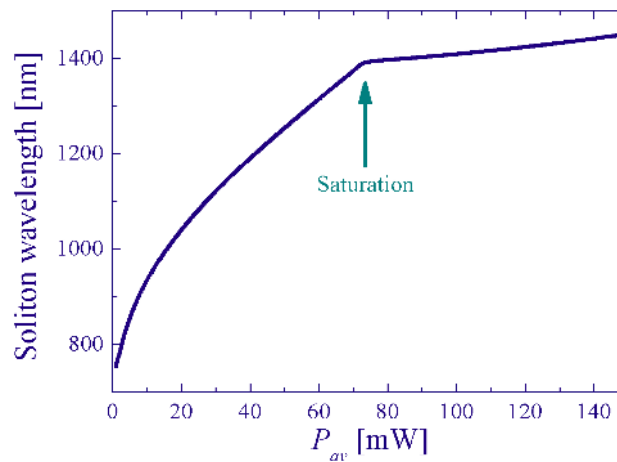
Figure 19. Simulated wavelength of the most Raman-shifted soliton as a function of average pump power. The magnitude of the OH absorption peak is taken to be 10 dB·m^{-1}.

On the short wavelength side, the bandwidth of the SC is limited by the high *UV*-losses and by the leakage of the propagating mode at these wavelengths, i.e., when the wavelength is much smaller than the core, the light tends to escape in the silica bridges between the holes surrounding the core of the fiber. For MF with a high air-filling fraction the leakage losses are, howver, not so severe and the main limitation comes from the dispersion curve which limits the restrain the phase-matching condition for the resonant waves to around 400 nm.

- Normal pumping

When the pump wavelength is located in the normal dispersion region of the fiber, the mechanism leading to SC generation differs from the case of anomalous pumping [171]. Indeed, solitons are not able to propagate in the normal dispersion region. The formation of the continuum results mainly from SPM and SRS. Figures 20 and 21 illustrate the simulated spectrum and the corresponding time trace of the SC generated along a 1 m-long MF with λ_{ZD} located at around 950 nm. The spectrum of the pulse broadens due to SPM. As the pulse propagates along the MF, it experiences temporal broadening due to the normal dispersion (see Fig. 21). Consequently, the peak power of the pulse decreases thereby stopping the spectral broadening.
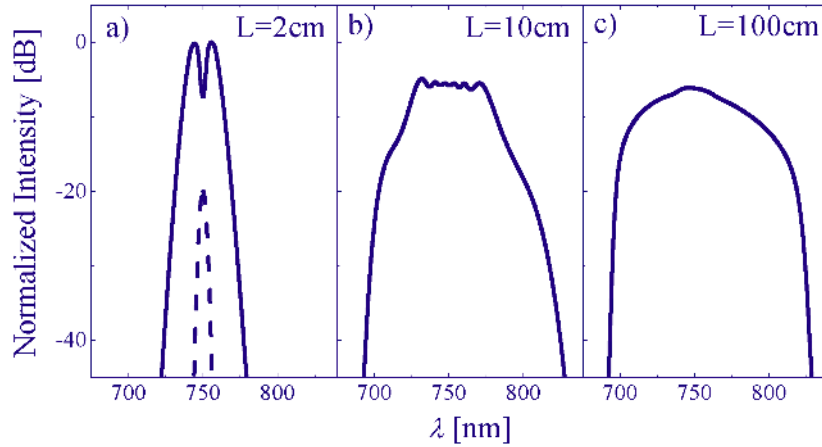
Figure 20. Simulated spectrum at the output of a MF after a) 2 cm, b) 10 cm, and c) 100 cm. λ_p=750 nm, T_{FWHM}=200 fs and P_p=6 kW (P_{av}=102 mW). The dashed curve represents the spectrum of the input pulses.
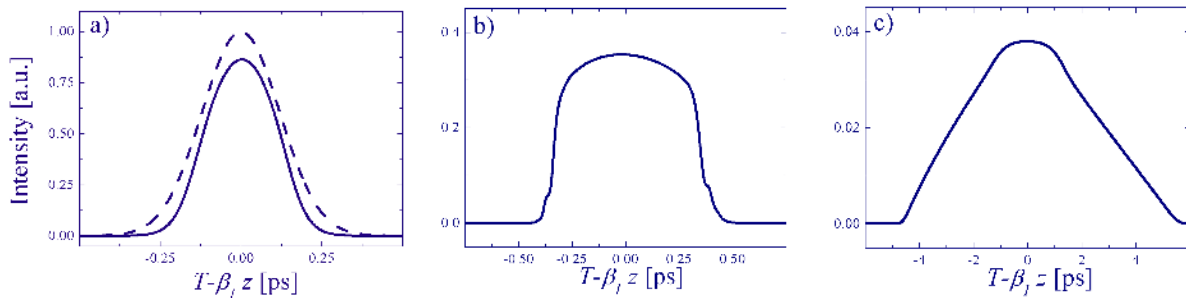
Figure 21. Simulated temporal profile of the pulse corresponding to Fig. 20 after a) 2 cm, b) 10 cm, and c) 100 cm. The dashed line represents the input pulse.

Effect of increasing the pump power

As a direct consequence of SPM, the spectral broadening increases with input peak power. Figure 22 shows the experimental spectrum obtained by launching 200 fs pulses into a MF having λ_{ZD} located at around 950 nm [I]. The pump wavelength was set to lie deep inside the normal dispersion region of the

fiber at 756 nm. The dispersion profile of the fiber is plotted as an inset in Fig. 22 and is similar to the one used for the simulations presented in Figs. 20 and 21.
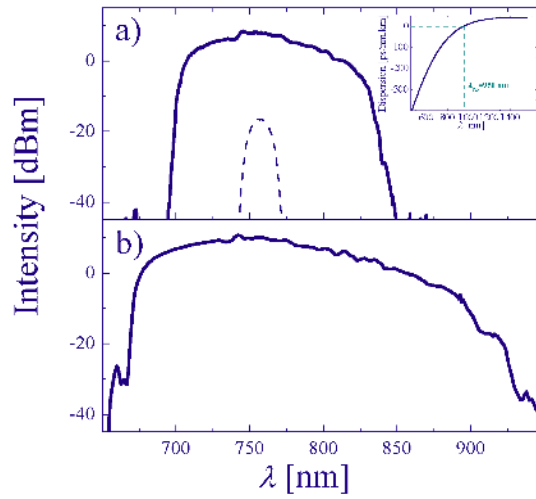
Figure 22. Experimentally recorded spectra of pulses after propagation inside a MF for average powers of a) 40 mW and b) 100 mW. λ_p=756 nm and T_{FWHM}=200 fs. The dashed curve represents the spectrum of the input pulses. Inset: dispersion of the fiber. L=14 m.

Effect of varying the pulse width

Keeping the average power constant and increasing the pulse width results in a decrease of the peak power. Therefore, the SPM broadening is less pronounced than in the case of shorter pulses [I].

Effect of detuning the pump wavelength

When the pump wavelength is tuned closer to λ_{ZD}, the spectral evolution, which is illustrated in Fig. 23, is initially similar to the case of pumping far from λ_{ZD} except for the fact that the dispersion value is smaller and the broadening caused by SMP is therefore enhanced. For high enough input power, the SPM induced frequencies extend in the vicinity of λ_{ZD}, acting as efficient seeds for FWM process [167,319]. The new frequencies generated by FWM appear beyond λ_{ZD}, in the anomalous dispersion region of the MF [167,319].
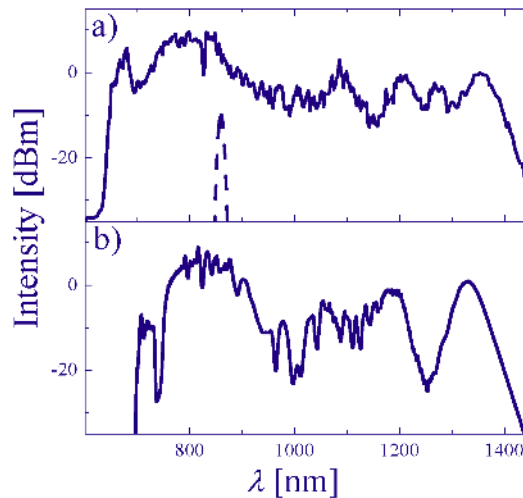
Figure 23. a) Experimental and b) simulated spectrum of pulses after 100 cm of propagation in a MF with λ_{ZD}=950 nm. λ_p=860 nm, T_{FWHM}=130 fs, and P_{av}=120 mW. The dashed curve represents the spectrum of the input pulses.

To emphasize the role of FWM when the spectrum extends to the vicinity of λ_{ZD}, it is interesting to plot the phase-matched Stokes and anti-Stokes wavelengths as a function of potential pump wavelength components already present in the spectrum. From Fig. 24 it can be seen that FWM can expand the spectrum of the SC far into the infrared.
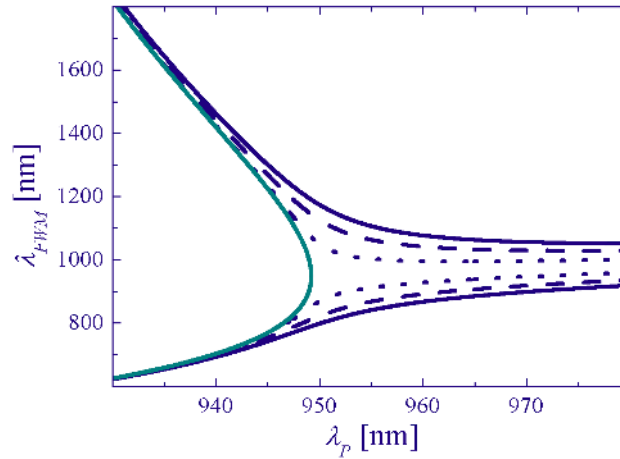
Figure 24. Calculated phase-matched wavelengths as a function of pump wavelength through degenerate FWM. The blue solid, dashed and dotted lines correspond to a pump peak power of 1, 0.5, and 0.1 kW respectively. The green solid line is calculated neglecting the nonlinear induced phase-shift (i.e. with P_p=0 kW). The dispersion profile of the MF corresponds to that of Fig. 22.

The wave packet transferred to the anomalous dispersion region of the MF subsequently forms bound states. The formation of solitons becomes possible and is accompanied by the process of soliton self-frequency shift that expands the continuum further into the infrared [I]. This sequence of events is conveniently observed in the simulated spectrograms of the pulses plotted in Fig. 25. The bandwidth of the SC is again mainly limited by the high losses due to OH absorption around 1400 nm.
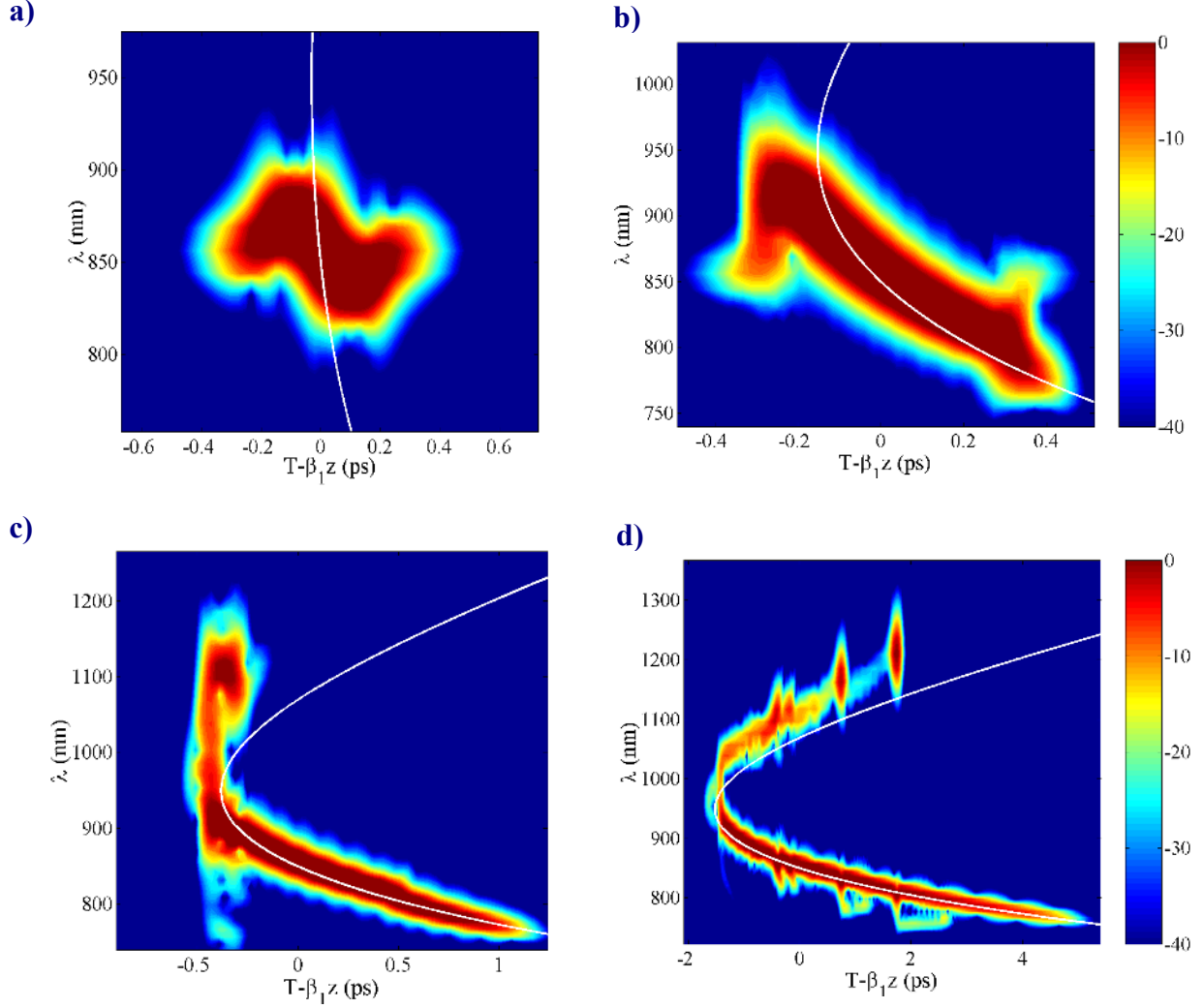
Figure 25. Simulated spectrogram of the pulses after a) 2 cm, b) 10 cm, c) 25 cm, and d) 100 cm of propagation inside the MF (see Fig. 22 for the dispersion profile). The white line represents the group delay of the fiber. The scale is in dB units. P_p=8 kW (P_{av}=136 mW), T_{FWHM}=200 fs and λ_p=850 nm.

3.4 Supercontinuum generation using ps and ns pulses

Supercontinuum can also be generated in MFs using ps and ns pulses [144,145,147,148,153,174]. In that case, the peak power of the pulses is much lower and SPM spectral broadening is negligible. The mechanism leading to SC generation relies on SRS and FWM [144,145,153]. Due to the relatively low peak power of the pulses, SC generation requires several meters of MF.

Figure 26 illustrates the simulated spectrum of 20 ps pulses at the output of a 3 m-long MF. Noise-seeded SRS generates a pair of Stokes and anti-Stokes bands in the spectrum which are coupled through parametric FWM [144]. This coupling is much stronger than in conventional fibers due to the high nonlinearity of the MF. This pair can serve as an efficient seed for further parametric amplification, which results in the appearance of multiple side bands in the spectrum. This process is particularly efficient when the pump wavelength is located around λ_{ZD} because the phase-matching condition for degenerate FWM to occur is then easily fulfilled. The fact that the pulse is ps-broad allows for the pump and side bands to overlap over few meters. Consequently, energy transfers continuously from the pump to the side bands which grow as the pulse propagates along the MF. The different frequency components eventually walk off after few meters of propagation and the spectral broadening ceases.

Cross-phase modulation broadens the side bands which subsequently merge, resulting in a smooth spectrum [144].
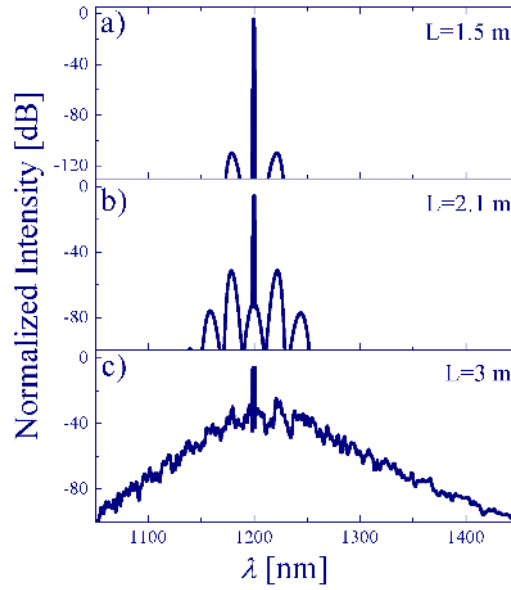
Figure 26. Simulated spectrum of SC generated in a MF with λ_{ZD}=950 nm (see Fig. 22 for the dispersion profile) after a) 1.5 m, b) 2.1 m, and c) 3 m. T_{FWHM}=20 ps pulses, λ_p=1200 nm, and P_p=400 W.

Supercontinuum generation using ns pulses has also been demonstrated using frequency-doubled Nd:YAG laser operating at 532 nm [153,174] or seeded Ytterbium amplifier at 1064 nm [147,148]. In the case of ns pulses, cascaded Raman scattering is mostly responsible for the generation of the continuum, i.e., multiple lines separated by 13.2 THz are amplified through SRS [153,174]. For this reason, the spectrum mainly extends towards the infrared. If the pump wavelength is located in the vicinity of λ_{ZD} FWM can contribute to the extension of the SC to the blue wavelengths [153,174]. At high enough power all the different Raman lines broaden due to XPM and subsequently merge leading to a smooth spectrum. Since the peak power of ns pulses is typically below the kW level, several meters of MFs are necessary to form the continuum.

3.5 Enhancement of supercontinuum generation

- Use of a highly birefringent MF

The flexibility in the design of MF allows for producing fibers with very high birefringence [213,214]. The use of highly birefringent MFs is particularly interesting in the context of SC generation because it not only enable to obtain all the frequency components of the SC in a single state of polarization but also introduces an extra degree of freedom for generating the SC by tuning the polarization state of the input pulses to match either of the principal axes of polarization (PAPs) of the MF [II].
Pulses with a state of polarization matching the direction of one of the PAPs of a highly birefringent MF maintain their polarization as they propagate along the fiber. This property can be exploited to generate SC with all the wavelength components exhibiting the same state of polarization [II]. Polarized continua can be essential for spectroscopic applications.
Furthermore, the preserved state of polarization enhances the various nonlinear processes inside the MF, which means that less input power is required to generate comparable SC than in non-polarization maintaining fibers.
The direction of the fast/slow axis corresponds to the narrowest/largest dimension of the core of the MF. Consequently, the two PAPs exhibit different λ_{ZD}, λ_{ZD} of the fast axis being located at a lower wavelength compared to that of the slow axis. For a pump wavelength located in the anomalous

26

dispersion region of a highly birefringent MF, the bandwidth of the SC is maximum when the direction of the polarization of the input light is set to match that of the fast axis. Indeed, the relative detuning between the wavelength of the pump pulses and λ_{ZD} is larger when the polarization of the input pulses matches the direction of the fast axis. On the blue side, the wavelength of the resonant waves is therefore shorter than in the case of pumping on the slow axis. On the red side, the multiple solitons experience a larger frequency shift on the fast axis. Pumping on the fast axis also results in an enhancement of the magnitude of the gap between the Stokes and anti-Stokes frequency components. Pumping on the slow axis reduces the magnitude of the gap at the expense of the generated bandwidth. Tuning the polarization of the input pulse at 45° between the directions of the PAPs leads to the generation of two distinct continua with half of the total input power and different characteristics. This is because the walk-off length is very short for highly birefringent MFs (of the order of few millimeters for 100 fs pulses) and, consequently, orthogonally polarized pulses do not interact with each other after this distance and the SC are generated independently of each other on each PAP. These features are in agreement with the experiments performed using a highly birefringent MF as is illustrated in Fig. 27 [II].
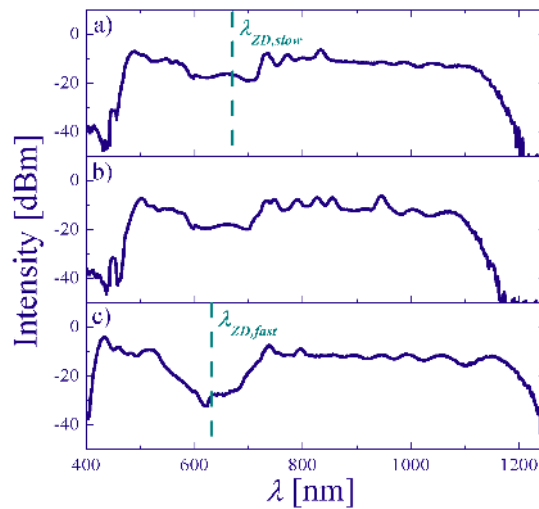
Figure 27. Experimental SC generated in a highly birefringent MF for an input polarization a) parallel to the slow PAP, b) at 45° between the PAPs, and c) parallel to the fast PAP. λ_p=730 nm, T_{FWHM}=200 fs, and P_{av}=60 mW.

- Higher-order mode phase-matching

Small core MFs with a large air-filling fraction exhibit a large index difference seen by the fundamental mode well confined into the core and higher-order modes that extends into the cladding region. It is therefore difficult to couple light into a higher-order mode in small core MFs [320]. However, increasing slightly the size of the core can allow for higher-order mode propagation provided the launching conditions are adequate. It is then possible to generate supercontinua that are partly divided between fundamental and higher-order modes [110,159,321-323]. Varying the angle of incidence between the laser beam and the MF can excite various forms of higher-order modes such as two-sided lobes or doughnut-like as is illustrated in Fig. 28.
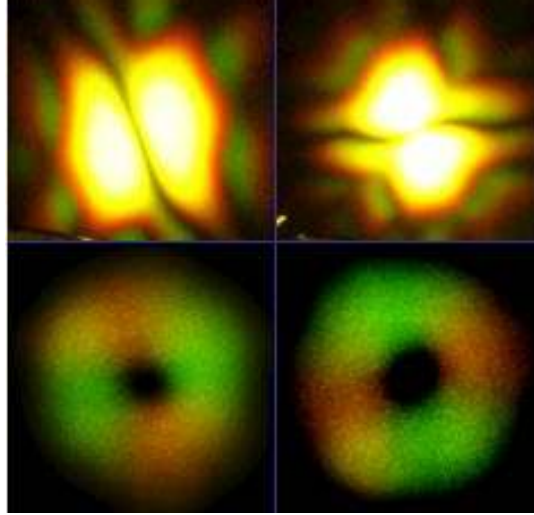
Figure 28. Visible far field patterns of SC generated in a multimode MF.

The coupling between the fundamental and higher-order modes allows for FWM interactions between the frequency components of various modes, which results in an extension of the continuum to the shorter wavelength side. Figure 29 shows the SC generated in two MFs which exhibit similar characteristics except for a slightly different core size. Extra high frequency components appear in the spectrum of the SC generated in the multimode MF. It has recently been demonstrated that *UV* light can be generated in this way [156,173].
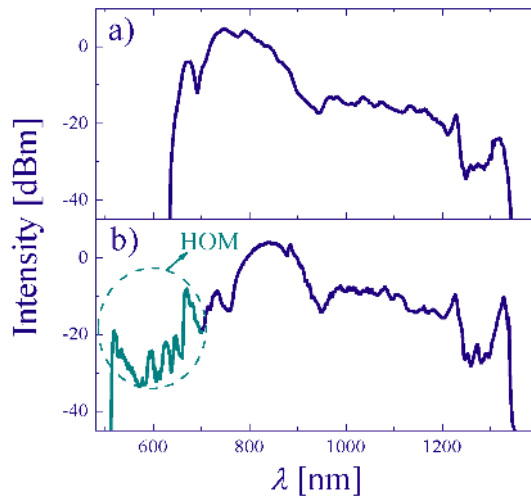
Figure 29. Experimental SC generated in the a) fundamental mode of a MF and b) both fundamental and higher-order modes. HOM: higher-order mode wavelengths components. λ_p=820 nm, T_{FWHM}=200 fs, and P_{av}=150 mW. For both MFs λ_{ZD} of the fundamental mode is located at around 950 nm.

- Introduction of a second λ_{ZD}

The limitation of the SC bandwidth on the long wavelength side results from the saturation of the SSFS due to the dispersion and various losses experienced by the solitons as they travel along the MF. One way to extend further the bandwidth of the SC towards the infrared is to introduce a second λ_{ZD} around the wavelength at which the SSFS ceases [168,324]. This can be easily achieved by a proper choice of the air-holes size and pitch of the lattice. When the center wavelengths of the solitons have shifted to the vicinity of this second λ_{ZD}, the spectrum of these solitons overlap with that of the resonant wave located in the second normal dispersion region of the MF. The resonant wave is subsequently amplified in the same manner that the resonant wave located in the first normal dispersion region of the MF. New

frequency components appear beyond the second λ_{ZD}, thus extending further the SC as is shown in Fig. 30.
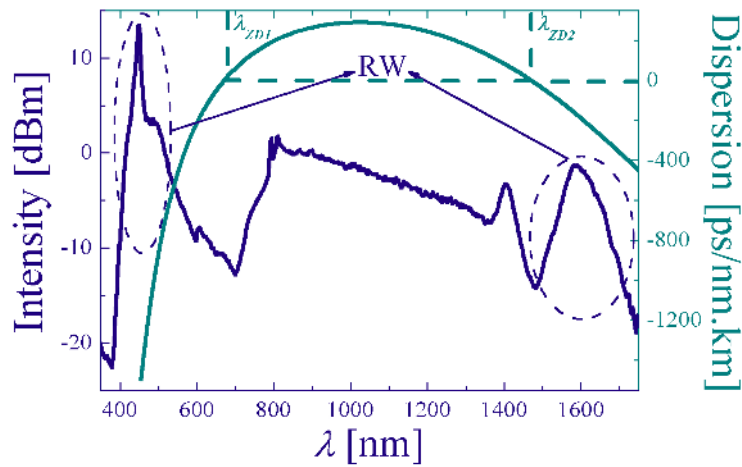
Figure 30. Experimental spectrum generated in a 1.1–μm core MF with two λ_{ZD}. RW: resonant wave. λ_p=813 nm, T_{FWHM}=200 fs, and P_{av}=200 mW.

The use of MF with an ultra-flattened dispersion profile or MF made of highly nonlinear material such as extruded SF6 glass allows for the generation of very broad SC using less input power and/or shorter fiber lengths [231]. This permits to overcome the saturation of the SSFS and extend the SC further to the infrared.

4. Novel optical measurement techniques

In general, light waves with different wavelengths travel at different speeds inside materials. The dependence of the speed of light on its wavelength is commonly referred to as dispersion. Dispersion is one of the most important parameter of optical fibers and components as it may strongly affect the performances of communication systems and fiber-optic nonlinear devices.

4.1 Dispersion of optical fibers and components

The various frequency components of an optical pulse travel inside a material of refractive index n with the phase velocity defined as

$$v_\varphi(\omega) = \frac{c}{n(\omega)} \ , \tag{31}$$

where c represents the speed of light in vacuum. The velocity at which the energy of the optical pulse travels along a fiber or inside a component is referred to as the group velocity and it is defined as [284]

$$v_g(\omega) = \frac{1}{\beta_1} = \frac{d\omega}{d\beta} = \frac{c}{n(\omega) + \omega\left[\left(\frac{\partial n}{\partial \omega}\right)_M + \left(\frac{\partial n}{\partial \omega}\right)_W\right]} , \tag{32}$$

where β is the propagation constant of the electromagnetic wave and the subscripts M and W refers to the material and waveguide dispersion, respectively. The sum of the material and waveguide dispersion constitutes the total dispersion. The quantity β_1 is called the group delay. In terms of wavelength Eq. (32) can be rewritten as [284]

$$v_g(\lambda) = \frac{c}{n(\lambda) - \lambda\left[\left(\frac{\partial n}{\partial \lambda}\right)_M + \left(\frac{\partial n}{\partial \lambda}\right)_W\right]} . \tag{33}$$

Material dispersion

The refractive index of a material depends on the wavelength of the electromagnetic wave interacting with the material. This dependence is referred to as the material dispersion and it can be represented using the Sellmeier approximation [284,325,326]

$$n(\lambda) = \sqrt{1 + \sum_{k \geq 1} \frac{B_k \lambda_k^2}{\lambda_k^2 - \lambda^2}} \ , \tag{34}$$

where B_k is the magnitude of the kth resonance of the material located at wavelength λ_k. Equation (31) includes all the resonances of the material that are of interest for a given wavelength range. For silica fibers, the refractive index is well approximated using the following values for B_k and λ_k: B_1=0.6961663, B_2=0.4079426, B_3=0.8974794 and λ_1=0.0684043 µm, λ_2=0.1162414 µm and λ_3=09.896161µm [325]. The wavelength dependence of the refractive index of fused-silica is illustrated in Fig. 31.
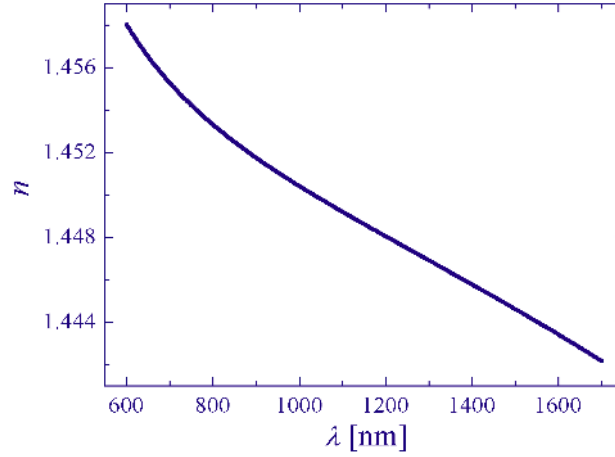
Figure 31. Refractive index *n* of silica as a function of wavelength.

Waveguide dispersion

Waveguide dispersion occurs due to the dependence of the light confinement on its frequency as it is guided along a waveguide (e.g., optical fibers). At higher frequencies, the mode propagating along the fiber is well confined in the core so that most of the energy travels inside the core. This results in an increase of the group velocity. Waveguide dispersion depends on the core diameter of the waveguide and the core-cladding refractive index difference of the waveguide.

Total dispersion

Both waveguide and material dispersion contribute to the group velocity dispersion of the fiber. The parameter β_2 represents the group velocity dispersion also referred to as the second-order dispersion and it is connected to the dispersion parameter D as [284]

$$\beta_2(\omega) = \frac{d\left(\frac{1}{v_g}\right)}{d\omega} = \frac{1}{c}\left[2\left(\frac{\partial n}{\partial \omega}\right)_M + 2\left(\frac{\partial n}{\partial \omega}\right)_W + \omega\left(\frac{\partial^2 n}{\partial \omega^2}\right)_M + \omega\left(\frac{\partial^2 n}{\partial \omega^2}\right)_W\right] = -\frac{2\pi c}{\omega^2}D(\omega). \quad (35)$$

The wavelength at which β_2 or D is equal to 0 is referred to as the zero-dispersion wavelength. The wavelength region for which $\beta_2 > 0$ (<0) is commonly referred to as the normal (anomalous) dispersion region. In the normal dispersion region higher frequency (blue wavelengths) components travel at a slower speed than lower frequency (red wavelengths) components. The opposite occurs in the anomalous dispersion region.

Whereas material dispersion is intrinsic to the material used to fabricate the waveguide or fiber and can not be changed, waveguide dispersion can be varied by modifying the design parameters of the waveguide or fiber, thus allowing tailoring of the total dispersion. For instance, by reducing the core diameter of conventional single-mode fibers down to 4 μm and using a core-cladding refractive index difference larger than 4×10^{-3}, it is possible to shift the zero-dispersion wavelength of the fiber from the 1.3 μm to the 1.55 μm region. Using multiple cladding designs it is also possible to manufacture fibers that exhibit a flat dispersion over the 1.3-1.6 μm wavelength range. Figure 32a illustrates the calculated material (solid line) and waveguide (dashed line) of a conventional single-mode optical fiber. Examples of the total dispersion of conventional single-mode and dispersion-shifted fibers are shown in Fig. 32b. The curves presented in Fig. 32 were calculated by solving the eigenvalues of the wave equation [284] and incorporating the material dispersion in the form of the Sellmaier equation (see Eq. (34)).
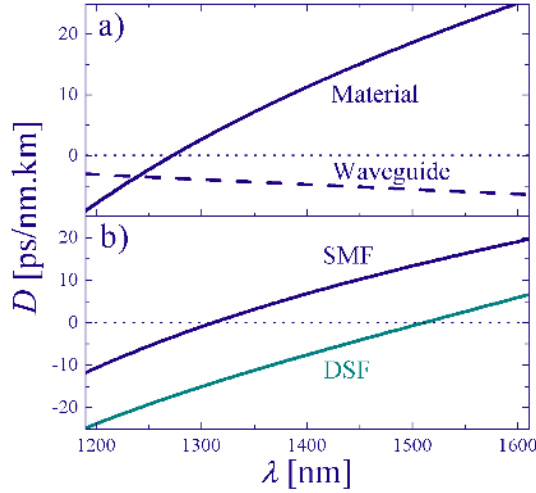
Figure 32. Dispersion parameter as a function of wavelength. a) The solid/dashed line represent the material/waveguide dispersion of a conventional single-mode fiber. b) Total dispersion of a conventional single-mode fiber (SMF) and a dispersion-shifted fiber (DSF).

Dispersion of optical components

The response of optical components such as filters can be modeled as

$$R_C(\omega) = \left| R_C(\omega) \right| e^{j\phi_C(\omega)}, \tag{36}$$

where $|R_C(\omega)|$ and $\phi_C(\omega)$ are the modulus and phase of the response of the component. The phase response of optical components results from multiple reflections or from wavelength dependent gain/loss inside the component [327]. Thus, as light passes through the component, it experiences a frequency-dependent group delay τ_c defined as

$$\tau_c(\omega) = -\frac{d\phi_C(\omega)}{d\omega}. \tag{37}$$

The wavelength-dependence of the time delay induces dispersion which is related to the phase response as

$$D(\omega) = -\frac{\omega^2}{2\pi c} \cdot \frac{d^2\phi_C(\omega)}{d\omega^2}. \tag{38}$$

4.2 Dispersion measurement techniques

Dispersion is responsible for temporal changes of an optical pulse traveling through a fiber or a component. For instance, transform limited pulses will broadened as they travel along a fiber whereas depending on the sign of the dispersion, non-transform limited pulses will be temporally broadened or compressed. Furthermore, when the strength of the nonlinearity of the fiber is not negligible, the spectral and temporal behavior of the pulse is different whether the center wavelength of the pulse is located in the anomalous or normal dispersion region of the fiber. Also, dispersion plays a critical role in supercontinuum generation in MFs. Therefore, it is important to characterize accurately the dispersive properties of these fibers. In addition, various optical components such as fiber Bragg gratings (FBGs) or thin-film filters are employed in fiber-optic communication systems. For optimization of these systems, precise knowledge of the dispersion of the components is necessary. For these reasons, it is of prime importance to develop measurement techniques that can accurately characterize the dispersion values of optical fibers and components.

Various techniques have been developed to measure the dispersion of optical fibers and components. They include pulse delay [328], phase measurement [329-332] and interferometric methods [330,333-335]. All these techniques are based on the fact that light waves with different wavelengths simultaneously launched into an optical fiber or component exit from it at a different time or with a

different phase. The measurement of the group delay or phase as a function of wavelength permits calculating the dispersion parameter by differentiation of the measured quantity.

Pulse delay technique

The pulse delay technique is mainly used to measure the dispersion of optical fibers. It measures the difference in arrival time of short light pulses traveling along the fiber as a function of wavelength [328,330,331]. The group delay of the fiber can be subsequently fitted with a multiple order polynomial and differentiated to obtain the dispersion. The technique has the disadvantage of requiring long fiber lengths so that the difference in arrival time is large enough to be detected. Typical fiber lengths are of the order of hundreds meters.

Phase-shift technique

The phase-shift technique allows for the measurement of the group delay as a function of wavelength [329-332]. The intensity of the output light of a CW tunable laser is sinusoidally modulated, which produces side bands around the carrier frequency in the spectral domain. As light passes through the device under test, the sidebands experience a phase-shift that is proportional to the group delay of the device. The resolution of the method depends on the sensitivity of the phase measurement and on the frequency of the sinusoidal modulation applied [336-338].

Interferometric technique

Interferometric methods make use of the short coherence time of partially coherent light and allow for very precise dispersion measurements [330,333-335]. The experimental setup consists of a Mach-Zehnder (MZ) or Michelson type interferometer. The light of a broadband source is divided between the two arms of the interferometer of which one is the reference path and the other one contains the device to be tested. The output light from the two arms is then recombined and the interference fringes are detected as the length of the optical path in the reference arm is changed. The phase response of the device is subsequently obtained by Fourier transformation of the interferogram and curve fitting [330,333]. The optical path length of the reference arm of the interferometer must be nearly equal to that of the arm containing the device under test. In practice, this limits the length of the device that can be measured. In addition, free-space interferometers are inherently extremely sensitive on the environmental conditions such as vibrations or temperature changes, which may affect the measurements results.

Examples of experimental setup of the aforementioned methods are presented in Fig. 33. Their main characteristics are summarized in Table 3.
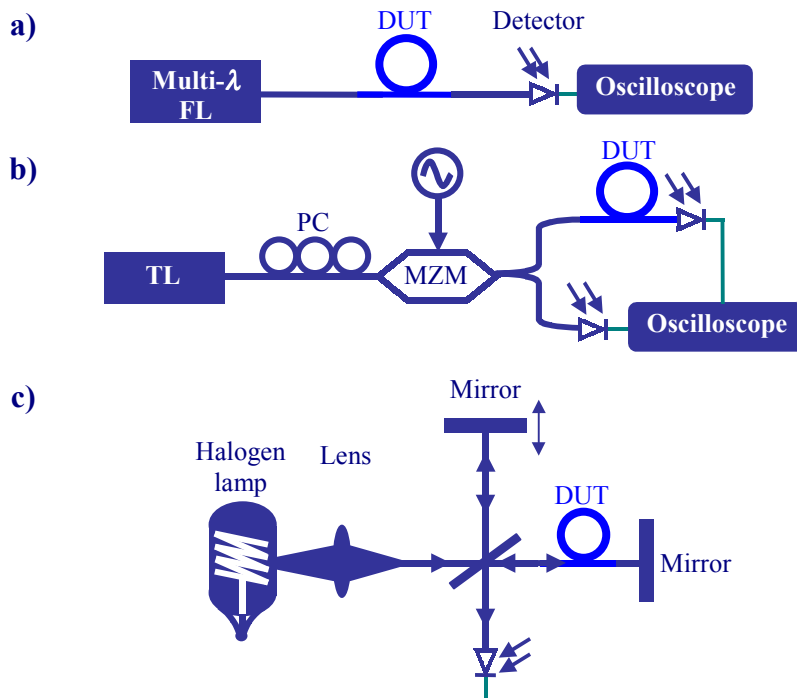
Figure 33. Example of experimental setup for a) time of flight, b) phase-shift, and c) interferometric techniques. FL: fiber laser, DUT: device under test, TL: tunable laser, MZM: Mach-Zehnder modulator, and PC: polarization controller.

Table 3. Characteristics of the most commonly used dispersion measurement techniques. GD: group delay.

Technique	Light source	GD resolution	Typical fiber length	Sensitivity to the environment
Time of flight	TL, Multi-λ FL	20 ps	100 m	low
Phase-shift	TL	1 ps	10 m	low
Interferometric	Halogen lamp, LED	0.1 ps	0.1 m	high

Another dispersion technique relies on the measurement of the amplitude response of a component. If the component fulfills the principle of causality [339,340], its phase response is directly connected to its amplitude response through Hilbert transformation [339]. The dispersion is subsequently obtained by double-differentiation of the phase response of the component. However, several optical components exhibit some rather complex phase response which can not be directly retrieved from their amplitude response. Mode-field diameter measurement technique or interferometric-pulse delay hybrid method have also been developed [330,341].

4.3 Measurement of anomalous dispersion in microstructured fibers using spectral modulation

Dispersion measurements of MFs can be difficult to perform using standard techniques. In particular, many applications employing MFs require short lengths of fiber to be utilized and, consequently, it is important to be able to characterize the dispersive properties of short fiber samples which can be problematic using pulse delay or phase-shift techniques. Furthermore, in the case of small core MFs, efficient coupling to the MF from low-coherent white-light may be difficult. Also, all the dispersion measurement techniques actually measure the group delay or phase response of the fiber and the dispersion is subsequently calculated by differentiation, which requires the group delay to be measured over a given wavelength interval and tends to amplify the noise of the measurements. Direct

measurement of the dispersion values of relatively short pieces of MFs can be performed by taking advantage of the interplay between dispersive and nonlinear effects [III].

Spectral modulation of short optical pulses

For pulses whose bandwidth does not exceed a few nanometers, Eq. (20) models accurately their propagation along optical fibers. If the time-dependent amplitude of the pulse launched into the fiber is so that $A(T)=N \, sech(T/T_0)$ with $N=1$, the pulse corresponds to a fundamental soliton which propagates undistorted [284]. Nevertheless, the parameters of the input pulse seldom match the requirements for the pulse to be a perfect fundamental soliton and in general $N=1\pm\varepsilon$. An optical pulse whose time-dependent amplitude is of the form $(1+\varepsilon)sech(T/T_0)$ evolves into the asymptotic solution of the NSE, i.e., a fundamental soliton whose amplitude is equal to $(1+2\varepsilon)sech[(1+2\varepsilon)T/T_0]$ [284,342]. The energy difference between the input pulse and the asymptotic soliton is equal to $2T_0\varepsilon^2$ and during the reshaping process, the excess of energy of the input pulse compared to that of the asymptotic fundamental soliton is shed away as a dispersive wave [342]. Such phenomenon occurs for $\varepsilon \in [-1/2, 1/2]$. The spectrum of the total field $A_T(\omega)$ after propagating inside the fiber is given by [342]

$$A_T(\omega) = A_S(\omega) + A_D(\omega), \tag{39}$$

with A_S and A_D being the spectral amplitude of the asymptotic soliton and dispersive field, respectively. It can be shown theoretically than the spectral amplitudes of the asymptotic soliton and dispersive field are given by [342]

$$A_S(\omega) = \sqrt{\frac{\pi}{2}}(1+2\varepsilon)\,sech\left[\frac{\pi}{2}\cdot\frac{(\omega-\omega_0)T_0}{1+2\varepsilon}\right]\cdot e^{j(1+2\varepsilon)^2\cdot\frac{L}{2T_0^2}|\beta_2|}, \tag{40}$$

$$A_D(\omega) = \varepsilon \, A_S(\omega)e^{-j\phi(\omega)}, \tag{41}$$

where ω_0 is the carrier frequency of the input pulse, L the fiber length and $\phi(\omega)$ a phase term defined by [342]

$$\phi(\omega) = \frac{(\omega-\omega_0)^2 T_0^2 + (1+2\varepsilon)^2}{2}\cdot\frac{L}{T_0^2}|\beta_2| + 2\,tan^{-1}\left(\frac{|\omega-\omega_0|T_0}{1+2\varepsilon}\right). \tag{42}$$

Here, β_2 represents the group velocity dispersion of the fiber. The phase difference $\phi(\omega)$ between the two coherent fields depends on both frequency and distance of propagation. The interference between the emerging soliton and the dispersive field results in the modulation of the optical spectrum [342]. The amplitude spectrum of the asymptotic soliton $A_S(\omega)$ determines the spectral envelope of the total field. Comparison between the theoretical model and the simulation using the NSE is presented in Fig. 34 for several values of ε. The agreement is improved for smaller values of ε. Varying the input peak power affects the characteristics of the spectral oscillations. In particular, as the peak power is increased, the value of ε increases and the spectral envelope of the spectrum broadens. Moreover, the amplitude of the oscillations reduces for higher $|\varepsilon|$ values.
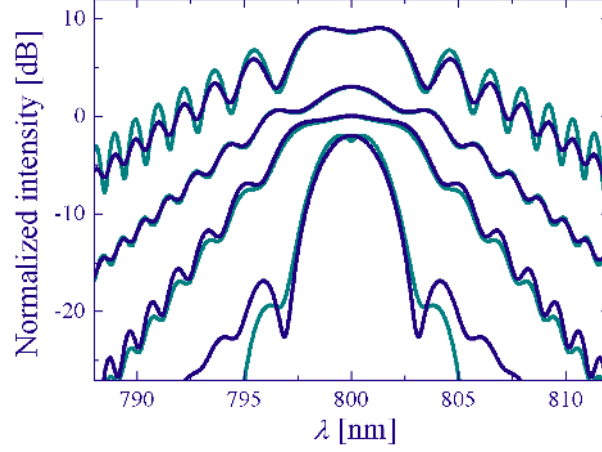
Figure 34. **Simulated spectrum at the output of a 2 m-long fiber. $\lambda_0=2\pi c/\omega_0$=800 nm, T_0=60 fs, D=100 ps/nm·km, γ=100 W^{-1}·km^{-1}. From top to bottom: ε=0.3, 0.1, -0.1, -0.3. The dark blue lines are obtained by solving Eq. (20) and the dark green lines correspond to the computed spectral intensity using Eq. (39). For clarity an arbitrary offset has been added to each curve.**

Figure 35a-c illustrates the simulated spectrum of 100 fs (FWHM) pulses whose initial amplitude is of the form $(1+\varepsilon)sech(T/T_0)$ with ε being equal to 0.2 after propagation along 0.5, 2 and 5 m of MF. The amplitude and period of the oscillations decrease as the propagation length increases. The time-dependent amplitude of the pulse after 0.25 m of propagation is plotted in Fig. 35d. The superimposition of the soliton and dispersive field is clearly observed. The dispersive field broadens as the pulse propagates further while the soliton remains nearly unchanged.
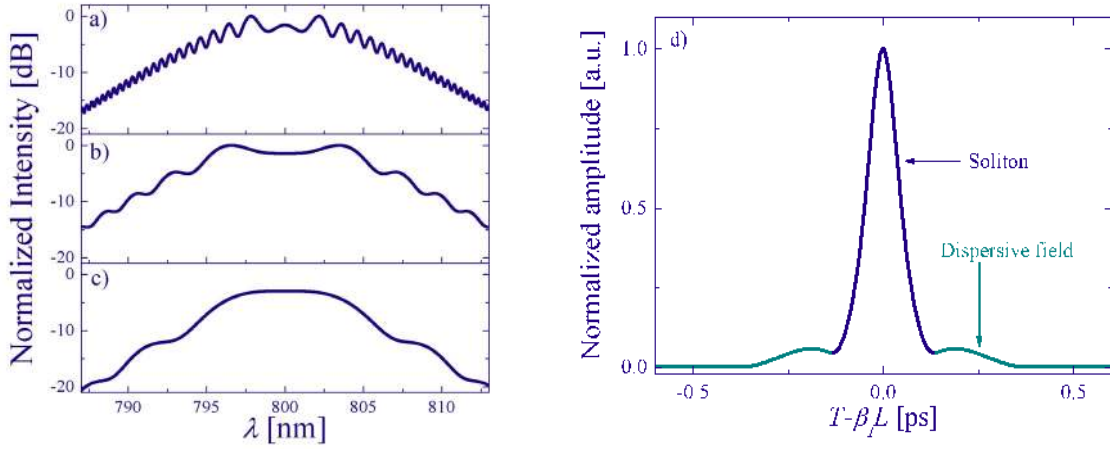
Figure 35. **Simulated spectrum and corresponding temporal profile of 100 fs pulses after propagating a) 0.5, b) 2, and c) 5 m inside a MF obtained by solving the NSE. $\lambda_0=2\pi c/\omega_0$=800 nm, D=100 ps/nm·km, γ=100 W^{-1}·km^{-1}. For clarity an arbitrary offset has been added to each curve. d) Time-dependent amplitude of the pulse after 0.25 m of propagation.**

From Eq. (42) it can be seen that the phase difference between the two interfering fields depends on the dispersion parameter β_2. By writing that the phase difference in the spectrum between two consecutive maxima or minima is equal to 2π and omitting the tan^{-1} terms in the calculation, the dispersion can be approximated to the first order as [III]

$$D(\omega_0) = -\frac{\omega_0^2}{2\pi c}\beta_2(\omega_0) \approx \frac{2}{cL} \cdot \frac{10^6}{\left(\dfrac{\omega_2}{\omega_0}-1\right)^2 - \left(\dfrac{\omega_1}{\omega_0}-1\right)^2} \quad \text{[ps/nm·km]}, \tag{43}$$

36

where ω_0 is the center frequency of the spectrum and ω_2 and ω_1 represent the frequency of the first and second maxima. Note that Eq. (43) does not depend either on the input pulse width T_0 or the ε value. The spectral modulation effect due to the input pulse reshaping into a fundamental soliton can therefore be exploited for direct dispersion measurement of MFs [III]. Since solitons cannot propagate in the normal dispersion regime, the method is intrinsically limited to the anomalous dispersion region of the fiber. A schematic layout of the experimental setup for dispersion measurement using this technique is shown in Fig. 36.

Figure 36. Experimental setup for dispersion measurement using the spectral modulation effect. I: isolator, $\lambda/2$: half-wave plate, VA: variable aperture, and OSA: optical spectrum analyzer.

The dispersion measurement procedure is as follows. Short optical pulses from a Ti:Sapphire laser are launched into the MF and the input power is gradually increased until oscillations are observed in the spectrum recorded at the output of the fiber. The dispersion is then calculated using Eq. (43). Tuning the wavelength of the pulses launched into the fiber allows for the measurement of the dispersion profile of the fiber as a function of wavelength [III]. Examples of dispersion measurement performed for two different types of MF are illustrated in Fig. 37. A typical experimental spectrum recorded at the output of the fiber is plotted as an inset in Fig. 37.
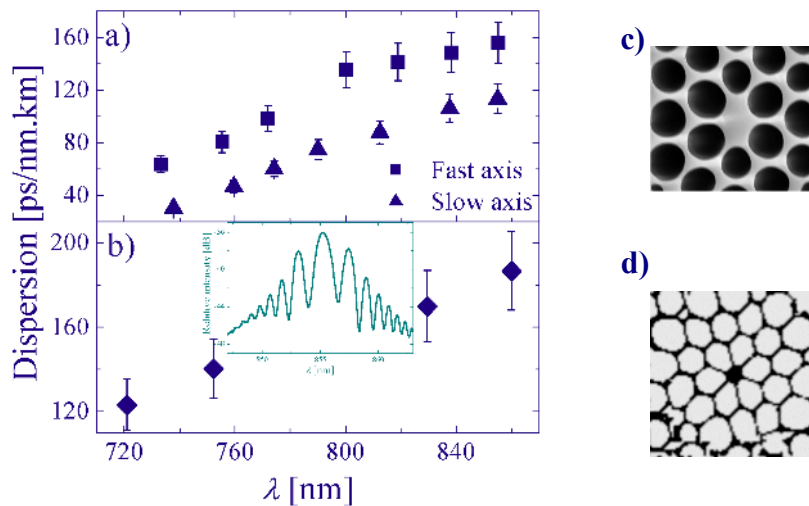
Figure 37. Dispersion profile measured using the spectral modulation technique for a) a highly birefringent MF and b) a small core MF. Inset: Typical experimental spectrum recorded at the output of the MF. Microscope image of c) the highly birefringent and d) the small core MF.

The measurement accuracy of the method is limited due to the omission of the tan^{-1} terms in the dispersion calculation [III]. It can be evaluated in a two-step process. The exact values of ω_1 and ω_2 are calculated numerically from Eq. (42) as a function of D and subsequently plugged into Eq. (43). The relative measurement error is then defined as $(D_a-D)/D$ where D_a represents the approximated dispersion value from Eq. (43). The relative measurement error is illustrated in Fig. 38 as a function of ε and L/L_D with L_D being the dispersion length defined by Eq. (22). The error calculation was performed only in the case of a good fringes visibility, i.e., when clear maxima and minima can be distinguished in the spectrum. This criteria must be fulfilled in practice to avoid any ambiguity in the location of the maxima. The measurement error is within a 10% limit depending on the value of ε and the ratio of the fiber length to the dispersion length. Even though the measurement error exhibit a rather complex pattern, it decreases as ε or the ratio L/L_D increases. To improve the accuracy, it is therefore preferable to perform the measurements with shorter pulses and/or longer fibers.
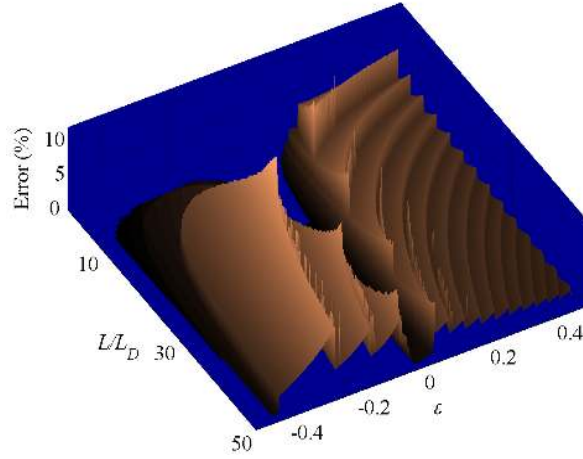
Figure 38. Plot of the measurement error of the spectral modulation technique as a function of ε and L/L_D.

4.4 Novel method to improve the measurement accuracy of the phase-shift technique

Measurement principle of the phase-shift technique

The phase-shift technique is based on the measurement of the phase-shift experienced by the sidebands of a sinusoidally modulated signal at angular frequency ω_m as it passes through the component to be characterized [329]. Assuming that the phase varies linearly in the interval $[-\omega_m, \omega_m]$ around the carrier frequency ω of the optical signal, the intensity of the signal detected by the photodetector can be written as [329]

$$I_D(t) = I_0 \left[1 + m\, cos(\omega_m t + \omega_m \tau_m) \right]. \tag{44}$$

where m is the modulation index and τ_m the measured group delay of the component. The measurement of the phase difference between the reference path and the path containing the component (see Fig. 33b) gives direct access to the group delay of the component

$$\tau_m(\omega) = \frac{\Delta\phi_E(\omega)}{\omega_m}, \tag{45}$$

where $\Delta\phi_E(\omega)$ is the electrical phase difference measured between the two paths at the angular carrier frequency ω. It can be seen from Eq. (45) that the resolution of the group delay measurement is enhanced when employing higher modulation frequencies. The group delay measurements are accurate for components whose group delay varies slowly with wavelength. This is the case, e.g., of optical fibers. However, components such as fiber Bragg gratings or thin-film filters may exhibit fast variations of the group delay with wavelength [343] and are more difficult to characterize using the phase-shift technique. In particular, the assumption of linear phase variation in the $[-\omega_m, \omega_m]$ interval may not be valid and the group delay measurements not accurate [IV]. Attempts have been made to modify the phase-shift technique in order to improve the accuracy of group delay measurement [344].

Instrument function of the phase-shift technique

The assumption of linear phase variation in the $[-\omega_m, \omega_m]$ interval is equivalent to assuming that the group delay of the component is constant over the angular frequency interval $[-\omega_m, \omega_m]$. Therefore, the instrument function of the phase-shift technique is simply a rectangular function whose width is equal to $2\omega_m$ and the measured group delay is the result of the true group delay of the component convoluted by the instrument function [IV]

38

$$\tau_m(\omega) = \tau_c(\omega) * rect\left(\frac{\omega}{2\omega_m}\right), \tag{46}$$

where τ_c and τ_m represent the true and measured group delay of the component at the frequency ω, respectively. The $*$ operator denotes the convolution and *rect* is the rectangular function. From Eq. (46), it can be seen that increasing the modulation frequency results in an increase of the measurement error [IV]. The effects of the instrument function on group delay measurements can be conveniently analyzed in the Fourier domain in which Eq. (46) can be rewritten as

$$\tilde{\tau}_m(u) = \tilde{\tau}_c(u) \cdot sinc(\omega_m u), \tag{47}$$

where $\sim$ denotes the Fourier transform and u is a Fourier variable. The Fourier components of the true group delay are attenuated, sign-reversed or vanished, depending on their location with respect to the modulation frequency $f_m=\omega_m/2\pi$ as is illustrated in Fig. 39 [IV].
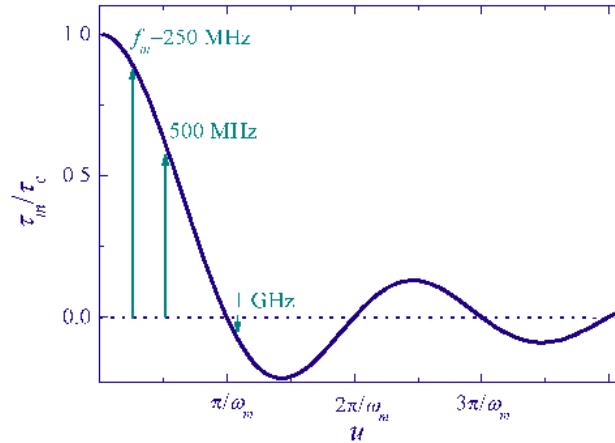
Figure 39. **Effect of the instrument function of the phase-shift technique on the Fourier components of the true group delay of the device under test. The arrows indicates the location of the main Fourier component of the grating as the modulation frequency applied is changed.**

In particular, Fourier components located beyond $2/\omega_m$ will experience an attenuation of more than 50%. Moreover, the amplitude of every Fourier component $\in \left[\frac{(2k-1)\pi}{\omega_m}, \frac{2k\pi}{\omega_m}\right]$ with k being an integer will be reversed. Experimental confirmation of these effects is presented in Fig. 40a. In this figure, the group delay of a 20 cm long dispersion compensating fiber Bragg grating measured as a function of frequency using the phase-shift technique is shown for f_m equal to a) 250 MHz, b) 500 MHz, and c) 1 GHz. The variation of the group delay is periodic with the main period of the ripples approximately equal to 1.9 GHz. The Fourier spectrum of the group delay therefore consists of a peak whose location with respect to ω_m is marked in Fig. 39 as an arrow. For f_m equal to 250 MHz, the amplitude of the measured group delay is slightly attenuated by the instrument function. When the modulation frequency is increased to 500 MHz, the attenuation rises to 40 %. Using f_m=1 GHz results in an attenuation of 95 % and reverses the sign of the group delay amplitude.

a)   b)
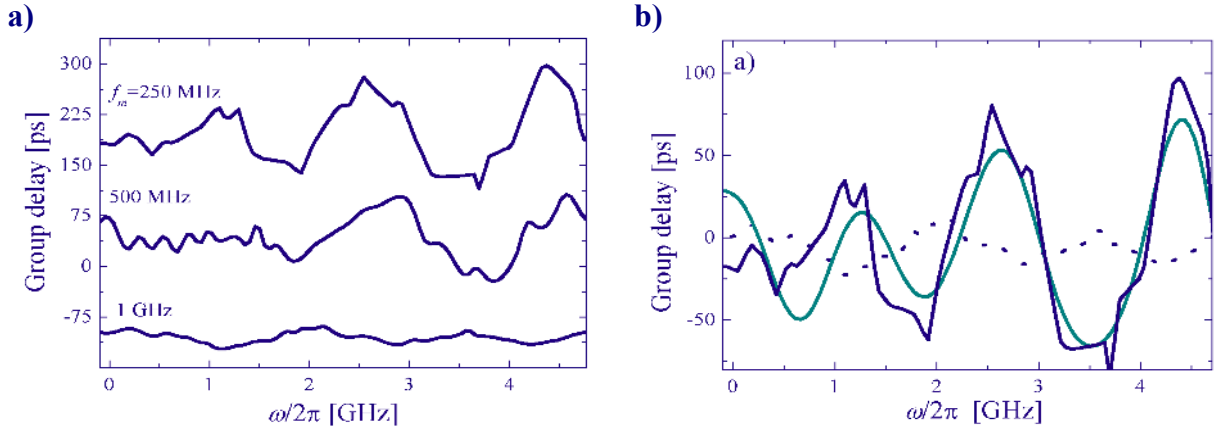
Figure 40.   **a) Effect of the modulation frequency used in the phase-technique on the experimentally measured amplitude of the group delay of a fiber Bragg grating. For clarity an arbitrary offset has been added to each curve.**

b) True (blue solid line), measured (dotted line) and reconstructed (green solid line) group delay for a fiber Bragg grating.

The derivation of the instrument function of the phase-shift technique is not only important for analyzing its effects on the measurement results but also because it allows for improving the accuracy of the measurements by post-processing of the data [IV]. Indeed, from Eqs. (46) and (47), the true group delay of the component can be restored by performing a deconvolution of the measured group delay by the instrument function [IV]

$$\tau_c(\omega) = FT^{-1}\left[\frac{\tilde{\tau}_m(u)}{sinc(\omega_m u)}\right]_\omega , \qquad (48)$$

where FT^{-1} represents the inverse Fourier transform. However, the deconvolution operation has undesirable effects on the data: division by zero for some particular values of u and amplification of the Fourier component with highest frequencies, these latter components arising from the noise of the measurements. To avoid such effects, the zero-points of the *sinc* function must be removed and a low-pass filter can be applied in the Fourier domain before performing the deconvolution operation. Based on the same principle, a variant of this method was recently developed and consists of performing two sets of group delay measurements utilizing different modulation frequency, which allows avoiding the division by zero in the post-processing of the data [345].

An example of post-data processing for improvement of the measurement accuracy are illustrated in Fig. 40b. The group delay of the fiber Bragg grating previously described was measured using $f_m=1$ GHz (dotted line in Fig. 40b). The data were subsequently processed according to the procedure described above. The reconstructed group delay is marked as a green line in Fig. 40b. For comparison, the group delay measured with a modulation frequency of 250 MHz is also plotted as a blue solid line. Due to the low value of f_m in that case, this latter measurement can be considered to very close to the true group delay of the grating. The reconstructed group delay from the 1 GHz f_m-value is in good agreement with the measurements performed employing a 250 MHz modulation frequency.

The technique can be applied to any arbitrary group delay and allows for improving the accuracy of the measurements when high modulation frequency are used for a better timing resolution.

4.5 Linewidth of external cavity lasers

4.5.1 Linewidth of semiconductor lasers

Laser linewidth

The random phase variations of the optical field results in the finite linewidth of lasers [346]. The linewidth is inversely proportional to the coherence time of the laser defined as the time period over which a phase shift occurs on average [184,346-348]. The phase fluctuations are due to two different types of noise: intrinsic and extrinsic. The extrinsic noise results from current fluctuations, temperature variations and vibrations in the laser system. It yields a Gaussian lineshape [349] which, in the case of semiconductor lasers, is small compared to the linewidth resulting from the intrinsic noise [349]. The intrinsic noise arises from the spontaneous emission of photons caused by the random hole-electron recombination in the semiconductor material [350]. Assuming white intrinsic noise and neglecting the amplitude variations, the electric field at the output of the laser can be written as [347,348]

$$E(t) = E_0 e^{j[2\pi v_0 t + \phi(t)]},$$
(49)

where v_0 is the center frequency of the field. The time-varying phase term $\phi(t)$ accounts for the random phase of the spontaneously emitted photons and it has a Gaussian statistical distribution [347]. The lineshape of the laser obtained from the Fourier transform of the autocorrelation of the electric field is therefore Lorenztian with a full-width at half maximum Δv_L given by the well-known Schalow-Townes formula [195,351-354]

$$\Delta v_L = \eta \frac{\pi h v_0}{P_{om}} \Delta v_c^{\ 2},$$
(50)

where η is the spontaneous emission coefficient (of the order of 2.5 for semiconductor materials [355]), P_{om} the power of the oscillating mode, h Planck's constant and Δv_c represents the linewidth of the cavity mode. The latter is defined as [356]

$$\Delta v_c = \frac{c}{2\pi n_d L_d} [\alpha_m - ln(r_1 r_2)],$$
(51)

with n_d and α_m being the refractive index and the modal loss coefficient of the semiconductor material. Here, r_1 and r_2 are the amplitude reflectivities of the mirrors forming the cavity of length L_d.

In semiconductor materials, the variation of the photon number due to spontaneous emission causes intensity fluctuations which in turn induce changes in the carrier density, thus affecting the gain. This process referred to as relaxation oscillation causes variations of the refractive index seen by the optical field, thereby inducing an extra delayed phase change [348,354,357]. This intensity-phase noise coupling results in an enhancement of the linewidth by a factor $(1+\alpha_L^{\ 2})$ where α_L designates the linewidth-enhancement factor defined as [348,354,357]

$$\alpha_L = -\frac{\omega}{c} \cdot \frac{dn/dN_c}{dg/dN_c} = \frac{\Delta Re\ (n)}{\Delta Im\ (n)}\ .$$
(52)

Here, n is the refractive index of the semiconductor material, g is the gain per unit length and N_c is the carrier density. The value of α_L depends on the semiconductor material and several parameters such as the structure and length of the laser cavity [357,358]. Typical α-values for semiconductor materials varies from 2 to 9 [357].

Furthermore, in addition to the power-dependent linewidth, a power-independent linewidth Δv_S resulting from the shot noise sets the ultimate limit for the value of the laser linewidth [359-363]. The shot noise stems from the statistical fluctuations of the carrier population and varies as $1/f$ with f being the frequency in the power spectrum. Furthermore, in the same way as the spontaneous emission affects the carrier population and brodens the linewidth, the statistical fluctuations of the shot noise leads to an extra-brodening of the linewidthof the form $\alpha^2 \kappa \Delta v_L$ with κ being the ratio of the shot noise fluctuations to the carrier population fluctuations. Hence, the total linewidth of a semiconductor diode laser is given by [359,364]

$$\Delta v = (1 + (1 + \kappa)\alpha_L^{\ 2})\Delta v_L + \Delta v_S.$$
(53)

The various noise terms present in the laser system and their respective contribution to the linewidth are displayed in Fig. 42.
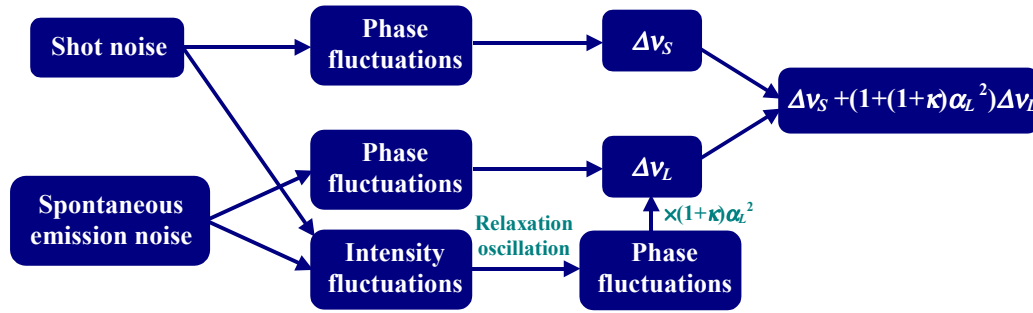
Figure 42. Noise mechanisms and their contribution to the linewidth.

4.5.2 Linewidth measurement techniques

Several techniques have been developed to measure the linewidth of lasers. They include the use of grating spectrometers or spectrum analyzers [365], Fabry-Pérot resonators (FP), coherent detection techniques [331] and self-homodyne/heterodyne interferometers [366-368].

Optical spectrum analyzer or grating spectrometer

The different frequency components of the laser line are diffracted at different angles by a grating. The spectrum of the laser light is then obtained by rotating the grating. The resolution depends mostly on the grating parameters and is usually limited to 1.25 GHz.

Fabry-Pérot interferometer

The transmission peaks of a FP interferometer are used to select the frequency components of the laser line. The linewidth of the laser can be measured by monitoring the intensity at the output of the interferometer as a function of the mirror spacing. The resolution of the technique depends on the finesse of the FP interferometer.

Coherent discrimination

The phase fluctuations of the optical field are converted into intensity fluctuations using a Michelson, MZ or FP type interferometer [331]. A time delay longer than the coherence length of the laser to be characterized is introduced in one arm of the interferometer. The interferometer is biased at the quadrature point by inserting a phase modulator in of its arms so that the frequency fluctuations of the laser are linearly proportional to the variations of the photocurrent detected [331]. Exact knowledge of the time delay and careful preliminary calibration of the linear conversion are required. The linewidth of the laser is then extracted from the RF spectrum of the photocurrent.

Self-heterodyne/homodyne techniques

The measurement principle is the same as for the coherent discrimination technique. However, the linewidth value is directly obtained from the spectrum of the beat signal displayed on an RF spectrum analyzer. In the case of self-heterodyne method, an acousto-optic modulator is placed in one arm of the MZ interferometer [367]. This shifts the beat signal at the frequency of the acousto-optic modulator and prevents the dependence of the power spectrum on the mean phase difference between the two arms of the interferometer. In the delayed self-homodyne technique, the two interfering fields share the same center frequencies, which causes the interference signal to strongly depend on the exact mean phase difference between the two arms of the interferometer [368]. To overcome this problem a modified delayed self-homodyne technique has been developed [369,370]. It includes a phase modulator inserted

in one arm of the interferometer to average out the mean phase dependence. Moreover, a microwave mixer is placed after the photodetector in order to shift the beat signal from 0 Hz to remove the noise contribution caused by the electrical spectrum analyzer itself. The modified delayed self-homodyne technique offers technical advantages since it does not require the use of an acousto-optic frequency shifter and therefore lower amplification of the beat signal is needed [370]. A typical experimental arrangement for a self-heterodyne/homodyne measurement of a laser linewidth is shown in Fig. 43.
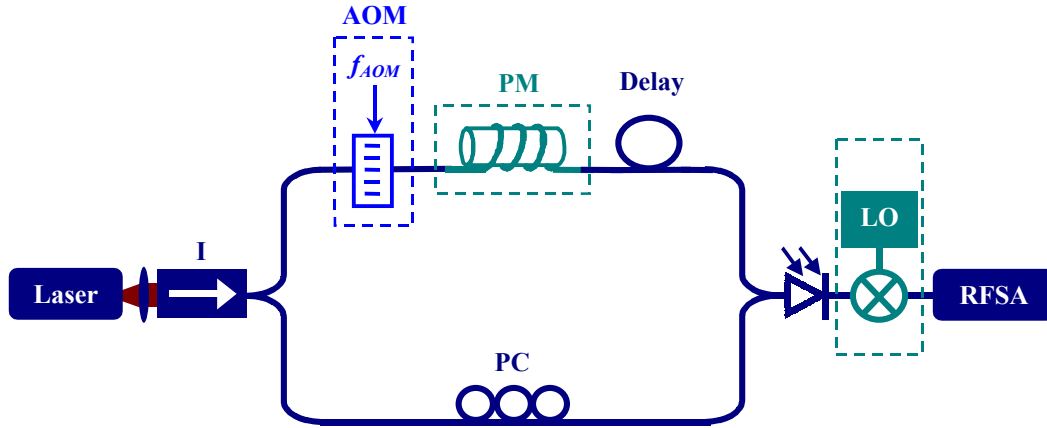
Figure 43. **Schematic layout of a self-homodyne (dark blue), self-heterodyne (light blue), and modified self-homodyne (green) linewidth measurement setup. I: isolator, AOM: acousto-optic modulator, PM: phase modulator, PC: polarization controller, LO: local oscillator, and RFSA: RF spectrum analyzer.**

The RF power spectrum recorded at the output of the MZ interferometer depends on the relative magnitude of the coherence time ($\tau_{coh}=1/\Delta\nu$) of the laser to be characterized and the delay line employed [367,368]. In particular, for a delay line much longer than the coherence time of the laser, the RF power spectrum is similar to the case of the beat signal obtained from two independent identical lasers [368]. Assuming a Lorentzian lineshape, the linewidth of the laser is equal to twice the linewidth of the measured RF power spectrum [368]. In the case of a delay line of the order of τ_{coh}, the two interfering fields are partially correlated which complicates the interpretation of the RF power spectrum thereby yielding the necessity of a fit by a theoretical function [367,368,371]. Nevertheless, it has been shown that the use of a short delay line effectively filters out the $1/f$ noise component of the laser linewidth and gives access to the pure Lorentzian linewidth [349,369,370] resulting from the white noise which is the parameter of interest for coherent communication systems [349,354,372,373].
Table 4 presents the main characteristics of the different linewidth measurement techniques.

Table 4. Characteristics of various linewidth measurement techniques.

Technique	Resolution	Setup	Disadvantages
Grating	1.25 GHZ	complex	
FP	~ MHz	simple	
Coherent discrimination	1 kHz	complex	calibration
Self-heterodyne	1 kHz	simple	frequency jitter, signal amplification
Self-homodyne	1 kHz	simple	frequency jitter

4.5.3 External cavity lasers

Wavelength tuning of diode lasers can be accomplished through the use of external cavity configurations [184,185,374]. The external cavity can be formed for instance between the front facet of the diode laser and an extra reflective elements that provides optical feedback to the diode laser. Due to their specific characteristics (e.g., broad wavelength tunability and narrow linewidth) external cavity

lasers (ECLs) find numerous applications in high-precision spectroscopy, optical metrology or optical telecommunications [184,185]. Various reflective elements have been used for providing the feedback. These include mirrors [186,187,375-378], gratings [185,193,195,373,379-383], electro-optic birefringent filters [384,385], acousto-optic filters [386,387] or liquid crystal arrays [388] as the wavelength selective element. The characteristics of several ECLs with different configurations and tuning elements are summarized in Table 5.

Table 5. Examples of ECLs. *LCA*: liquid crystal array, *EO*: electro-optic, *AO*: acousto-optic.

Tuning element	*Tunability*	*λ-center*	*Δν*	*P_out*	*Ref.*
Mirror	10 nm	1370 nm			[378]
Grating	244 nm	1570 nm		5 mW	[379]
LCA	11 nm	670 nm	<30 MHz		[388]
EO filter	7 nm	1552 nm	60 kHz	0.4 mW	[385]
AO filter	83 nm	1300 nm	<10 MHz	<1mW	[387]

Principle of operation and modeling of ECLs

Optical feedback strongly affects the dynamic and spectral properties of semiconductor diode lasers [185,187,195,354,389-392]. In particular, the injection of optical feedback allows control the tuning properties of the laser and a reducion of its linewidth [195,354,390,391,393-396]. The operation principle of an external cavity laser can be conveniently analyzed by replacing the amplitude reflectivity r_2 of the front facet of the diode laser with a frequency-dependent effective reflectivity defined as [397-399]

$$r_{eff}(\omega) = \frac{r_2 + r_3(\omega)\ e^{j\omega\tau_e}}{1 + r_2 r_3(\omega)\ e^{j\omega\tau_e}},$$ (54)

where $\tau_e = c/(2L_e)$ is the round-trip time of photons inside the external cavity. Here, r_3 represents the amplitude reflectivity of the feedback element. The effective reflictivity model enables analyze the operation characteristics of the laser in a similar way as a Fabry-Pérot laser. In particular, the steady state oscillation condition as well as the dynamical properties can be conveniently investigated using the well established rate equations. Note that the effective reflectivity model is accurate since it includes exaclty all the multiple reflections in the external cavity and should, consequently, be valid independently of the feedback level. In general, a numerical treatment of the rate equations modified to account for the effect of optical feedback is necessary to correctly model the transient behavior of the laser and especially the presence of multiple satellite peaks in the optical spectrum of the laser steming from the relaxation oscillation. In the following, the analysis is restricted to the stady state operation of the external cavity laser and its corresponding linewidth.

The steady state oscillation condition imposes the electric field to retain its amplitude and phase after one cavity round-trip [184,346,395,400]

$$r_1 r_{eff}(\omega)\ e^{2j\beta L_d} = 1,$$ (55)

where r_1 is the amplitude reflectivity of the rear facet of the diode laser, L_d the length of the solitary diode laser cavity and β the propagation constant of the electric field. The propagation constant is a complex number that includes both the phase and amplitude changes inside the cavity [184]

$$\beta(\omega) = n_d \frac{\omega}{c} - j[\Gamma g(\omega) - \alpha_m],$$ (56)

with $g(\omega)$ and α_m being the frequency-dependent semiconductor gain and modal losses. Here, Γ designates the confinement factor which represents the fraction of the power effectively traveling inside the active region of the semiconductor material [184,346]. The oscillation frequency of the ECL is then obtained by combining Eqs. (55) and (56). Taking into account the dependence of the refractive index on the frequency (see Eq. 52), the oscillation frequency of the ECL is determined by [191,395,400]

$$\omega = \omega_{qo} - \frac{1}{\tau_d}\left[arg(r_{eff}(\omega)) + \alpha_L\, ln\left(\frac{|r_{eff}(\omega)|}{r_2}\right)\right],\qquad (57)$$

where $\tau_d = c/(2n_dL_d)$ is the round-trip time of photons inside the solitary diode laser cavity and $\omega_{qo}=2\pi q/\tau_d$ is the oscillation frequency of the diode laser in the absence of optical feedback, i.e., when r_3=0. Here, q is an integer number that represents the longitudinal oscillating mode. It is determined by the relative detuning between the modes of the solitary diode laser cavity and the peak of the gain medium. It can be seen from Eq. (57) that the addition of an external cavity to the solitary diode laser results in the shift of its oscillation frequency. The frequency dependence of the effective reflectivity produces a modulation of the cavity losses. Any change in the strength or phase of the optical feedback will affect the relative detuning between the compound cavity losses and semiconductor gain curves thereby allowing for tuning the oscillation frequency of the ECL to a different external cavity mode [V]. In general, the oscillating external cavity mode is determined by the condition of minimum threshold gain [390,393,395,401].

The phase of the optical feedback can be varied by changing the length of the external cavity [390,402] whereas the strength of the optical feedback can be varied by the use of a dispersive reflective element such as a grating [191,395]. The use of a grating as a reflective element is advantageous since it provides additional wavelength selectivity through its dispersion profile. In particular, a rotation of the grating permits the tuning of the reflected frequency and, consequently, of the lasing frequency of the ECL [191,195,400,403]. The operation principles of an *AlGaAs* solitary diode laser and an *AlGaAs* grating cavity laser are illustrated in Fig. 44.
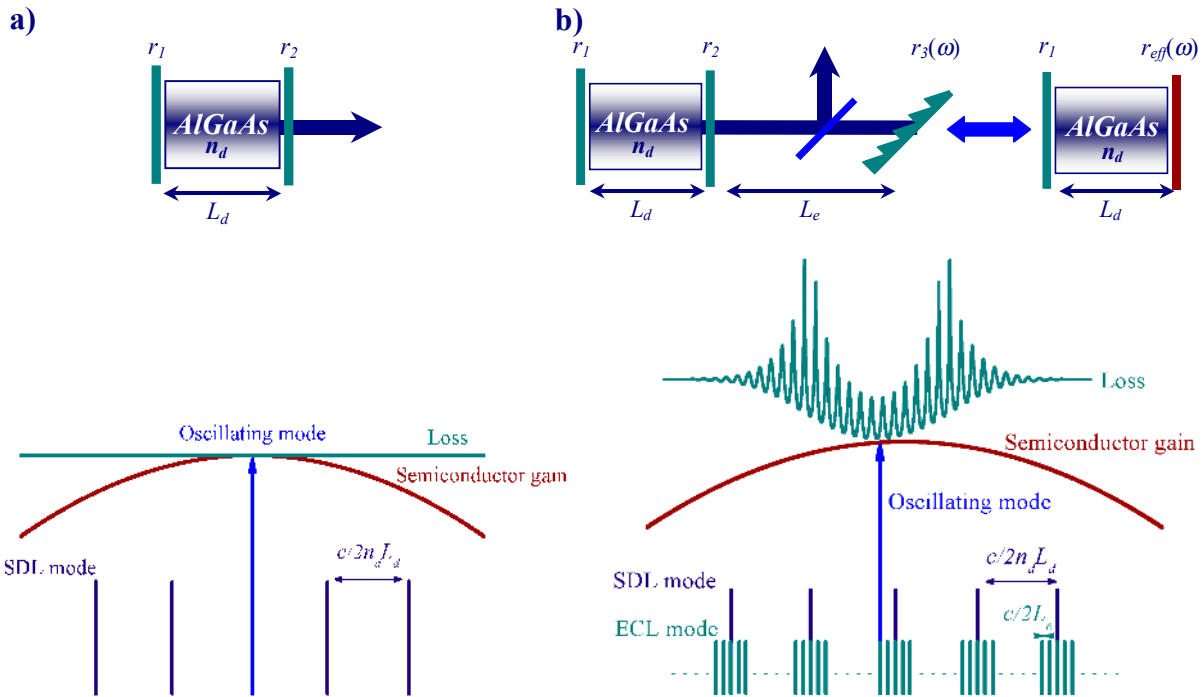
Figure 44. a) Operation principle of a solitary diode laser. SDL: solitary diode laser.   **b) Operation principle of a grating cavity laser.**

As the grating orientation is changed, the oscillation frequency hops between the different external cavity modes leading to discrete tuning [V]. The frequency range over which the ECL can be tuned discretely before returning to its original oscillation frequency depends on the ratio of the internal to external cavity lengths [346]. Figure 45 shows the simulated oscillation frequency of an *AlGaAs* grating cavity laser as a function of the rotation angle of the grating θ. The grating is assumed to have a Gaussian frequency-dependent reflectivity profile [400]. The parameters of the ECL and the

characteristics of the grating are summarized in Table 6 [V, VI]. The step-like fine structure is due to the mode-hopping between the different external cavity modes.
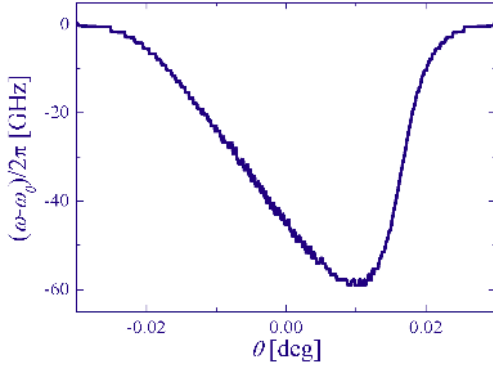
Figure 45. **Illustration of the frequency tuning of a _AlGaAs_ grating cavity laser by rotation of the grating.**

Table 6. **Parameters corresponding to the ECL of Fig. 45. Δf_G represents the spectral width of the dispersion of the grating reflectivity (FWHM).** _SDL_: solitary diode laser.

SDL	Grating cavity
r_1=0.97	r_3=0.5
r_2=0.22	Δf_G=100 GHz
L_d=400 μm	L_e=12 cm
n_d=3.65	
α_m=20 cm^{-1}	

Continuous tuning can be achieved through simultaneous translation and rotation of the grating so that the reflected frequency from the grating and the location of the external cavity modes shift simultaneously [404-406]. The tunability of ECLs is ultimately limited by the width of the gain of the semiconductor material which typically exceeds several tens of nanometers.

4.5.4 Fine structure linewidth variations of external cavity lasers

Linewidth of ECLs

The dynamic behavior of ECLs strongly depends on the strength and phase of the optical feedback. Five distinct regimes of operation with different properties have been identified and are commonly referred to as regimes _I-V_ [389,394,407,408]. In particular, the linewidth of ECLs follows a different behavior depending on which regime the ECL operates. In the following, the discussion is restricted to the case where the ECL operates in regime _V_ for which stable single-mode operation and broad tuning range can be achieved. This type of regime corresponds in practice to a fraction of optical feedback greater than 10%.

The spontaneous emission rate η of a semiconductor laser corresponds to the number of photons spontaneously emitted into an oscillating mode per unit time [346]. In the presence of optical feedback, the mode spacing of the compound cavity laser and, therefore η, is inversely proportional to the external cavity length L_e. Besides, the photon lifetime increases with the length of the external cavity. This results in an increase of the photon number at a given output power. As a direct consequence of Eq. (50), these two facts yield a reduction of the linewidth proportional to $1/L_e^2$. An exact mathematical description of the linewidth reduction phenomenon in ECLs can be obtained from the definition of the chirp reduction factor F which links the change in the oscillation frequency $d\omega_0$ of the solitary diode laser per unit change in the ECL oscillating frequency $d\omega$ [391,395,400,409]

$$F = \frac{d\omega_0}{d\omega}. \tag{58}$$

The phase noise of the solitary diode laser is then reduced by the same quantity [354,390,400,409], which leads to the following relationship between the linewidth of the diode laser with and without optical feedback [354,400,409-411]

$$\Delta\nu_{ECL} = \frac{\Delta\nu_{SDL}}{F^2} , \tag{59}$$

where $\Delta\nu_{ECL}$ and $\Delta\nu_{SDL}$ represent the linewidth of the solitary diode laser and ECL, respectively. From Eq. (57) it can be seen that the linewidth reduction depends on the strength and phase of the optical feedback as well as on the α-factor of the semiconductor material. A typical order of magnitude for the

46

linewidth of a diode laser with 1 mW output power is 100 MHz. The addition of an external cavity allows for a reducion of the linewidth to the kHz level.

Linewidth variations in a grating cavity laser

Due to the dependence of the chirp reduction factor on the oscillation frequency of the grating cavity laser, the linewidth is affected when tuning the orientation of the grating. In particular, as the grating position is changed, the oscillation frequency of the laser is tuned through several external cavity modes [412,413]. Consequently, the linewidth variations follow pseudo-periodic variations whose period is determined by the external cavity modes spacing [V]. The amplitude variations of the linewidth within one external cavity mode depend on the strength of the feedback at that particular oscillation frequency [V]. Experimental measurements of linewidth variations within one external cavity mode of an *AlGaAs* grating cavity laser using the modified self-homodyne technique are presented in Fig. 46a. These variations have been observed by slightly changing the grating orientation [VI]. The characteristics of the ECL correspond to the ones used for the simulation of Fig. 45 and are shown in Table 6. The measurements were performed using an experimental setup similar to the one depicted in Fig. 43 and with a delay shorter than the coherence time of the ECL to access the pure Lorentzian component of the laser linewidth. A typical experimental RF spectrum recorded at the output of the MZ interferometer is shown in Fig. 46b. The spectrum consists of a dc peak sitting on the top of a Lorentzian envelope with delayed-dependent oscillations on the wings [369]

$$S(f) \propto \frac{1}{2\pi}\left[(1+\beta^2)^2 + 2\beta^2 e^{-2\pi\tau_{delay}\Delta v_{ECL}}\right]\delta(f) +$$

$$\frac{\beta_r^2}{\pi^2} B \frac{\Delta v_{ECL}}{f^2 + \Delta v_{ECL}^2}\left[1 - e^{-2\pi\tau_{delay}\Delta v_{ECL}} \times \left\{ cos(2\pi f\tau_{delay}) + 2\pi\Delta v_{ECL}\tau_{delay} sinc(2\pi f\tau_{delay})\right\}\right] \tag{60}$$

where f is frequency, β_r the amplitude ratio between the interfering fields, and Δv_{ECL} the Lorentzian linewidth of the ECL (FWHM). The scaling factor B in the AC-part of the spectrum accounts for the limited bandwidth of the measurement system. Here, τ_{delay} is the delay introduced by the fiber placed in the delay arm of the MZ interferometer.
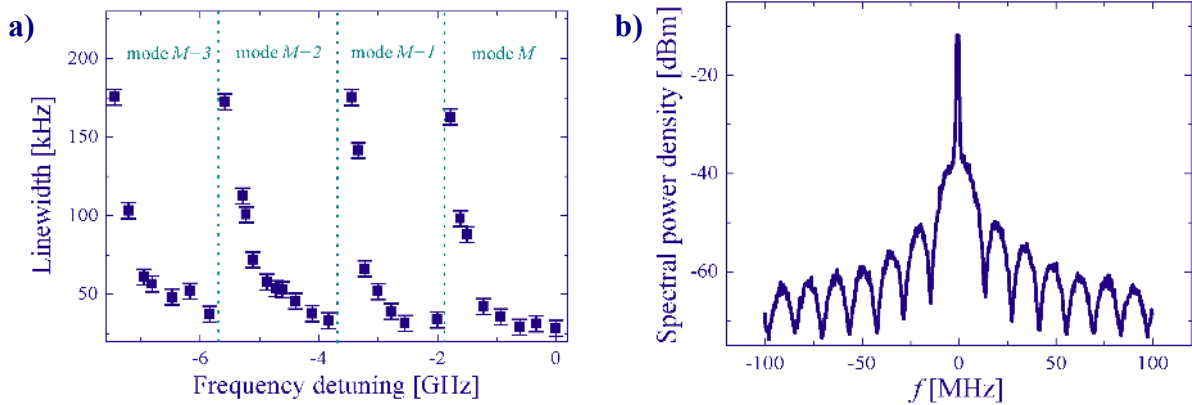
Figure 46. a) Linewidth variations within external cavity modes measured as a function of lasing frequency detuning by rotating the grating.

b) Typical RF power spectrum recorded employing the modified self-homodyne delayed technique.

The linewidth value is extracted from the RF spectrum using a least-square fitting procedure with the linewidth as the fitting parameter [370]. Mode hopping between several external modes is clearly seen. The linewidth variations within one external mode can be as high as 100 kHz [VI], which can be detrimental for applications requiring a fixed narrow linewidth.

4.6 Thermal poling of planar waveguides

Silica is by essence an amorphous material and possesses a centrosymmetric structure which implies that its second-order susceptibility $\chi^{(2)}$ is extremely low [196,414]. The second-order susceptibility is responsible for phenomena such as second harmonic generation (SHG), sum/difference frequency generation, electro-optic effect or optical rectification [299]. These effects find applications in optical telecommunications (e.g., for the fabrication of wavelength converters or modulators) and in optical memory systems (e.g., CDs, DVDs, holographic storage). The prospect of using silica as a nonlinear material for active functionalities has been the subject of extensive research for obvious reasons such as cost, transparency, and monolithic integration with other silica-based components. Poling has proven to be a promising way to induce a $\chi^{(2)}$-type nonlinearity in silica materials and has recently received considerable attention [197,415-418]. The poling technique consists in heating or illuminating with a *UV* radiation a material while applying to it a strong electric field [419]. These two types of poling are commonly referred to as thermal and *UV* poling, respectively [197,419-421]. Optical poling by launching simultaneously a fundamental light wave and its second-harmonic into the material has also been demonstrated [422]. Even though the magnitude of the poling-induced $\chi^{(2)}_{eff}$ are barely high enough for the generation of new optical components, it is important to develop characterization techniques for gaining physical insight into the poling process which is, to date, not fully understood.

4.6.1 Types of poling

In the following, the different poling techniques for silica glasses are briefly reviewed.

Optical poling

The co-propagation of fundamental and second harmonic waves allows for recording a periodic dc electric field inside an optical fiber [284,422-425]. The periodicity of the dc field fulfills the requirement for SHG enhancement through quasi-phase matching when the fiber is subsequently pumped by an intense pump radiation. The recording of the dc field can be considerably accelerated if the fiber is pre-exposed to blue, green or *UV* light [426-428]. More than 10% conversion efficiency from the pump to the second harmonic have been reported, mainly due to the rather long interaction length between the fundamental and second-harmonic along the fiber.

UV poling

The sample is simultaneously subjected to an intense electric field and illuminated with a *UV* radiation [419,429]. Typical *UV* light sources used for poling experiments include *ArF* [430,431] and *KrF* [432,433] excimer lasers. This type of poling can be performed both in fibers and bulk silica media. This technique presents the advantage of an improved spatial resolution, which could be proven to be useful for creating periodically poled structures.

Thermal poling

The silica device is heated up to several hundred degrees with simultaneous application of an electric field [75,197,418,420,434-444]. This type of poling can be performed with bulk silica [418,420,440,445], waveguides [444] or fibers [75,416,421,443,446,447]. The glass is subsequently cooled down to room temperature while maintaining the applied voltage. The value of the induced $\chi^{(2)}_{eff}$ strongly depends on the heating temperature and on the poling time [415,448,449]. Second-order nonlinearity induced by thermal poling seems to be the most reproducible and stable. Nevertheless, thermal poling has the disadvantage of poor spatial resolution when realized in air. Poling in vacuum permits improving the resolution and enables the fabrication of periodically poled structures [450,451]. Furthermore, it has been shown that the magnitude and physical origin of the induced second-order susceptibility vary whether the voltage is positive or negative [452]. In particular, using positive voltage allows for an increase of the magnitude of $\chi^{(2)}_{eff}$ possibly due to the injection of cations from the electrodes to the poled device. The presence of these cations results in higher losses and a wavelength

dependence of $\chi^{(2)}_{eff}$ [452]. Employing negative voltage permits reducing considerably the risk of electrical breakdown [452]. Figure 47 illustrates the different poling techniques and Table 7 summarizes some of the important results achieved in poling experiments [197,421,422].

Figure 47. Different poling methods a) optical, b) UV-assisted and c) thermal. HV: high voltage.
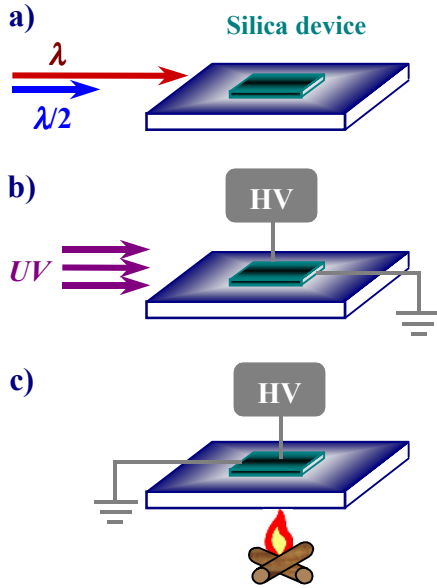
Table 7. Examples of poling experiments. *SHG$_{eff}$*: second harmonic generation efficiency.

Poling technique	Device	Parameter	SHG$_{eff}$ or $\chi^{(2)}_{eff}$
Optical	fiber	λ=1064 nm P_{av}~300 mW	~5%
UV-assisted	fiber	λ_{UV}=193 nm HV=800 V	11.6 pm/V
Thermal	fused silica	T~ 300 °C HV=3-5 kV	1 pm/V

4.6.2 Physical aspects of thermal poling

The polarization of a dielectric medium subjected to an intense external electric field can be expressed as [326]

$$P = \varepsilon_0 \chi^{(1)} E + \varepsilon_0 \chi^{(2)} E \cdot E + \varepsilon_0 \chi^{(3)} E \cdot E \cdot E + ... \tag{61}$$

The corresponding change in the material refractive index is given by [326]

$$\Delta n = \frac{1}{2} r n^3 E_{app} + \frac{1}{2} s n^3 E_{app}{}^2 , \tag{62}$$

where E_{app} is the applied external field, n denotes the refractive index of the material and r and s designate the linear electro-optic (LEO) and quadratic electro-optic (QEO) coefficients, respectively. The LEO and QEO are related to the second-order and third-order susceptibilities by [326]

$$r = 2 \frac{\chi^{(2)}}{n^4} , \tag{63}$$

and

$$s = 3 \frac{\chi^{(3)}}{n^4} . \tag{64}$$

In centrosymmetric materials $\chi^{(2)}$ and therefore r are null. When such a material is poled, an intense internal electric field E_{dc} is recorded inside the material and Eq. (62) can be rewritten as

$$\Delta n = \frac{1}{2} s n^3 (E_{dc} + E_{app})^2 . \tag{65}$$

Therefore, E_{dc} induces an effective LEO coefficient through the third-order susceptibility of the material

$$r_{eff} = 2 \frac{\chi_{eff}{}^{(2)}}{n^4} = 2 \frac{3 \chi^{(3)} E_{dc}}{n^4} . \tag{66}$$

The physical mechanism leading to the generation of an internal electric field inside the poled material has not been clarified yet. Attempts have been made to understand the physical phenomena

49

[419,442,447,453-456]. In particular, two models have been proposed to describe the poling effects but neither of them can fully explain the experimental observations. Both models are illustrated in Fig 48.
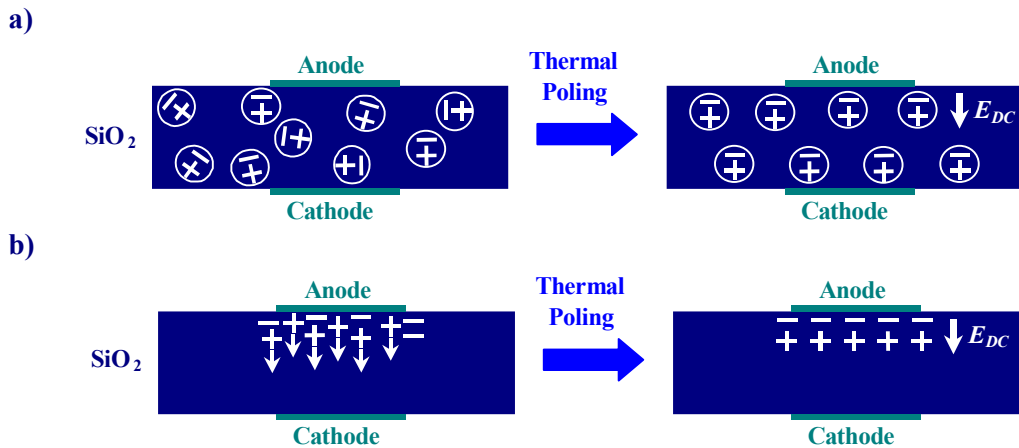
Figure 48. Physical interpretation of thermal poling a) oriented dipole model and b) space-charge separation model.

Oriented dipole model

As the material is subjected to heat, the molecular dipoles align themselves with the applied electric field. When the material is cooled down with the external electric field still applied, the orientation of the dipoles freezes, which results in reordering of the material. Thus the symmetry of the glass is broken and an effective $\chi^{(2)}$ is created. According to this model the third-order susceptibility $\chi^{(3)}$ of the poled glass should also be affected [419,453,455].

Space-charge separation model

The mobile ions, e.g. Na^+ from the glass itself or Ag^+ from the electrode, migrate towards the cathode as the material is subjected to heat and high voltage. As a consequence, the region of the material under the anode is depleted of these mobile ions and it becomes negatively charged while the cathode is positively charged. The location of the ions is maintained while cooling, yielding a built-in internal electric field. This internal electric field is then responsible for an effective $\chi^{(2)}$ through interaction with the third-order susceptibility of the material [419,453].

4.6.3 Measurement techniques of the poling-induced $\chi^{(2)}{}_{eff}$

Characterization of the poled region of the sample can provide useful information for a better understanding of the physics of poling. It can be accomplished using second harmonic imaging, etching or ion mass spectroscopy. The measurements of the induced $\chi^{(2)}{}_{eff}$ can be performed using several techniques such as interferometry, second harmonic generation, ion mass spectroscopy [457], current measurements [458] or inscription of a Bragg grating prior to poling.

Interferometric method

The poled device is placed in one arm of a MZ interferometer and its refractive index is modulated by applying a sinusoidal voltage [455]. The phase difference between the two arms of the interferometer is directly proportional to the LEO which can be subsequently extracted from the intensity variations at the output of the interferometer.

Second harmonic generation

The effective second-order susceptibility of poled glass allows for second harmonic generation. This phenomenon can be exploited for measuring the $\chi^{(2)}_{eff}$ value since the power of the second harmonic wave is directly proportional to $\chi^{(2)}_{eff}$.

Inscription of a Bragg grating

The wavelength of the peak reflection of a Bragg grating is proportional to the refractive index of the grating. This effect can be efficiently used for the determination of $\chi^{(2)}_{eff}$ induced by poling a glass sample [VII]. When an external electric field is applied to the poled sample, the refractive index changes, which in turn affects the wavelength of the peak reflection of the Bragg grating

$$\Delta\lambda = \lambda_0 \Delta n, \tag{67}$$

with λ_0 being the wavelength in vacuum of the grating reflection peak and $\Delta\lambda$ and Δn the change in the wavelength of the reflection peak and refractive index, respectively. Assuming that the space-charge separation model is valid and inserting Eq. (65) into Eq. (67) yields a relationship of parabolic-type between the change of the wavelength of the peak reflection of the grating and the applied external electric field E_{app} after the glass has been poled

$$\Delta\lambda(E_{app}) = \frac{\lambda_0}{2n} \chi^{(2)}_{eff} E_{dc} + \frac{\lambda_0}{n} \chi^{(2)}_{eff} E_{app} + \frac{\lambda_0}{2n} \chi^{(2)}_{eff} \frac{E_{app}^2}{E_{dc}} \ . \tag{68}$$

Consequently, writing a Bragg grating into a silica-based device such as a waveguide prior to poling enables to measure the effective second-order susceptibility induced by the poling. The Bragg grating can be written onto the waveguide by illumination with *UV* light through a phase-mask. After poling, the change in the wavelength of the peak reflection of the grating is recorded with an optical spectrum analyzer as it is subjected to a strong external electric field. A least square method fitting procedure employing a second-order polynomial is subsequently utilized to extract $\chi^{(2)}_{eff}$. Note that the last term of Eq. (68) solely depends on the third-order susceptibility since $\chi^{(2)}_{eff}/E_{dc} = 3\chi^{(3)}$. This allows for monitoring any change in the third-order susceptibility that would stem from the poling experiment. A typical experimental setup for $\chi^{(2)}_{eff}$ measurements using this technique is depicted in Fig. 49.
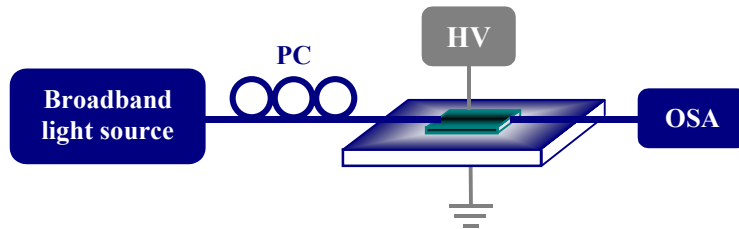
Figure 49. Experimental setup for measurement of $\chi^{(2)}_{eff}$ using the Bragg grating inscription technique. PC: polarization controller, HV: high voltage and OSA: optical spectrum analyzer.

4.6.4 Experimental measurement of the negative poling-induced $\chi^{(2)}_{eff}$ in germanium-doped silica waveguides

The novel technique of Bragg grating inscription for measurement of the LEO induced by thermal poling of planar slab waveguides was successfully demonstrated [VII]. The method also permits the measurement of the internal electric field E_{dc} and the third-order susceptibility $\chi^{(3)}$ [VII].

Fabrication of the waveguides and inscription of the grating

The slab waveguides were fabricated by growing three layers of glass on top of a silicon wafer. The two cladding layers (top and bottom) consist of pure silica. The bottom layer was produced by thermal oxidation while the core and top layers were made by plasma-enhanced chemical vapor deposition. The

core of the waveguides was doped with germanium and nitrogen. The samples were subsequently annealed during two hours at 800 °C and loaded with deuterium for increasing the photosensitivity of the core. A patterned aluminum mask was then deposited on top of the samples which were exposed to *UV* light from a *KrF* laser for modifying the refractive index profile of the core layer and thus producing waveguides. Figure 50 summarizes the different steps of the fabrication process of the slab waveguides.
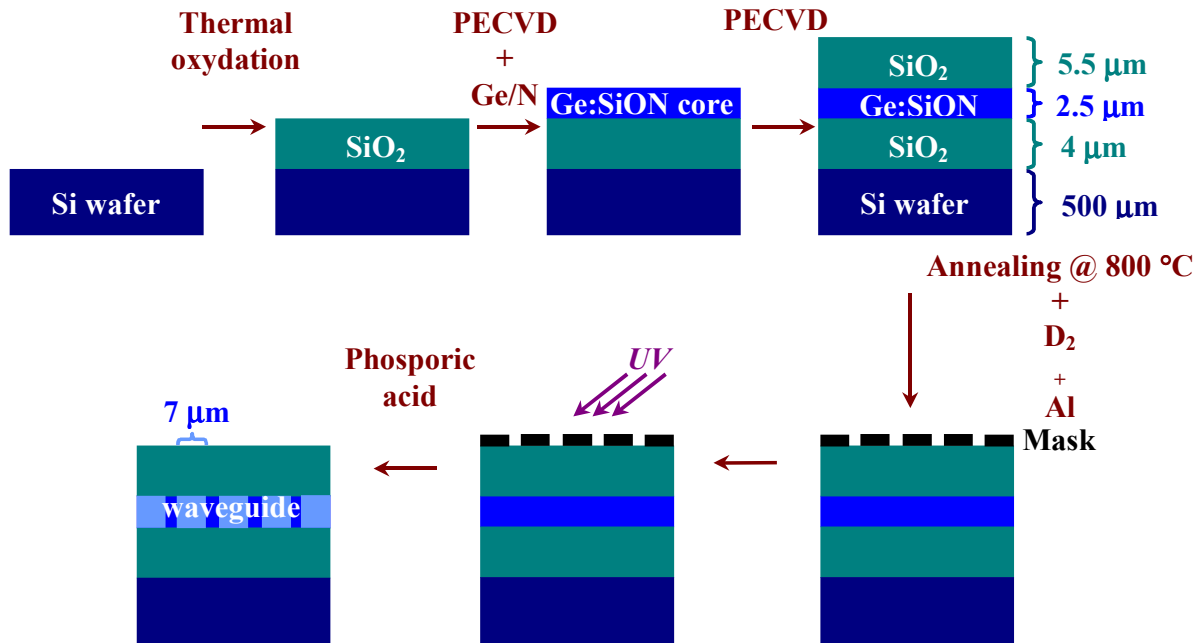
Figure 50. **Fabrication of the slab waveguides. The refractive indices of the core and cladding layers are equal to 1.493 and 1.458, respectively.**

Subsequently, Bragg gratings were written in the waveguides using a phase-mask and exposure to the *UV* light of the *KrF* laser. Finally, the samples were annealed two times at 375 °C for 1.5 h.

Poling and characterization of the linear electro-optic coefficient

Thermal poling of the waveguides was performed by heating the samples to 375 °C and simultaneously applying a 2 kV negative voltage. In order to apply the high voltage, a thin silver electrode was attached to the top of the waveguides using a conductive silver paint while the Si wafer was grounded. The poling time was set to about 30 minutes.

The change in the wavelength of the maximum reflection peak of the grating was monitored as a function of an external voltage applied to the sample before and after poling. Following the procedure described above, the poling-induced LEO could be measured for both transverse electric (TE) and transverse magnetic polarizations. A typical experimental spectrum recorded with the OSA and the variations of the grating peak reflection wavelength are displayed in Figure 51. A value of $\chi^{(2)}_{eff}$=0.06 pm/V was measured for the TE polarization which corresponds to an effective value of ~0.02 pm/V for the LEO. The magnitude of the LEO is almost high enough for practical applications such as EO-modulation [436]. Furthermore, the third-order nonlinearity was found to be unaffected by the poling process, which could partly confirm the validity of the space-charge separation model.

a)

b)
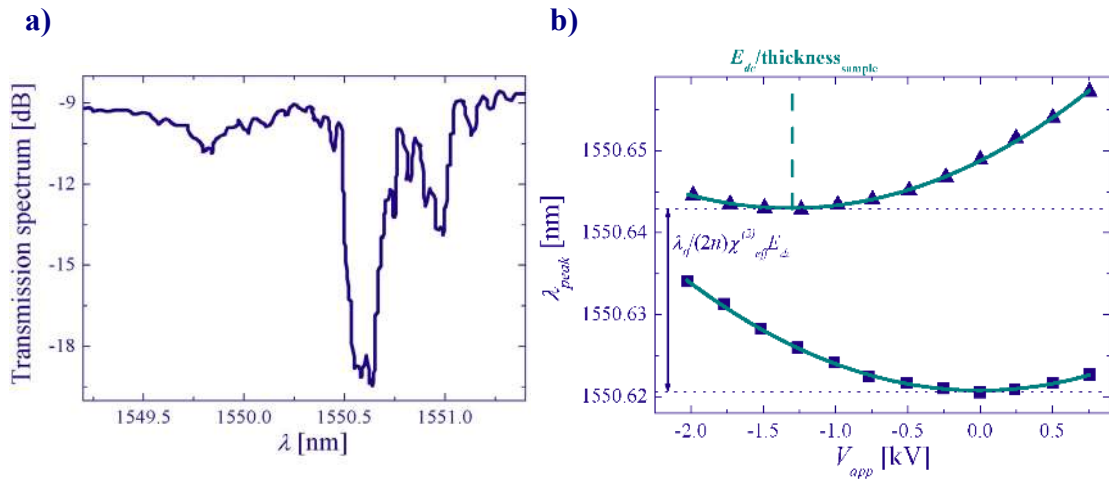
Figure 51. **a) Transmission spectrum of the waveguides after inscription of the Bragg grating.**

b) Wavelength of the reflection peak of the grating as a function of applied voltage before (squares) and after (triangles) thermal poling. The solid lines represent a quadratic fit.

5. Summary

The recent development of photonic crystal fibers has opened up new prospects in the field of optical science. Microstructured fibers constitute one particular class of photonic crystal fibers that guide light in the same way as conventional optical fibers. This type of fiber offers a great flexibility in the design of the properties of the guided mode. In particular, the unique dispersion characteristics of small core MF in combination with their enhanced nonlinearities have enabled efficient generation of ultra-broad supercontinua spanning from near *UV* to near infrared wavelengths. In this thesis, the physics of supercontinuum generation in MFs has been investigated in details for a wide variety of the pump pulse parameters such as wavelength, power and width. A comprehensive analysis of the relative contributions of the various nonlinear processes was also provided. The mechanisms leading to SC generation in MFs was shown to be different depending on whether the pump wavelength is located in the anomalous or normal dispersion region of the fiber. Several ways for controlling and extending further the bandwidth of SC were also proposed. In particular, it was demonstrated that employing highly birefringent microstructured fibers provides several advantages for supercontinuum generation: less power required, control of the polarization of the SC and wavelength tunability.

As dispersion properties play a crucial role in the applications of MFs, for instance in spectroscopy or telecommunications, a simple technique for measuring the anomalous dispersion of microstructured fibers was demonstrated. The technique is based on the modulation of the spectrum of a short laser pulse resulting from its reshaping into a soliton wave along the fiber. The dispersion of the fiber is directly related to the period of the spectral oscillations, and is, to the first order, independent of the power and temporal width of the input pulse. The measurement accuracy was estimated to be around 10%.

The phase-shift technique is one of the most commonly used techniques for measuring the group delay of optical components. However, the accuracy of this technique may be limited in the case of components for which the group delay varies strongly with wavelength. A new method based on the standard phase-shift technique that improves the accuracy of group delay measurement was presented. It allows access to the actual value of the group delay of the component by performing a deconvolution of the measured data with the instrument function of the phase-shift technique. Considerable improvement of the accuracy may be achieved, especially, when high modulation frequencies are employed in order to obtain good timing resolution. Furthermore, the method is applicable to the measurement of any arbitrary group delay profile.

The injection of optical feedback from a distant reflective element to solitary diode lasers can greatly enhance their performance. For instance, their wavelength tunability may be substantially increased and their linewidth reduced by more than an order of magnitude through the use of an external cavity configuration. In this work, the effects of optical feedback on the linewidth and tunability of a GaAlAs grating-cavity laser operating at 780 nm were studied. The analysis provided evidence of the linewidth dependence on the relative detuning between the grating dispersion curve and the oscillating external cavity mode. Furthermore, this dependence was experimentally measured employing the modified self-homodyne technique. Linewidth variations by as much as 150 kHz within one external cavity mode were observed when rotating the grating. Such variations can be minimized if the rotation of the grating is coupled to a translation in a very accurate fashion. However, accurate coupling is difficult to achieve in practice and the experiments performed show that a small mismatch may result in a substantial variation of the laser linewidth.

The development of silica-based active components for optical telecommunications is of high interest since it would allow for the reduction of loss and a better transparency of the networks. Poling of glass is one promising way for enhancing the intrinsically very low second-order susceptibility of silica. Inscription of Bragg gratings was demonstrated to be an efficient method for measuring the second-order susceptibility induced by thermal poling of doped-silica planar waveguides. The method is based on the change of refractive index of the material induced by poling. The technique also provides better understanding of the poling mechanisms.

In conclusion, the dissertation presented studies on supercontinuum generation in the newly developed microstructured fibers. These studies lay the basis for generating SC with flexibility in the center wavelength and bandwidth utilizing this type of fiber and future design of microstructured fibers intended for SC generation. Besides, several novel optical measurement techniques were successfully

demonstrated. These include the characteriztion of the dispersion properties of optical components, linewidth of external cavity lasers and poling-induced second-order nonlinearity.

List of acronyms and symbols

AO	Acousto-optic
DSF	Dispersion-shifted fiber
DUT	Device under test
ECL	External cavity laser
EO	Electro-optic
FBG	Fiber Bragg grating
FL	Fiber laser
FP	Fabry-Pérot
FWM	Four-wave mixing
GD	Group delay
HOM	Higher-order mode
HV	High voltage
I	Isolator
LCA	Liquid crystal array
LEO	Linear electro-optic coefficient
LO	Local oscillator
MF	Microstructured fiber
MFD	Mode field diameter
MMF	Multimode fiber
MZ	Mach-Zehnder
NSE	Nonlinear Schrödinger equation
OSA	Optical spectrum analyzer
PAP	Principal axis of polarization
PBF	Photonic bandgap fiber
PC	Polarization controller
PCF	Photonic crystal fiber
QEO	Quadratic electro-optic coefficient
RFSA	RF spectrum analyzer
RW	Resonant wave
SC	Supercontinuum
SDL	Solitary diode laser
SHG	Second harmonic generation
SPM	Self-phase modulation
SRS	Stimulated Raman scattering
SS	Self-steepening
SSFS	Soliton self-frequency shift
TE	Transverse electric
TL	Tunable laser
VA	Variable aperture
XPM	Cross-phase modulation
XPM-IW	Cross-phase modulation induced wave

a	core diameter
c	speed of light in vacuum
d	hole diameter
f_r	fractional contribution of the delayed response
f_{AOM}	frequency of acousto-optic modulator
g	gain of the semiconductor
h	Planck's constant
h_R	delayed response of the fiber
m	modulation index
n	refractive index
n_a	core refractive index
n_{cl}	cladding refractive index
n_d	semiconductor refractive index
n_L	linear part of the refractive index
n_2	nonlinear part of the refractive index

Symbol	Definition
r	linear electro-optic coefficient
r_{eff}	effective reflectivity
r_1	rear facet laser reflectivity
r_2	front facet laser reflectivity
r_3	external element reflectivity
s	quadratic electro-optic coefficient
z	distance

Symbol	Definition
A	slowly-varying envelope of the electric field
A_D	spectral amplitude of the dispersive field
A_S	spectral amplitude of the soliton
A_T	total field amplitude
A_{eff}	effective area
B	scaling factor
B_k	magnitude of the kth resonance
D	dispersion
D_a	approximated dispersion value
E	electric field
E_{app}	applied electric field
E_{dc}	frozen electric field
F	chirp reduction factor
I_D	intensity of the detected signal
L	fiber length
L_d	solitary diode laser cavity length
L_e	external cavity length
L_D	dispersion length
L_{NL}	nonlinear fiber length
N	soliton order
P	polarization
P_{om}	power of the oscillating mode
P_p	peak power
P_{av}	average power
P_k	peak power of the kth soliton
R	nonlinear response of fiber
R_C	response of optical component
T_{FWHM}	temporal full-width at half maximum
T_k	width of the kth soliton
T_0	temporal width
V	normalized frequency parameter
V_{app}	applied voltage

Symbol	Definition
α	fiber loss
α_L	linewidth-enhancement factor
α_m	modal loss coefficient
β_k	k^{th} order dispersion
β_r	amplitude ratio between the interfering fields
β_1	group delay
β_2	second-order dispersion
ε	deviation-value from fundamental soliton
η	spontaneous emission coefficient
λ_p	pump wavelength
λ_{FWM}	wavelength generated through four-wave-mixing
λ_{ZD}	zero-dispersion wavelength
β	propagation constant
γ	nonlinear coefficient
ε_0	vacuum permittivity
λ	wavelength
μ_0	vacuum permeability

v_g	group velocity	
v_ϕ	phase velocity	
v_0	center frequency of the field	
τ_c	group delay of optical component	
τ_{coh}	coherence time of the laser	
τ_{delay}	delay	
τ_m	measured group delay	
τ_1, τ_2	relaxation parameters	
ϕ_C	phase response of optical component	
ϕ_{NL}^{SPM}	SPM-induced phase-shift	
ϕ_{NL}^{XPM}	XPM-induced phase-shift	
ϕ_R	phase of resonant wave	
ϕ_S	phase of soliton	
$\chi^{(j)}$	j^{th} order susceptibility	
$\chi^{(2)}$	2nd order susceptibility	
$\chi^{(2)}_{eff}$	effective second-order susceptibility	
$\chi^{(3)}$	3rd order susceptibility	
ω	angular frequency	
ω_{as}	anti-Stokes frequency	
ω_m	angular modulation frequency	
ω_{off}	offset frequency	
ω_p	pump frequency	
ω_{qo}	oscillation frequency of the qth longitudinal mode without optical feedback	
ω_r	repetition rate	
ω_{st}	Stokes frequency	
ω_S	center angular frequency of the soliton	
ω_R	center angular frequency of the resonant wave	
Δf	frequency difference	
Δf_G	grating full width at half maximum reflectivity	
Δv	linewidth	
Δv_c	linewidth of the cavity mode	
Δv_{ECL}	linewidth of the external cavity laser	
Δv_L	Schalow-Townes linewidth	
Δv_S	linewidth resulting from the shot noise	
Δv_{SDL}	linewidth of the solitary diode laser	
$\Delta \phi_E$	electrical phase difference	
Γ	confinement factor	
Λ	pitch of the lattice	

References

[1]   P. Kaiser, E. A. J. Marcatili, and S. E. Miller, "A new optical fiber", *Bell Syst. Tech. J.* **52**, 265-269 (1973).

[2]   J. C. Knight, T. A. Birks, P. S. Russell, and D. M. Atkin, "All-silica single-mode optical fiber with photonic crystal cladding", *Opt. Lett.* **21**, 1547-1549 (1996).

[3]   J. C. Knight, T. A. Birks, P. S. J. Russell, and D. M. Atkin, "All-silica single-mode optical fiber with photonic crystal cladding: Errata", *Opt. Lett.* **22**, 484-485 (1997).

[4]   P. Rigby, "Optics - A photonic crystal fibre", *Nature* **396**, 415-416 (1998).

[5]   P. S. J. Russell, T. A. Birks, J. C. Knight, R. F. Cregan, B. Mangan, and J. P. De Sandro, "Silica/air photonic crystal fibres", *Jpn. J. Appl. Phys. Part 1 - Regul. Pap. Short Notes Rev. Pap.* **37**, 45-48 (1998).

[6]   M. D. Wheeler, "Photonic crystal portends fiber optics breakthrough", *Photon. Spect.* **32**, 34-34 (1998).

[7]   J. Broeng, D. Mogilevstev, S. E. Barkou, and A. Bjarklev, "Photonic crystal fibers: A new class of optical waveguides", *Opt. Fiber Technol.* **5**, 305-330 (1999).

[8]   P. M. Noaker, "Fiberoptics - Fabrication of long holey fibers gets practical", *Laser Focus World* **35**, 20-+ (1999).

[9]   A. M. Zheltikov, "Holey fibers", *Uspekhi Fiz. Nauk* **170**, 1203-1215 (2000).

[10]   T. A. Birks, J. C. Knight, B. J. Mangan, and P. S. Russell, "Photonic crystal fibres: An endless variety", *IEICE Trans. Electron.* **E84C**, 585-592 (2001).

[11]   T. A. Birks, J. C. Knight, B. J. Mangan, and P. S. J. Russell, "Photonic crystal fibres: An endless variety", *IEICE Trans. Commun.* **E84B**, 1211-1218 (2001).

[12]   J. Hecht, "Holes in photonic crystal fibers open new possibilities", *Laser Focus World* **37**, 207-216 (2001).

[13]   J. C. Knight, T. A. Birks, B. J. Mangan, and P. S. J. Russell, "Microstructured silica as an optical-fiber material", *MRS Bull.* **26**, 614-617 (2001).

[14]   K. W. Koch, "Focus issue: Photonic crystal fiber - Introduction", *Opt. Express* **9**, 675-675 (2001).

[15]   J. C. Knight, and R. S. J. Russell, "Microstructured glass for optical fibers", *Glass Sci. Technol.* **75**, 54-62 (2002).

[16]   P. Russell, "Holey fiber concept spawns optical-fiber renaissance", *Laser Focus World* **38**, 77-82 (2002).

[17]   A. Bjarklev, J. Broeng, and A. S. Bjarklev, "Photonic Crystal Fibres", *Kluwer Academic Publishers Boston* (2003).

[18]   H. Ebendorff-Heidepriem, T. Monro, and D. Richardson, "Fundamentals and applications of silica and non-silica holey fibers", *Glass Sci. Technol.* **76**, 35-40 (2003).

[19]   J. C. Knight, "Photonic crystal fibres", *Nature* **424**, 847-851 (2003).

[20]   T. M. Monro, and D. J. Richardson, "Holey optical fibres: Fundamental properties and device applications", *C. R. Phys.* **4**, 175-186 (2003).

[21]   W. H. Reeves, D. V. Skryabin, F. Biancalana, J. C. Knight, P. S. Russell, F. G. Omenetto, A. Efimov, and A. J. Taylor, "Transformation and control of ultra-short pulses in dispersion-engineered photonic crystal fibres", *Nature* **424**, 511-515 (2003).

[22]   P. J. Bennett, T. M. Monro, and D. J. Richardson, "Toward practical holey fiber technology: fabrication, splicing, modeling, and characterization", *Opt. Lett.* **24**, 1203-1205 (1999).

[23] B. J. Mangan, J. Arriaga, T. A. Birks, J. C. Knight, and P. S. Russell, "Fundamental-mode cutoff in a photonic crystal fiber with a depressed-index core", *Opt. Lett.* **26**, 1469-1471 (2001).

[24] P. Russell, "Photonic crystal fibers", *Science* **299**, 358-362 (2003).

[25] J. Broeng, S. E. Barkou, A. Bjarklev, J. C. Knight, T. A. Birks, and P. S. Russell, "Highly increased photonic band gaps in silica/air structures", *Opt. Commun.* **156**, 240-244 (1998).

[26] J. C. Knight, J. Broeng, T. A. Birks, and P. S. J. Russel, "Photonic band cap guidance in optical fibers", *Science* **282**, 1476-1478 (1998).

[27] S. E. Barkou, J. Broeng, and A. Bjarklev, "Silica-air photonic crystal fiber design that permits waveguiding by a true photonic bandgap effect", *Opt. Lett.* **24**, 46-48 (1999).

[28] J. Broeng, T. Sondergaard, S. E. Barkou, P. M. Barbeito, and A. Bjarklev, "Waveguidance by the photonic bandgap effect in optical fibres", *J. Opt. A-Pure Appl. Opt.* **1**, 477-482 (1999).

[29] J. Broeng, S. E. Barkou, T. Sondergaard, and A. Bjarklev, "Analysis of air-guiding photonic bandgap fibers", *Opt. Lett.* **25**, 96-98 (2000).

[30] J. Hecht, "Interest grows in components based on holey fibers", *Laser Focus World* **39**, 99-+ (2003).

[31] S. Kawanishi, and H. Kubota, "Photonic crystal fibers and their application to optical communications", *Ntt Rev.* **15**, 28-34 (2003).

[32] C. Peucheret, B. Zsigri, P. A. Andersen, K. S. Berg, A. Tersigni, P. Jeppesen, K. P. Hansen, and M. D. Nielsen, "40Gbit/s transmission over photonic crystal fibre using mid-span spectral inversion in highly nonlinear photonic crystal fibre", *Electron. Lett.* **39**, 919-921 (2003).

[33] B. Zsigri, C. Peucheret, M. D. Nielsen, and P. Jeppesen, "Transmission over 5.6 km large effective area and low-loss (1.7 dB/km) photonic crystal fibre", *Electron. Lett.* **39**, 796-798 (2003).

[34] K. Suzuki, H. Kubota, S. Kawanishi, M. Tanaka, and M. Fujita, "High-speed bi-directional polarisation division multiplexed optical transmission in ultra low-loss (1.3 dB/km) polarisation-maintaining photonic crystal fibre", *Electron. Lett.* **37**, 1399-1401 (2001).

[35] N. A. Mortensen, M. Stach, J. Broeng, A. Petersson, H. R. Simonsen, and R. Michalzik, "Multi-mode photonic crystal fibers for VCSEL based data transmission", *Opt. Express* **11**, 1953-1959 (2003).

[36] "Holey fibers lead to 2R-regenerative all-optical switch", *Laser Focus World* **37**, 11-11 (2001).

[37] P. Petropoulos, T. M. Monro, W. Belardi, K. Furusawa, J. H. Lee, and D. J. Richardson, "2R-regenerative all-optical switch based on a highly nonlinear holey fiber", *Opt. Lett.* **26**, 1233-1235 (2001).

[38] J. E. Sharping, M. Fiorentino, P. Kumar, and R. S. Windeler, "All-optical switching base in cross-phase modulation in microstructure fiber (vol 14, pg 77, 2002)", *IEEE Photonics Technol. Lett.* **14**, 420-420 (2002).

[39] J. E. Sharping, M. Fiorentino, P. Kumar, and R. S. Windeler, "All-optical switching based on cross-phase modulation in microstructure fiber", *IEEE Photonics Technol. Lett.* **14**, 77-79 (2002).

[40] J. H. Lee, W. Belardi, K. Furusawa, P. Petropoulos, Z. Yusoff, T. M. Monro, and D. J. Richardson, "Four-wave mixing based 10-Gb/s tunable wavelength conversion using a holey fiber with a high SBS threshold", *IEEE Photonics Technol. Lett.* **15**, 440-442 (2003).

[41] J. H. Lee, Z. Yusoff, W. Belardi, M. Ibsen, T. M. Monro, and D. J. Richardson, "A tunable WDM wavelength converter based on cross-phase modulation effects in normal dispersion holey fiber", *IEEE Photonics Technol. Lett.* **15**, 437-439 (2003).

[42]   J. E. Sharping, M. Fiorentino, A. Coker, P. Kumar, and R. S. Windeler, "Four-wave mixing in microstructure fiber", *Opt. Lett.* **26**, 1048-1050 (2001).

[43]   K. S. Abedin, J. T. Gopinath, E. P. Ippen, C. E. Kerbage, R. S. Windeler, and B. J. Eggleton, "Highly nondegenerate femtosecond four-wave mixing in tapered microstructure fiber", *Appl. Phys. Lett.* **81**, 1384-1386 (2002).

[44]   G. Millot, A. Sauter, J. M. Dudley, L. Provino, and R. S. Windeler, "Polarization mode dispersion and vectorial modulational instability in air-silica microstructure fiber", *Opt. Lett.* **27**, 695-697 (2002).

[45]   M. Fiorentino, J. E. Sharping, P. Kumar, and A. Porzio, "Amplitude squeezing in a Mach-Zehnder fiber interferometer: Numerical analysis of experiments with microstructure fiber", *Opt. Express* **10**, 128-138 (2002).

[46]   M. Fiorentino, J. E. Sharping, P. Kumar, A. Porzio, and R. S. Windeler, "Soliton squeezing in microstructure fiber", *Opt. Lett.* **27**, 649-651 (2002).

[47]   B. J. Eggleton, C. Kerbage, P. S. Westbrook, R. S. Windeler, and A. Hale, "Microstructured optical fiber devices", *Opt. Express* **9**, 698-713 (2001).

[48]   G. Kakarantzas, A. Ortigosa-Blanch, T. A. Birks, P. S. Russell, L. Farr, F. Couny, and B. J. Mangan, "Structural rocking filters in highly birefringent photonic crystal fiber", *Opt. Lett.* **28**, 158-160 (2003).

[49]   C. Kerbage, and B. J. Eggleton, "Numerical analysis and experimental design of tunable birefringence in microstructured optical fiber", *Opt. Express* **10**, 246-255 (2002).

[50]   C. Kerbage, P. Steinvurzel, A. Hale, R. S. Windeler, and B. J. Eggleton, "Microstructured optical fibre with tunable birefringence", *Electron. Lett.* **38**, 310-312 (2002).

[51]   C. Kerbage, P. Steinvurzel, P. Reyes, P. S. Westbrook, R. S. Windeler, A. Hale, and B. J. Eggleton, "Highly tunable birefringent microstructured optical fiber", *Opt. Lett.* **27**, 842-844 (2002).

[52]   A. I. Siahlo, L. K. Oxenlowe, K. S. Berg, A. T. Clausen, P. A. Andersen, C. Peucheret, A. Tersigni, P. Jeppesen, K. P. Hansen, and J. R. Folkenberg, "A high-speed demultiplexer based on a nonlinear optical loop mirror with a photonic crystal fiber", *IEEE Photonics Technol. Lett.* **15**, 1147-1149 (2003).

[53]   N. G. R. Broderick, T. M. Monro, P. J. Bennett, and D. J. Richardson, "Nonlinearity in holey optical fibers: measurement and future opportunities", *Opt. Lett.* **24**, 1395-1397 (1999).

[54]   C. J. S. de Matos, K. P. Hansen, and J. R. Taylor, "Experimental characterisation of Raman gain efficiency of holey fibre", *Electron. Lett.* **39**, 424-425 (2003).

[55]   R. F. Cregan, J. C. Knight, P. S. Russell, and P. J. Roberts, "Distribution of spontaneous emission from an Er3+-doped photonic crystal fiber", *J. Lightwave Technol.* **17**, 2138-2141 (1999).

[56]   T. Sondergaard, "Photonic crystal distributed feedback fiber lasers with Bragg gratings", *J. Lightwave Technol.* **18**, 589-597 (2000).

[57]   W. J. Wadsworth, J. C. Knight, W. H. Reeves, P. S. Russell, and J. Arriaga, "Yb3+-doped photonic crystal fibre laser", *Electron. Lett.* **36**, 1452-1454 (2000).

[58]   K. Furusawa, A. Malinowski, J. H. V. Price, T. M. Monro, J. K. Sahu, J. Nilsson, and D. J. Richardson, "Cladding pumped Ytterbium-doped fiber laser with holey inner and outer cladding", *Opt. Express* **9**, 714-720 (2001).

[59]   K. Furusawa, T. M. Monro, P. Petropoulos, and D. J. Richardson, "Modelocked laser based on ytterbium doped holey fibre", *Electron. Lett.* **37**, 560-561 (2001).

[60]   J. Wallace, "Ultrafast lasers - Holey-fiber pulse source is tunable", *Laser Focus World* **37**, 20-20 (2001).

[61]   H. Lim, F. O. Ilday, and F. W. Wise, "Femtosecond ytterbium fiber laser with photonic crystal fiber for dispersion control", *Opt. Express* **10**, 1497-1502 (2002).

[62]   J. H. V. Price, K. Furusawa, T. M. Monro, L. Lefort, and D. J. Richardson, "Tunable, femtosecond pulse source operating in the range 1.06-1.33 mu m based on an Yb3+-doped holey fiber amplifier", *J. Opt. Soc. Am. B-Opt. Phys.* **19**, 1286-1294 (2002).

[63]   J. E. Sharping, M. Fiorentino, P. Kumar, and R. S. Windeler, "Optical parametric oscillator based on four-wave mixing in microstructure fiber", *Opt. Lett.* **27**, 1675-1677 (2002).

[64]   Z. Yusoff, J. H. Lee, W. Belardi, T. M. Monro, P. C. Teh, and D. J. Richardson, "Raman effects in a highly nonlinear holey fiber: amplification and modulation", *Opt. Lett.* **27**, 424-426 (2002).

[65]   J. Canning, N. Groothoff, E. Buckley, T. Ryan, K. Lyytikainen, and J. Digweed, "All-fibre photonic crystal distributed Bragg reflector (PC-DBR) fibre laser", *Opt. Express* **11**, 1995-2000 (2003).

[66]   A. Cucinotta, F. Poli, S. Selleri, L. Vincetti, and M. Zoboli, "Amplification properties of Er3+-doped photonic crystal fibers", *J. Lightwave Technol.* **21**, 782-788 (2003).

[67]   C. J. S. de Matos, S. V. Popov, and J. R. Taylor, "Short-pulse, all-fiber, Raman laser with dispersion compensation in a holey fiber", *Opt. Lett.* **28**, 1891-1893 (2003).

[68]   K. G. Hougaard, J. Broeng, and A. Bjarklev, "Low pump power photonic crystal fibre amplifiers", *Electron. Lett.* **39**, 599-600 (2003).

[69]   J. Lasri, P. Devgan, R. Y. Tang, J. E. Sharping, and P. Kumar, "A microstructure-fiber-based 10-GHz synchronized tunable optical parametric oscillator in the 1550-nm regime", *IEEE Photonics Technol. Lett.* **15**, 1058-1060 (2003).

[70]   J. Limpert, T. Schreiber, S. Nolte, H. Zellmer, A. Tunnermann, R. Iliew, F. Lederer, J. Broeng, G. Vienne, A. Petersson, and C. Jakobsen, "High-power air-clad large-mode-area photonic crystal fiber laser", *Opt. Express* **11**, 818-823 (2003).

[71]   R. Tang, J. Lasri, P. Devgan, J. E. Sharping, and P. Kumar, "Microstructure-fibre-based optical parametric amplifier with gain slope of similar to 200 dB/W/km in the telecom range", *Electron. Lett.* **39**, 195-196 (2003).

[72]   W. J. Wadsworth, R. M. Percival, G. Bouwmans, J. C. Knight, and P. S. J. Russel, "High power air-clad photonic crystal fibre laser", *Opt. Express* **11**, 48-53 (2003).

[73]   D. G. Ouzounov, K. D. Moll, M. A. Foster, W. R. Zipfel, W. W. Webb, and A. L. Gaeta, "Delivery of nanojoule femtosecond pulses through large-core microstructured fibers", *Opt. Lett.* **27**, 1513-1515 (2002).

[74]   W. R. Zipfel, D. G. Ouzounov, A. L. Gaeta, and W. W. Webb, "The use of air-silica microstructured optical fibers for delivery of femtosecond pulses in the near IR", *Biophys. J.* **82**, 496A-496A (2002).

[75]   D. Faccio, A. Busacca, W. Belardi, V. Pruneri, P. G. Kazansky, T. M. Monro, D. J. Richardson, B. Grappe, M. Cooper, and C. N. Pannell, "Demonstration of thermal poling in holey fibres", *Electron. Lett.* **37**, 107-108 (2001).

[76]   D. G. Ouzounov, F. R. Ahmad, D. Muller, N. Venkataraman, M. T. Gallagher, M. G. Thomas, J. Silcox, K. W. Koch, and A. L. Gaeta, "Generation of megawatt optical solitons in hollow-core photonic band-gap fibers", *Science* **301**, 1702-1704 (2003).

[77]   F. Benabid, J. C. Knight, G. Antonopoulos, and P. S. J. Russell, "Stimulated Raman scattering in hydrogen-filled hollow-core photonic crystal fiber", *Science* **298**, 399-402 (2002).

[78]   Y. L. Hoo, W. Jin, H. L. Ho, D. N. Wang, and R. S. Windeler, "Evanescent-wave gas sensing using microstructure fiber", *Opt. Eng.* **41**, 8-9 (2002).

[79]   Y. L. Hoo, W. Jin, C. Z. Shi, H. L. Ho, D. N. Wang, and S. C. Ruan, "Design and modeling of a photonic crystal fiber gas sensor", *Appl. Optics* **42**, 3509-3515 (2003).

[80]   F. Benabid, J. C. Knight, and P. S. Russell, "Particle levitation and guidance in hollow-core photonic crystal fiber", *Opt. Express* **10**, 1195-1203 (2002).

[81]   S. L. Chin, S. Petit, F. Borne, and K. Miyazaki, "The white light supercontinuum is indeed an ultrafast white light laser", *Jpn. J. Appl. Phys. Part 2 - Lett.* **38**, L126-L128 (1999).

[82]   F. Futami, and K. Kikuchi, "Low-noise multiwavelength transmitter using spectrum-sliced supercontinuum generated from a normal group-velocity dispersion fiber", *IEEE Photonics Technol. Lett.* **13**, 73-75 (2001).

[83]   T. Hashimoto, H. Sotobayashi, K. Kitayama, and W. Chujo, "Photonic conversion of OC-192OTDM-to-4 x OC-48WDM by supercontinuum generation", *Electron. Lett.* **36**, 1133-1135 (2000).

[84]   J. Inoue, H. Sotobayashi, and W. Chujo, "Sub-picosecond transform-limited 160 Gbit/s optical pulse compression using supercontinuum generation", *IEICE Trans. Electron.* **E85C**, 1718-1719 (2002).

[85]   S. Kawanishi, H. Takara, T. Morioka, O. Kamatani, and M. Saruwatari, "200gbit/S, 100km Time-Division-Multiplexed Optical-Transmission Using Supercontinuum Pulses with Prescaled Pll Timing Extraction and All-Optical Demultiplexing", *Electron. Lett.* **31**, 816-817 (1995).

[86]   Y. Takushima, and K. Kikuchi, "10-GHz, over 20-channel multiwavelength pulse source by slicing super-continuum spectrum generated in normal-dispersion fiber", *IEEE Photonics Technol. Lett.* **11**, 322-324 (1999).

[87]   L. Boivin, and B. C. Collings, "Invited paper - Spectrum slicing of coherent sources in optical communications", *Opt. Fiber Technol.* **7**, 1-20 (2001).

[88]   L. Boivin, S. Taccheo, C. R. Doerr, P. Schiffer, L. W. Stulz, R. Monnard, and W. Lin, "400Gbit/s transmission over 544km from spectrum-sliced supercontinuum source", *Electron. Lett.* **36**, 335-336 (2000).

[89]   O. Boyraz, J. Kim, M. N. Islam, F. Coppinger, and B. Jalali, "10 Gb/s multiple wavelength, coherent short pulse source based on spectral carving of supercontinuum generated in fibers", *J. Lightwave Technol.* **18**, 2167-2175 (2000).

[90]   R. Calvani, R. Caponi, C. Naddeo, and D. Roccato, "Subpicosecond Pulses at 2.5ghz from Filtered Supercontinuum in a Fiber Pumped by a Chirp Compensated Gain-Switched Dfb Laser", *Electron. Lett.* **31**, 1685-1686 (1995).

[91]   K. Morioka, K. Mori, S. Kawanishi, and M. Saruwatari, "Pulse-Width Tunable, Self-Frequency Conversion of Short Optical Pulses over 200 Nm Based on Supercontinuum Generation", *Electron. Lett.* **30**, 1960-1962 (1994).

[92]   T. Morioka, K. Mori, and M. Saruwatari, "More Than 100-Wavelength-Channel Picosecond Optical Pulse Generation from Single Laser Source Using Supercontinuum in Optical Fibers", *Electron. Lett.* **29**, 862-864 (1993).

[93]   D. J. Jones, S. A. Diddams, J. K. Ranka, A. Stentz, R. S. Windeler, J. L. Hall, and S. T. Cundiff, "Carrier-envelope phase control of femtosecond mode-locked lasers and direct optical frequency synthesis", *Science* **288**, 635-639 (2000).

[94]   S. A. Diddams, D. J. Jones, J. Ye, T. Cundiff, J. L. Hall, J. K. Ranka, R. S. Windeler, R. Holzwarth, T. Udem, and T. W. Hansch, "Direct link between microwave and optical frequencies with a 300 THz femtosecond laser comb", *Phys. Rev. Lett.* **84**, 5102-5105 (2000).

[95]   S. T. Cundiff, J. Ye, and J. L. Hall, "Optical frequency synthesis based on mode-locked lasers", *Rev. Sci. Instrum.* **72**, 3749-3771 (2001).

[96]   J. L. Hall, J. Ye, S. A. Diddams, L. S. Ma, S. T. Cundiff, and D. J. Jones, "Ultrasensitive spectroscopy, the ultrastable lasers, the ultrafast lasers, and the seriously nonlinear fiber: A new alliance for physics and metrology", *IEEE J. Quantum Electron.* **37**, 1482-1492 (2001).

[97]   S. T. Cundiff, and J. Ye, "Colloquium: Femtosecond optical frequency combs", *Rev. Mod. Phys.* **75**, 325-342 (2003).

[98]   L. Hollberg, C. W. Oates, E. A. Curtis, E. N. Ivanov, S. A. Diddams, T. Udem, H. G. Robinson, J. C. Bergquist, R. J. Rafac, W. M. Itano, R. E. Drullinger, and D. J. Wineland, "Optical frequency standards and measurements", *IEEE J. Quantum Electron.* **37**, 1502-1513 (2001).

[99]   R. Holzwarth, M. Zimmermann, T. Udem, and T. W. Hansch, "Optical clockworks and the measurement of laser frequencies with a mode-locked frequency comb", *IEEE J. Quantum Electron.* **37**, 1493-1501 (2001).

[100] M. Bellini, and T. W. Hansch, "Phase-locked white-light continuum pulses: toward a universal optical frequency-comb synthesizer", *Opt. Lett.* **25**, 1049-1051 (2000).

[101] M. Bellini, and T. W. Hansch, "Generation and applications of phase-locked white-light continuum pulses", *Laser Part. Beams* **19**, 157-162 (2001).

[102] T. M. Ramond, S. A. Diddams, L. Hollberg, and A. Bartels, "Phase-coherent link from optical to microwave frequencies by means of the broadband continuum from a 1-GHz Ti : sapphire femtosecond oscillator", *Opt. Lett.* **27**, 1842-1844 (2002).

[103] I. Thomann, A. Bartels, K. L. Corwin, N. R. Newbury, L. Hollberg, S. A. Diddams, J. W. Nicholson, and M. F. Yan, "420-MHz Cr : forsterite femtosecond ring laser and continuum generation in the 1-2-mu m range", *Opt. Lett.* **28**, 1368-1370 (2003).

[104] S. A. Diddams, D. J. Jones, J. Ye, S. T. Cundiff, J. L. Hall, J. K. Ranka, and R. S. Windeler, "Direct RF to optical frequency measurements with a femtosecond laser comb", *IEEE Trans. Instrum. Meas.* **50**, 552-555 (2001).

[105] T. Udem, R. Holzwarth, and T. W. Hansch, "Optical frequency metrology", *Nature* **416**, 233-237 (2002).

[106] K. Robinson, "Photonic crystal fiber enables optical clock", *Photon. Spect.* **36**, 45-46 (2002).

[107] S. N. Bagayev, A. K. Dmitriyev, S. V. Chepurov, A. S. Dychkov, V. M. Klementyev, D. B. Kolker, S. A. Kuznetsov, Y. A. Matyugin, M. V. Okhapkin, V. S. Pivtsov, M. N. Skvortsov, V. F. Zakharyash, T. A. Birks, W. J. Wadsworth, P. S. Russell, and A. M. Zheltikov, "Femtosecond frequency combs stabilized with a He-Ne/CH4 laser: Toward a femtosecond optical clock", *Laser Phys.* **11**, 1270-1282 (2001).

[108] R. Holzwarth, T. Udem, T. W. Hansch, J. C. Knight, W. J. Wadsworth, and P. S. J. Russell, "Optical frequency synthesizer for precision spectroscopy", *Phys. Rev. Lett.* **85**, 2264-2267 (2000).

[109] A. B. Fedotov, A. M. Zheltikov, A. A. Ivanov, M. V. Alfimov, D. Chorvat, V. I. Beloglazov, L. A. Mel'nikov, N. B. Skibina, A. P. Tarasevitch, and D. von der Linde, "Supercontinuum-generating holey fibers as new broadband sources for spectroscopic applications", *Laser Phys.* **10**, 723-726 (2000).

[110] A. B. Fedotov, P. Zhou, A. P. Tarasevitch, K. V. Dukel'skii, Y. N. Kondrat'ev, V. S. Shevandin, V. B. Smirnov, D. von der Linde, and A. M. Zheltikov, "Microstructure-fiber sources of mode-separable supercontinuum emission for wave-mixing spectroscopy", *J. Raman Spectrosc.* **33**, 888-895 (2002).

[111] G. S. He, T. C. Lin, and P. N. Prasad, "New technique for degenerate two-photon absorption spectral measurements using femtosecond continuum generation", *Opt. Express* **10**, 566-574 (2002).

[112] S. T. Sanders, "Wavelength-agile fiber laser using group-velocity dispersion of pulsed super-continua and application to broadband absorption spectroscopy", *Appl. Phys. B-Lasers Opt.* **75**, 799-802 (2002).

[113] I. Hartl, X. D. Li, C. Chudoba, R. K. Ghanta, T. H. Ko, J. G. Fujimoto, J. K. Ranka, and R. S. Windeler, "Ultrahigh-resolution optical coherence tomography using continuum generation in an air-silica microstructure optical fiber", *Opt. Lett.* **26**, 608-610 (2001).

[114] A. A. Ivanov, M. V. Alfimov, A. B. Fedotov, A. A. Podshivalov, D. Chorvat, and A. M. Zheltikov, "An all-solid-state sub-40-fs self-starting Cr4+: Forsterite laser with holey-fiber beam delivery and chirp control for coherence-domain and nonlinear-optical biomedical applications", *Laser Phys.* **11**, 158-163 (2001).

[115] Y. M. Wang, Y. H. Zhao, J. S. Nelson, Z. P. Chen, and R. S. Windeler, "Ultrahigh-resolution optical coherence tomography by broadband continuum generation from a photonic crystal fiber", *Opt. Lett.* **28**, 182-184 (2003).

[116] D. L. Marks, A. L. Oldenburg, J. J. Reynolds, and S. A. Boppart, "Study of an ultrahigh-numerical-aperture fiber continuum generation source for optical coherence tomography", *Opt. Lett.* **27**, 2010-2012 (2002).

[117] B. Povazay, K. Bizheva, A. Unterhuber, B. Hermann, H. Sattmann, A. F. Fercher, W. Drexler, A. Apolonski, W. J. Wadsworth, J. C. Knight, P. S. J. Russell, M. Vetterlein, and E. Scherzer, "Submicrometer axial resolution optical coherence tomography", *Opt. Lett.* **27**, 1800-1802 (2002).

[118] L. Boivin, S. Taccheo, C. R. Doerr, L. W. Stulz, R. Monnard, W. Lin, and W. C. Fang, "A supercontinuum source based on an electroabsorption-modulated laser for long distance DWDM transmission", *IEEE Photonics Technol. Lett.* **12**, 1695-1697 (2000).

[119] H. Takara, T. Ohara, K. Mori, K. Sato, E. Yamada, Y. Inoue, T. Shibata, M. Abe, T. Morioka, and K. I. Sato, "More than 1000 channel optical frequency chain generation from single supercontinuum source with 12.5 GHz channel spacing", *Electron. Lett.* **36**, 2089-2090 (2000).

[120] K. Y. Kim, I. Alexeev, and H. M. Milchberg, "Single-shot supercontinuum spectral interferometry", *Appl. Phys. Lett.* **81**, 4124-4126 (2002).

[121] K. Mori, T. Morioka, and M. Saruwatari, "Ultrawide Spectral Range Group-Velocity Dispersion Measurement Utilizing Supercontinuum in an Optical-Fiber Pumped by a 1.5 Mu-M Compact Laser Source", *IEEE Trans. Instrum. Meas.* **44**, 712-715 (1995).

[122] K. Mori, T. Morioka, and M. Saruwatari, "Group-Velocity Dispersion Measurement Using Supercontinuum Picosecond Pulses Generated in an Optical-Fiber", *Electron. Lett.* **29**, 987-989 (1993).

[123] J. Jasapara, T. H. Her, R. Bise, R. Windeler, and D. J. DiGiovanni, "Group-velocity dispersion measurements in a photonic bandgap fiber", *J. Opt. Soc. Am. B-Opt. Phys.* **20**, 1611-1615 (2003).

[124] F. Koch, S. V. Chernikov, and J. R. Taylor, "Characterization of dispersion in components for ultrafast lasers", *Opt. Commun.* **180**, 133-135 (2000).

[125] R. R. Alfano, and S. L. Shapiro, "Emission in the region 4000 to 7000 Å via four-photon coupling in glass", *Phys. Rev. Lett.* **24**, 584-587 (1970).

[126] P. B. Corkum, C. Rolland, and T. Srinivasanrao, "Supercontinuum Generation in Gases", *Phys. Rev. Lett.* **57**, 2268-2271 (1986).

[127] V. Francois, F. A. Ilkov, and S. L. Chin, "Supercontinuum Generation in Co2 Gas Accompanied by Optical-Breakdown", *J. Phys. B-At. Mol. Opt. Phys.* **25**, 2709-2724 (1992).

[128] T. R. Gosnell, A. J. Taylor, and D. P. Greene, "Supercontinuum Generation at 248nm Using High-Pressure Gases", *Opt. Lett.* **15**, 130-132 (1990).

[129] P. P. Ho, Q. X. Li, T. Jimbo, Y. L. Ku, and R. R. Alfano, "Supercontinuum Pulse Generation and Propagation in a Liquid Carbontetrachloride", *Appl. Optics* **26**, 2700-2702 (1987).

[130] T. Jimbo, V. L. Caplan, Q. X. Li, Q. Z. Wang, P. P. Ho, and R. R. Alfano, "Enhancement of Ultrafast Supercontinuum Generation in Water by the Addition of Zn-2+ and K+ Cations", *Opt. Lett.* **12**, 477-479 (1987).

[131] T. A. Birks, W. J. Wadsworth, and P. S. Russell, "Supercontinuum generation in tapered fibers", *Opt. Lett.* **25**, 1415-1417 (2000).

[132] J. M. Harbold, F. O. Ilday, F. W. Wise, T. A. Birks, W. J. Wadsworth, and Z. Chen, "Long-wavelength continuum generation about the second dispersion zero of a tapered fiber", *Opt. Lett.* **27**, 1558-1560 (2002).

[133] K. Igarashi, S. Saito, M. Kishi, and M. Tsuchiya, "Broad-band and extremely flat super-continuum generation via optical parametric gain extended spectrally by fourth-order dispersion in anomalous-dispersion-flattened fibers", *IEEE J. Sel. Top. Quantum Electron.* **8**, 521-526 (2002).

[134] K. Mori, H. Takara, S. Kawanishi, M. Saruwatari, and T. Morioka, "Flatly broadened supercontinuum spectrum generated in a dispersion decreasing fibre with convex dispersion profile", *Electron. Lett.* **33**, 1806-1808 (1997).

[135] K. Mori, H. Takara, and S. Kawanishi, "Analysis and design of supercontinuum pulse generation in a single-mode optical fiber", *J. Opt. Soc. Am. B-Opt. Phys.* **18**, 1780-1792 (2001).

[136] V. A. Arkhireev, A. E. Korolev, D. A. Nolan, and V. V. Solov'ev, "High-efficiency generation of a supercontinuum in an optical fiber", *Opt. Spectrosc.* **94**, 632-637 (2003).

[137] F. Futami, Y. Takushima, and K. Kikuchi, "Generation of wideband and flat supercontinuum over a 280-nm spectral range from a dispersion-flattened optical fiber with normal group-velocity dispersion", *IEICE Trans. Electron.* **E82C**, 1531-1538 (1999).

[138] A. Mussot, T. Sylvestre, L. Provino, and H. Maillotte, "Generation of a broadband single-mode supercontinuum in a conventional dispersion-shifted fiber by use of a subnanosecond microchip laser", *Opt. Lett.* **28**, 1820-1822 (2003).

[139] G. A. Nowak, J. Kim, and M. N. Islam, "Stable supercontinuum generation in short lengths of conventional dispersion-shifted fiber", *Appl. Optics* **38**, 7364-7369 (1999).

[140] T. Okuno, M. Onishi, T. Kashiwada, S. Ishikawa, and M. Nishimura, "Silica-based functional fibers with enhanced nonlinearity and their applications", *IEEE J. Sel. Top. Quantum Electron.* **5**, 1385-1391 (1999).

[141] J. K. Ranka, R. S. Windeler, and A. J. Stentz, "Visible continuum generation in air-silica microstructure optical fibers with anomalous dispersion at 800 nm", *Opt. Lett.* **25**, 25-27 (2000).

[142] J. K. Ranka, R. S. Windeler, and A. J. Stentz, "Efficient visible continuum generation in air-silica microstructure optical fibers with anomalous dispersion at 800 nm", *Conference on Lasers and Electro-Optics CLEO '99* CPD8/1 -CPD8/2 (1999).

[143] K. L. Corwin, N. R. Newbury, J. M. Dudley, S. Coen, S. A. Diddams, K. Weber, and R. S. Windeler, "Fundamental noise limitations to supercontinuum generation in microstructure fiber", *Phys. Rev. Lett.* **90**, (2003).

[144] S. Coen, A. H. L. Chau, R. Leonhardt, J. D. Harvey, J. C. Knight, W. J. Wadsworth, and P. S. J. Russell, "Supercontinuum generation by stimulated Raman scattering and parametric four-wave mixing in photonic crystal fibers", *J. Opt. Soc. Am. B-Opt. Phys.* **19**, 753-764 (2002).

[145] S. Coen, A. H. L. Chan, R. Leonhardt, J. D. Harvey, J. C. Knight, W. J. Wadsworth, and P. S. J. Russell, "White-light supercontinuum generation with 60-ps pump pulses in a photonic crystal fiber", *Opt. Lett.* **26**, 1356-1358 (2001).

[146] G. Q. Chang, T. B. Norris, and H. G. Winful, "Optimization of supercontinuum generation in photonic crystal fibers for pulse compression", *Opt. Lett.* **28**, 546-548 (2003).

[147] P. A. Champert, S. V. Popov, and J. R. Taylor, "Generation of multiwatt, broadband continua in holey fibers", *Opt. Lett.* **27**, 122-124 (2002).

[148] P. A. Champert, S. V. Popov, M. A. Solodyankin, and J. R. Taylor, "Multiwatt average power continua generation in holey fibers pumped by kilowatt peak power seeded ytterbium fiber amplifier", *Appl. Phys. Lett.* **81**, 2157-2159 (2002).

[149] A. V. Avdokhin, S. V. Popov, and J. R. Taylor, "Continuous-wave, high-power, in Raman continuum generation holey fibers", *Opt. Lett.* **28**, 1353-1355 (2003).

[150] Q. Cao, X. Gu, E. Zeek, M. Kimmel, R. Trebino, J. Dudley, and R. S. Windeler, "Measurement of the intensity and phase of supercontinuum from an 8-mm-long microstructure fiber", *Appl. Phys. B-Lasers Opt.* **77**, 239-244 (2003).

[151] A. Apolonski, B. Povazay, A. Unterhuber, W. Drexler, W. J. Wadsworth, J. C. Knight, and P. S. Russell, "Spectral shaping of supercontinuum in a cobweb photonic-crystal fiber with sub-20-fs pulses", *J. Opt. Soc. Am. B-Opt. Phys.* **19**, 2165-2170 (2002).

[152] J. N. Ames, S. Ghosh, R. S. Windeler, A. L. Gaeta, and S. T. Cundiff, "Excess noise generation during spectral broadening in a microstructured fiber", *Appl. Phys. B-Lasers Opt.* **77**, 279-284 (2003).

[153] J. M. Dudley, L. Provino, N. Grossard, H. Maillotte, R. S. Windeler, B. J. Eggleton, and S. Coen, "Supercontinuum generation in air-silica microstructured fibers with nanosecond and femtosecond pulse pumping", *J. Opt. Soc. Am. B-Opt. Phys.* **19**, 765-771 (2002).

[154] J. M. Dudley, X. Gu, L. Xu, M. Kimmel, E. Zeek, P. O'Shea, R. Trebino, S. Coen, and R. S. Windeler, "Cross-correlation frequency resolved optical gating analysis of broadband continuum generation in photonic crystal fiber: simulations and experiments", *Opt. Express* **10**, 1215-1221 (2002).

[155] J. M. Dudley, and S. Coen, "Coherence properties of supercontinuum spectra generated in photonic crystal and tapered optical fibers", *Opt. Lett.* **27**, 1180-1182 (2002).

[156] A. Efimov, and A. J. Taylor, "Nonlinear generation of very high-order UV modes in microstructured fibers", *Opt. Express* **11**, 910-918 (2003).

[157] X. J. Fang, N. Karasawa, R. Morita, R. S. Windeler, and M. Yamashita, "Nonlinear propagation of a-few-optical-cycle pulses in a photonic crystal fiber - Experimental and theoretical studies beyond the slowly varying-envelope approximation", *IEEE Photonics Technol. Lett.* **15**, 233-235 (2003).

[158] A. B. Fedotov, P. Zhou, A. N. Naumov, V. V. Temnov, V. I. Beloglazov, N. B. Skibina, L. A. Mel'nikov, A. V. Shcherbakov, A. P. Tarasevitch, D. von der Linde, and A. M. Zheltikov, "Spectral broadening of 40-fs Ti : sapphire laser pulses in photonic-molecule modes of a cobweb-microstructure fiber", *Appl. Phys. B-Lasers Opt.* **75**, 621-627 (2002).

[159] A. B. Fedotov, P. Zhou, Y. N. Kondrat'ev, S. N. Bagayev, V. S. Shevandin, K. V. Dukel'skii, V. B. Smirnov, A. P. Tarasevitch, D. von der Linde, and A. M. Zheltikov, "The mode structure and spectral properties of supercontinuum emission from microstructure fibers", *J. Exp. Theor. Phys.* **95**, 851-860 (2002).

[160] A. B. Fedotov, A. N. Naumov, A. M. Zheltikov, I. Bugar, D. Chorvat, A. P. Tarasevitch, and D. von der Linde, "Frequency-tunable supercontinuum generation in photonic-crystal fibers by femtosecond pulses of an optical parametric amplifier", *J. Opt. Soc. Am. B-Opt. Phys.* **19**, 2156-2164 (2002).

[161] A. B. Fedotov, I. Bugar, D. A. Sidorov-Biryukov, E. E. Serebryannikov, D. Chorvat, M. Scalora, and A. M. Zheltikov, "Pump-depleting four-wave mixing in supercontinuum-generating microstructure fibers", *Appl. Phys. B-Lasers Opt.* **77**, 313-317 (2003).

[162] A. L. Gaeta, "Nonlinear propagation and continuum generation in microstructured optical fibers", *Opt. Lett.* **27**, 924-926 (2002).

[163] X. Gu, L. Xu, M. Kimmel, E. Zeek, P. O'Shea, A. P. Shreenath, R. Trebino, and R. S. Windeler, "Frequency-resolved optical gating and single-shot spectral measurements reveal fine structure in microstructure-fiber continuum", *Opt. Lett.* **27**, 1174-1176 (2002).

[164] X. Gu, M. Kimmel, A. P. Shreenath, R. Trebino, J. M. Dudley, S. Coen, and R. S. Windeler, "Experimental studies of the coherence of microstructure-fiber supercontinuum", *Opt. Express* **11**, 2697-2703 (2003).

[165] K. M. Hilligsoe, H. N. Paulsen, J. Thogersen, S. R. Keiding, and J. J. Larsen, "Initial steps of supercontinuum generation in photonic crystal fibers", *J. Opt. Soc. Am. B-Opt. Phys.* **20**, 1887-1893 (2003).

[166] A. V. Husakou, and J. Herrmann, "Supercontinuum generation of higher-order solitons by fission in photonic crystal fibers", *Phys. Rev. Lett.* **8720**, (2001).

[167] A. V. Husakou, and J. Herrmann, "Supercontinuum generation, four-wave mixing, and fission of higher-order solitons in photonic-crystal fibers", *J. Opt. Soc. Am. B-Opt. Phys.* **19**, 2171-2182 (2002).

[168] A. V. Husakou, and J. Herrmann, "Supercontinuum generation in photonic crystal fibers made from highly nonlinear glasses", *Appl. Phys. B-Lasers Opt.* **77**, 227-234 (2003).

[169] V. L. Kalashnikov, P. Dombi, T. Fuji, W. J. Wadsworth, J. C. Knight, P. S. J. Russell, R. S. Windeler, and A. Apolonski, "Maximization of supercontinua in photonic crystal fibers by using double pulses and polarization effects", *Appl. Phys. B-Lasers Opt.* **77**, 319-324 (2003).

[170] N. R. Newbury, B. R. Washburn, K. L. Corwin, and R. S. Windeler, "Noise amplification during supercontinuum generation in microstructure fiber", *Opt. Lett.* **28**, 944-946 (2003).

[171] A. Ortigosa-Blanch, J. C. Knight, and P. S. J. Russell, "Pulse breaking and supercontinuum generation with 200-fs pump pulses in photonic crystal fibers", *J. Opt. Soc. Am. B-Opt. Phys.* **19**, 2567-2572 (2002).

[172] J. H. V. Price, W. Belardi, T. M. Monro, A. Malinowski, A. Piper, and D. J. Richardson, "Soliton transmission and supercontinuum generation in holey fiber, using a diode pumped Ytterbium fiber source", *Opt. Express* **10**, 382-387 (2002).

[173] J. H. V. Price, T. M. Monro, K. Furusawa, W. Belardi, J. C. Baggett, S. Coyle, C. Netti, J. J. Baumberg, R. Paschotta, and D. J. Richardson, "UV generation in a pure-silica holey fiber", *Appl. Phys. B-Lasers Opt.* **77**, 291-298 (2003).

[174] L. Provino, J. M. Dudley, H. Maillotte, N. Grossard, R. S. Windeler, and B. J. Eggleton, "Compact broadband continuum source based on microchip laser pumped microstructured fibre", *Electron. Lett.* **37**, 558-560 (2001).

[175] L. Tartara, I. Cristiani, V. Degiorgio, F. Carbone, D. Faccio, and M. Romagnoli, "Nonlinear propagation of ultrashort laser pulses in a microstructured fiber", *J. Nonlinear Opt. Phys. Mater.* **11**, 409-419 (2002).

[176] L. Tartara, I. Cristiani, and V. Degiorgio, "Blue light and infrared continuum generation by soliton fission in a microstructured fiber", *Appl. Phys. B-Lasers Opt.* **77**, 307-311 (2003).

[177] W. J. Wadsworth, A. Ortigosa-Blanch, J. C. Knight, T. A. Birks, T. P. M. Man, and P. S. Russell, "Supercontinuum generation in photonic crystal fibers and optical fiber tapers: a novel light source", *J. Opt. Soc. Am. B-Opt. Phys.* **19**, 2148-2155 (2002).

[178] B. R. Washburn, S. E. Ralph, and R. S. Windeler, "Ultrashort pulse propagation in air-silica microstructure fiber", *Opt. Express* **10**, 575-580 (2002).

[179] T. Yamamoto, H. Kubota, S. Kawanishi, M. Tanaka, and S. Yamaguchi, "Supercontinuum generation at 1.55 mu m in a dispersion-flattened polarization-maintaining photonic crystal fiber", *Opt. Express* **11**, 1537-1540 (2003).

[180] M. Seefeldt, A. Heuer, and R. Menzel, "Compact white-light source with an average output power of 2.4 W and 900 nm spectral bandwidth", *Opt. Commun.* **216**, 199-202 (2003).

[181] T. A. Birks, J. C. Knight, and P. S. Russell, "Endlessly single-mode photonic crystal fiber", *Opt. Lett.* **22**, 961-963 (1997).

[182] J. C. Knight, J. Arriaga, T. A. Birks, A. Ortigosa-Blanch, W. J. Wadsworth, and P. S. Russell, "Anomalous dispersion in photonic crystal fiber", *IEEE Photonics Technol. Lett.* **12**, 807-809 (2000).

[183] G. P. Agrawal, "Fiber-Optic Communication Systems", Second Edition, *John Wiley & Sons New York* (1997).

[184] M. C. Amann, and J. Buus, "Tunable Laser Diodes", *Hartech House Publishers Boston* (1998).

[185] C. E. Wieman, and L. Hollberg, "Using diode lasers for atomic physics", *Rev. Sci. Instrum.* **62**, 1-20 (1991).

[186] R. P. Salathé, "Diode lasers coupled to external resonators", *Appl. Phys.* **20**, 1-18 (1979).

[187] R. Lang, and K. Kobayashi, "External optical feedback effects on semiconductor injection laser properties", *IEEE J. Quantum Electron.* **16**, 347-355 (1980).

[188] B. Dahmani, L. Hollberg, and R. Drullinger, "Frequency Stabilization of Semiconductor-Lasers by Resonant Optical Feedback", *Opt. Lett.* **12**, 876-878 (1987).

[189] H. Patrick, and C. E. Wieman, "Frequency stabilization of a diode laser using simultaneous optical feedback from a diffraction grating and a narrowband Fabry-Perot cavity", *Rev. Sci. Instrum.* **62**, 2593-2595 (1991).

[190] A. Hemmerich, D. H. McIntyre, D. Schropp, D. Meschede, and T. W. Hansch, "Optically Stabilized Narrow Linewidth Semiconductor-Laser for High-Resolution Spectroscopy", *Opt. Commun.* **75**, 118-122 (1990).

[191] J. O. Binder, G. D. Cormack, and A. Somani, "Intermodal Tuning Characteristics of an Ingaasp Laser with Optical Feedback from an External-Grating Reflector", *IEEE J. Quantum Electron.* **26**, 1191-1199 (1990).

[192] D. T. Cassidy, and M. J. Hamp, "Diffractive optical element used in an external feedback configuration to tune the wavelength of uncoated Fabry-Perot diode lasers", *J. Mod. Opt.* **46**, 1071-1078 (1999).

[193] K. C. Harvey, and C. J. Myatt, "External-Cavity Diode-Laser Using a Grazing-Incidence Diffraction Grating", *Opt. Lett.* **16**, 910-912 (1991).

[194] T. Kiguchi, A. Uematsu, M. Kitano, and H. Ogura, "Grating external cavity diode lasers with broad tunable range and narrow spectral linewidth for high-resolution spectroscopy", *Jpn. J. Appl. Phys. Part 1 - Regul. Pap. Short Notes Rev. Pap.* **35**, 5890-5895 (1996).

[195] M. Fleming, and A. Mooradian, "Spectral characteristics of external-cavity controlled semiconductor lasers", *IEEE J. Quantum Electron.* **17**, 44-59 (1981).

[196] A. J. Ikushima, T. Fujiwara, and K. Saito, "Silica glass: A material for photonics", *J. Appl. Phys.* **88**, 1201-1213 (2000).

[197] R. A. Myers, N. Mukherjee, and S. R. J. Brueck, "Large 2nd-Order Nonlinearity in Poled Fused-Silica", *Opt. Lett.* **16**, 1732-1734 (1991).

[198] J. C. Baggett, T. M. Monro, K. Furusawa, and D. J. Richardson, "Comparative study of large-mode holey and conventional fibers", *Opt. Lett.* **26**, 1045-1047 (2001).

[199] J. C. Knight, T. A. Birks, R. F. Cregan, P. S. Russell, and J. P. de Sandro, "Large mode area photonic crystal fibre", *Electron. Lett.* **34**, 1347-1348 (1998).

[200] M. J. Gander, R. McBride, J. D. C. Jones, D. Mogilevtsev, T. A. Birks, J. C. Knight, and P. S. Russell, "Experimental measurement of group velocity dispersion in photonic crystal fibre", *Electron. Lett.* **35**, 63-64 (1999).

[201] H. Chi, Q. J. Zeng, H. D. Zhao, H. Liu, S. L. Xiao, and J. X. Wang, "Analysis on dispersion characteristics of photonic crystal fiber", *J. Infrared Millim. Waves* **22**, 149-153 (2003).

[202] R. K. Sinha, and S. K. Varshney, "Dispersion properties of photonic crystal fibers", *Microw. Opt. Technol. Lett.* **37**, 129-132 (2003).

[203] A. Ferrando, E. Silvestre, J. J. Miret, J. A. Monsoriu, M. V. Andres, and P. S. Russell, "Designing a photonic crystal fibre with flattened chromatic dispersion", *Electron. Lett.* **35**, 325-327 (1999).

[204] A. Ferrando, E. Silvestre, J. J. Miret, and P. Andres, "Nearly zero ultraflattened dispersion in photonic crystal fibers", *Opt. Lett.* **25**, 790-792 (2000).

[205] A. Ferrando, E. Silvestre, P. Andres, J. J. Miret, and M. V. Andres, "Designing the properties of dispersion-flattened photonic crystal fibers", *Opt. Express* **9**, 687-697 (2001).

[206] K. P. Hansen, "Dispersion flattened hybrid-core nonlinear photonic crystal fiber", *Opt. Express* **11**, 1503-1509 (2003).

[207] W. H. Reeves, J. C. Knight, P. S. J. Russell, and P. J. Roberts, "Demonstration of ultra-flattened dispersion in photonic crystal fibers", *Opt. Express* **10**, 609-613 (2002).

[208] G. Renversez, B. Kuhlmey, and R. McPhedran, "Dispersion management with microstructured optical fibers: ultraflattened chromatic dispersion with low losses", *Opt. Lett.* **28**, 989-991 (2003).

[209] K. Saitoh, M. Koshiba, T. Hasegawa, and E. Sasaoka, "Chromatic dispersion control in photonic crystal fibers: application to ultra-flattened dispersion", *Opt. Express* **11**, 843-852 (2003).

[210] T. M. Monro, D. J. Richardson, N. G. R. Broderick, and P. J. Bennett, "Holey optical fibers: An efficient modal model", *J. Lightwave Technol.* **17**, 1093-1102 (1999).

[211] A. M. Zheltikov, "Limiting efficiencies of nonlinear-optical processes in microstructure fibers", *J. Exp. Theor. Phys.* **97**, 505-521 (2003).

[212] N. A. Mortensen, M. D. Nielsen, J. R. Folkenberg, A. Petersson, and H. R. Simonsen, "Improved large-mode-area endlessly single-mode photonic crystal fibers", *Opt. Lett.* **28**, 393-395 (2003).

[213] T. P. Hansen, J. Broeng, S. E. B. Libori, E. Knudsen, A. Bjarklev, J. R. Jensen, and H. Simonsen, "Highly birefringent index-guiding photonic crystal fibers", *IEEE Photonics Technol. Lett.* **13**, 588-590 (2001).

[214] K. Suzuki, H. Kubota, S. Kawanishi, M. Tanaka, and M. Fujita, "Optical properties of a low-loss polarization-maintaining photonic crystal fiber", *Opt. Express* **9**, 676-680 (2001).

[215] J. Ju, W. Jin, and M. S. Demokan, "Properties of a highly birefringent photonic crystal fiber", *IEEE Photonics Technol. Lett.* **15**, 1375-1377 (2003).

[216] D. Mogilevtsev, J. Broeng, S. E. Barkou, and A. Bjarklev, "Design of polarization-preserving photonic crystal fibres with elliptical pores", *J. Opt. A-Pure Appl. Opt.* **3**, S141-S143 (2001).

[217] A. Ortigosa-Blanch, J. C. Knight, W. J. Wadsworth, J. Arriaga, B. J. Mangan, T. A. Birks, and P. S. J. Russell, "Highly birefringent photonic crystal fibers", *Opt. Lett.* **25**, 1325-1327 (2000).

[218] K. Saitoh, and M. Koshiba, "Single-polarization single-mode photonic crystal fibers", *IEEE Photonics Technol. Lett.* **15**, 1384-1386 (2003).

[219] A. B. Fedotov, S. O. Konorov, Y. N. Kondrat'ev, S. N. Bagayev, V. S. Shevandin, K. V. Dukel'skii, D. A. Sidorov-Biryukov, A. V. Khokhlov, V. B. Smirnov, and A. M. Zheltikov, "Measurement of optical losses

for a family of microstructure fibers with a sequentially increasing number of hexagonal cycles of air holes", *Laser Phys.* **13**, 856-860 (2003).

[220] D. Ferrarini, L. Vincetti, M. Zoboli, A. Cucinotta, and S. Selleri, "Leakage properties of photonic crystal fibers", *Opt. Express* **10**, 1314-1319 (2002).

[221] V. Finazzi, T. M. Monro, and D. J. Richardson, "The role of confinement loss in highly nonlinear silica holey fibers", *IEEE Photonics Technol. Lett.* **15**, 1246-1248 (2003).

[222] M. H. Frosz, K. Hougaard, S. E. B. Libori, J. Laegsgaard, and A. Bjarklev, "Radial deformation losses in photonic crystal fibres", *J. Opt. A-Pure Appl. Opt.* **5**, 268-271 (2003).

[223] M. Koshiba, and K. Saitoh, "Polarization-dependent confinement losses in actual holey fibers", *IEEE Photonics Technol. Lett.* **15**, 691-693 (2003).

[224] J. T. Lizier, and G. E. Town, "Splice losses in holey optical fibers", *IEEE Photonics Technol. Lett.* **13**, 794-796 (2001).

[225] M. D. Nielsen, N. A. Mortensen, and J. R. Folkenberg, "Reduced microdeformation attenuation in large-mode-area photonic crystal fibers for visible applications", *Opt. Lett.* **28**, 1645-1647 (2003).

[226] M. D. Nielsen, G. Vienne, J. R. Folkenberg, and A. Bjarklev, "Investigation of microdeformation-induced attenuation spectra in a photonic crystal fiber", *Opt. Lett.* **28**, 236-238 (2003).

[227] T. Sorensen, J. Broeng, A. Bjarklev, E. Knudsen, and S. E. B. Libori, "Macro-bending loss properties of photonic crystal fibre", *Electron. Lett.* **37**, 287-289 (2001).

[228] T. Sorensen, J. Broeng, A. Bjarklev, T. P. Hansen, E. Knudsen, S. E. B. Libori, H. R. Simonsen, and J. R. Jensen, "Spectral macro-bending loss considerations for photonic crystal fibres", *IEE Proc.-Optoelectron.* **149**, 206-210 (2002).

[229] T. P. White, R. C. McPhedran, C. M. de Sterke, L. C. Botten, and M. J. Steel, "Confinement losses in microstructured optical fibers", *Opt. Lett.* **26**, 1660-1662 (2001).

[230] K. M. Kiang, K. Frampton, T. M. Monro, R. Moore, J. Tucknott, D. W. Hewak, D. J. Richardson, and H. N. Rutt, "Extruded singlemode non-silica glass holey optical fibres", *Electron. Lett.* **38**, 546-547 (2002).

[231] V. Kumar, A. K. George, W. H. Reeves, J. C. Knight, P. S. Russell, F. G. Omenetto, and A. J. Taylor, "Extruded soft glass photonic crystal fiber for ultrabroad supercontinuum generation", *Opt. Express* **10**, 1520-1525 (2002).

[232] T. M. Monro, Y. D. West, D. W. Hewak, N. G. R. Broderick, and D. J. Richardson, "Chalcogenide holey fibres", *Electron. Lett.* **36**, 1998-2000 (2000).

[233] J. Arriaga, and B. Meneses, "Band structure for the cladding of a hollow core photonic crystal fibre", *Rev. Mex. Fis.* **49**, 335-337 (2003).

[234] A. B. Fedotov, M. V. Alfimov, A. A. Ivanov, A. V. Tarasishin, V. I. Beloglazov, A. P. Tarasevitch, D. von der Linde, B. A. Kirillov, S. A. Magnitskii, D. Chorvat, A. N. Naumov, E. A. Vlasova, D. A. Sidorov-Biryukov, A. A. Podshivalov, O. A. Kolevatova, L. A. Mel'nikov, D. A. Akimov, V. A. Makarov, Y. S. Skibina, and A. M. Zheltikov, "Holey fibers with 0.4-32-mu m-lattice-constant photonic band-gap cladding: Fabrication, characterization, and nonlinear-optical measurements", *Laser Phys.* **11**, 138-145 (2001).

[235] T. M. Monro, D. J. Richardson, N. G. R. Broderick, and P. J. Bennett, "Modeling large air fraction holey optical fibers", *J. Lightwave Technol.* **18**, 50-56 (2000).

[236] M. J. Steel, and R. M. Osgood, "Elliptical-hole photonic crystal fibers", *Opt. Lett.* **26**, 229-231 (2001).

[237] J. Arriaga, J. C. Knight, and P. S. Russell, "Modelling photonic crystal fibres", *Physica E* **17**, 440-442 (2003).

[238] A. V. Belov, and E. M. Dianov, "Waveguide characteristics of single-mode microstructural fibres with a complicated refractive index distribution profile", *Quantum Electron.* **32**, 641-644 (2002).

[239] F. Brechet, J. Marcou, D. Pagnoux, and P. Roy, "Complete analysis of the characteristics of propagation into photonic crystal fibers, by the finite element method", *Opt. Fiber Technol.* **6**, 181-191 (2000).

[240] A. Cucinotta, S. Selleri, L. Vincetti, and M. Zoboli, "Holey fiber analysis through the finite-element method", *IEEE Photonics Technol. Lett.* **14**, 1530-1532 (2002).

[241] C. A. De Francisco, B. V. Borges, and M. A. Romero, "A semivectorial method for the modeling of photonic crystal fibers", *Microw. Opt. Technol. Lett.* **38**, 418-421 (2003).

[242] I. Del Villar, I. R. Matias, F. J. Arregui, and R. O. Claus, "Analysis of one-dimensional photonic band gap structures with a liquid crystal defect towards development of fiber-optic tunable wavelength filters", *Opt. Express* **11**, 430-436 (2003).

[243] A. Ferrando, E. Silvestre, J. J. Miret, P. Andres, and M. V. Andres, "Full-vector analysis of a realistic photonic crystal fiber", *Opt. Lett.* **24**, 276-278 (1999).

[244] J. M. Fini, "Analysis of microstructure optical fibers by radial scattering decomposition", *Opt. Lett.* **28**, 992-994 (2003).

[245] A. D. Fitt, K. Furusawa, T. M. Monro, C. P. Please, and D. J. Richardson, "The mathematical modelling of capillary drawing for holey fibre manufacture", *J. Eng. Math.* **43**, 201-227 (2002).

[246] F. Fogli, L. Saccomandi, P. Bassi, G. Bellanca, and S. Trillo, "Full vectorial BPM modeling of Index-Guiding Photonic Crystal Fibers and Couplers", *Opt. Express* **10**, 54-59 (2002).

[247] T. Fujisawa, and M. Koshiba, "Finite element characterization of chromatic dispersion in nonlinear holey fibers", *Opt. Express* **11**, 1481-1489 (2003).

[248] R. Ghosh, A. Kumar, and J. P. Meunier, "Waveguiding properties of holey fibres and effective-V model", *Electron. Lett.* **35**, 1873-1875 (1999).

[249] N. Guan, S. J. Habu, K. Takenaga, K. Himeno, and A. Wada, "Boundary element method for analysis of holey optical fibers", *J. Lightwave Technol.* **21**, 1787-1792 (2003).

[250] S. Guenneau, A. Nicolet, F. Zolla, and S. Lasquellec, "Modeling of photonic crystal optical fibers with finite elements", *IEEE Trans. Magn.* **38**, 1261-1264 (2002).

[251] Y. Z. He, and F. G. Shi, "Finite-difference imaginary-distance beam propagation method for modeling of the fundamental mode of photonic crystal fibers", *Opt. Commun.* **225**, 151-156 (2003).

[252] Y. L. Hsueh, E. S. T. Hu, M. E. Marhic, and L. G. Kazovsky, "Opposite-parity orthonormal function expansion for efficient full-vectorial modeling of holey optical fibers", *Opt. Lett.* **28**, 1188-1190 (2003).

[253] N. A. Issa, and L. Poladian, "Vector wave expansion method for leaky modes of microstructured optical fibers", *J. Lightwave Technol.* **21**, 1005-1012 (2003).

[254] C. E. Kerbage, B. J. Eggleton, P. S. Westbrook, and R. S. Windeler, "Experimental and scalar beam propagation analysis of an air-silica microstructure fiber", *Opt. Express* **7**, 113-122 (2000).

[255] J. C. Knight, T. A. Birks, P. S. J. Russell, and J. P. de Sandro, "Properties of photonic crystal fiber and the effective index model", *J. Opt. Soc. Am. A-Opt. Image Sci. Vis.* **15**, 748-752 (1998).

[256] E. Knudsen, and A. Bjarklev, "Modelling photonic crystal fibres with Hermite-Gaussian functions", *Opt. Commun.* **222**, 155-160 (2003).

[257] M. Koshiba, "Full-vector analysis of photonic crystal fibers using the finite element method", *IEICE Trans. Electron.* **E85C**, 881-888 (2002).

[258] B. T. Kuhlmey, T. P. White, G. Renversez, D. Maystre, L. C. Botten, C. M. de Sterke, and R. C. McPhedran, "Multipole method for microstructured optical fibers. II. Implementation and results", *J. Opt. Soc. Am. B-Opt. Phys.* **19**, 2331-2340 (2002).

[259] J. Laegsgaard, A. Bjarklev, and S. E. B. Libori, "Chromatic dispersion in photonic crystal fibers: fast and accurate scheme for calculation", *J. Opt. Soc. Am. B-Opt. Phys.* **20**, 443-448 (2003).

[260] M. Midrio, M. P. Singh, and C. G. Someda, "The space filling mode of holey fibers: An analytical vectorial solution", *J. Lightwave Technol.* **18**, 1031-1037 (2000).

[261] W. S. Mohammed, L. Vaissie, and E. G. Johnson, "Hybrid mode calculations for novel photonic crystal fibers", *Opt. Eng.* **42**, 2311-2317 (2003).

[262] M. D. Nielsen, and N. A. Mortensen, "Photonic crystal fiber design based on the V-parameter", *Opt. Express* **11**, 2762-2768 (2003).

[263] A. Peyrilloux, S. Fevrier, J. Marcou, L. Berthelot, D. Pagnoux, and P. Sansonetti, "Comparison between the finite element method, the localized function method and a novel equivalent averaged index method for modelling photonic crystal fibres", *J. Opt. A-Pure Appl. Opt.* **4**, 257-262 (2002).

[264] M. Qiu, "Analysis of guided modes in photonic crystal fibers using the finite-difference time-domain method", *Microw. Opt. Technol. Lett.* **30**, 327-330 (2001).

[265] K. Saitoh, and M. Koshiba, "Full-vectorial imaginary-distance beam propagation method based on a finite element scheme: Application to photonic crystal fibers", *IEEE J. Quantum Electron.* **38**, 927-933 (2002).

[266] M. J. Steel, T. P. White, C. M. de Sterke, R. C. McPhedran, and L. C. Botten, "Symmetry and degeneracy in microstructured optical fibers", *Opt. Lett.* **26**, 488-490 (2001).

[267] M. J. Steel, and R. M. Osgood, "Polarization and dispersive properties of elliptical-hole photonic crystal fibers", *J. Lightwave Technol.* **19**, 495-503 (2001).

[268] Z. Wang, G. B. Ren, S. Q. Lou, and S. S. Jian, "Supercell lattice method for photonic crystal fibers", *Opt. Express* **11**, 980-991 (2003).

[269] T. P. White, R. C. McPhedran, L. C. Botten, G. H. Smith, and C. M. de Sterke, "Calculations of air-guided modes in photonic crystal fibers using the multipole method", *Opt. Express* **9**, 721-732 (2001).

[270] T. P. White, B. T. Kuhlmey, R. C. McPhedran, D. Maystre, G. Renversez, C. M. de Sterke, and L. C. Botten, "Multipole method for microstructured optical fibers. I. Formulation", *J. Opt. Soc. Am. B-Opt. Phys.* **19**, 2322-2330 (2002).

[271] T. P. White, B. T. Kuhlmey, R. C. McPhedran, D. Maystre, G. Renversez, C. M. De Sterke, and L. C. Botten, "Multipole method for microstructured optical fibers. Iota. Formulation (vol 19, pg 2322, 2002)", *J. Opt. Soc. Am. B-Opt. Phys.* **20**, 1581-1581 (2003).

[272] Z. M. Zhu, and T. G. Brown, "Analysis of the space filling modes of photonic crystal fibers", *Opt. Express* **8**, 547-554 (2001).

[273] Z. M. Zhu, and T. G. Brown, "Full-vectorial finite-difference analysis of microstructured optical fibers", *Opt. Express* **10**, 853-864 (2002).

[274] Y. J. Zhu, Y. C. Chen, P. Huray, and X. P. Dong, "Application of a 2D-CFDTD algorithm to the analysis of photonic crystal fibers (PCFs)", *Microw. Opt. Technol. Lett.* **35**, 10-14 (2002).

[275] D. Mogilevtsev, T. A. Birks, and P. S. Russell, "Localized function method for modeling defect modes in 2-D photonic crystals", *J. Lightwave Technol.* **17**, 2078-2081 (1999).

[276] A. Ferrando, E. Silvestre, J. J. Miret, P. Andres, and M. V. Andres, "Vector description of higher-order modes in photonic crystal fibers", *J. Opt. Soc. Am. A-Opt. Image Sci. Vis.* **17**, 1333-1340 (2000).

[277] R. Ghosh, A. Kumar, J. P. Meunier, and E. Marin, "Modal characteristics of few-mode silica-based photonic crystal fibres", *Opt. Quantum Electron.* **32**, 963-970 (2000).

[278] B. T. Kuhlmey, R. C. McPhedran, and C. M. de Sterke, "Modal cutoff in microstructured optical fibers", *Opt. Lett.* **27**, 1684-1686 (2002).

[279] A. S. Sudbo, "Film mode matching: a versatile numerical method for vector mode field calculations in dielectric waveguides", *Pure Appl. Opt.* **2**, 211-233 (1993).

[280] S. T. Peng, and A. A. Oliner, "Guidance and leakage properties of a class of open dielectric waveguides: Part I", **29**, 843-845 (1981).

[281] D. F. G. Gallagher, and T. P. Felici, "Eigenmode expansion methods for simulation of optical propagation in photonic - pros and cons", *Photonics West 2003*, San Jose, paper 4987-10.

[282] T. A. Birks, D. Mogilevtsev, J. C. Knight, and P. S. Russell, "Dispersion compensation using single-material fibers", *IEEE Photonics Technol. Lett.* **11**, 674-676 (1999).

[283] F. Poli, A. Cucinotta, M. Fuochi, S. Selleri, and L. Vincetti, "Characterization of microstructured optical fibers for wideband dispersion compensation", *J. Opt. Soc. Am. A-Opt. Image Sci. Vis.* **20**, 1958-1962 (2003).

[284] G. P. Agrawal, "Nonlinear Fiber Optics", Third edition, *Academic Press San Diego* (2001).

[285] A. B. Fedotov, A. M. Zheltikov, A. P. Tarasevitch, M. V. Alfimov, A. A. Ivanov, L. A. Golovan, P. K. Kashkarov, A. A. Podshivalov, V. I. Beloglazov, J. W. Haus, and D. von der Linde, "Controlled light localisation and nonlinear-optical interactions of short laser pulses in holey fibres", *Quantum Electron.* **31**, 387-390 (2001).

[286] M. Koshiba, and K. Saitoh, "Structural dependence of effective area and mode field diameter for holey fibers", *Opt. Express* **11**, 1746-1756 (2003).

[287] N. A. Mortensen, "Effective area of photonic crystal fibers", *Opt. Express* **10**, 341-348 (2002).

[288] N. A. Mortensen, and J. R. Folkenberg, "Low-loss criterion and effective area considerations for photonic crystal fibres", *J. Opt. A-Pure Appl. Opt.* **5**, 163-167 (2003).

[289] R. R. Alfano, "The Supercontinuum Laser Source", *Springer-Verlag New York* (1989).

[290] V. Francois, F. A. Ilkov, and S. L. Chin, "Experimental-Study of the Supercontinuum Spectral Width Evolution in Co2 Gas", *Opt. Commun.* **99**, 241-246 (1993).

[291] R. L. Fork, C. V. Shank , C. Hirlimann, R. Yen, and W. J. Tomlinson, "Femstosecond white-light continuum pulses", *Opt. Lett.* **8**, (1983).

[292] W. Lee Smith, P. Liu, and N. Bloembergen, "Superbroadenning in H2O and D2O by self-focused picosecond pulses from a YAlG:Nd laser", *Phys. Rev. A* **15**, (1977).

[293] P. L. Baldeck, and R. R. Alfano, "Intensity effects on the stimulated four photon spectra generated by picosecond pulses in optical fibers", *J. Lightwave Technol.* **5**, 1712-1715 (1987).

[294] J. Herrmann, U. Griebner, N. Zhavoronkov, A. Husakou, D. Nickel, J. C. Knight, W. J. Wadsworth, P. S. J. Russell, and G. Korn, "Experimental evidence for supercontinuum generation by fission of higher-order solitons in photonic fibers", *Phys. Rev. Lett.* **88**, (2002).

[295] J. M. Dudley, and S. Coen, "Numerical simulations and coherence properties of supercontinuum generation in photonic crystal and tapered optical fibers", *IEEE J. Sel. Top. Quantum Electron.* **8**, 651-659 (2002).

[296] A. B. Fedotov, I. Bugar, A. N. Naumov, D. Chorvat, D. A. Sidorov-Biryukov, and A. M. Zheltikov, "Light confinement and supercontinuum generation switching in photonic-molecule modes of a microstructure fiber", *Jetp Lett.* **75**, 304-308 (2002).

[297] A. B. Fedotov, A. N. Naumov, I. Bugar, D. Chorvat, D. A. Sidorov-Biryukov, and A. M. Zheltikov, "Supercontinuum generation in photonic-molecule modes of microstructure fibers", *IEEE J. Sel. Top. Quantum Electron.* **8**, 665-674 (2002).

[298] R. H. Stolen, and C. Lin, "Self-phase modulation in silica optical fibers", *Phys. Rev. A* **17**, 1448-1453 (1978).

[299] E. G. Sauter, "Nonlinear Optics", *John Wiley & Sons New York* (1996).

[300] K. J. Blow, and D. Wood, "Theoretical Description of Transient Stimulated Raman-Scattering in Optical Fibers", *IEEE J. Quantum Electron.* **25**, 2665-2673 (1989).

[301] P. V. Mamyshev, and S. V. Chernikov, "Ultrashort-Pulse Propagation in Optical Fibers", *Opt. Lett.* **15**, 1076-1078 (1990).

[302] A. S. Akhmanov, R. V. Khohhlov, and A. P. Sukhorukov, "Laser Handbook", *North-Holland Amsterdam* (1972).

[303] C. V. Raman, "A new radiation", *Indian J. Phys.* **2**, 387 (1928).

[304] R. H. Stolen, *Private communication* (2001).

[305] V. E. Zakharov, and E. A. Kuznetsov, "Optical solitons and quasisolitons", *J. Exp. Theor. Phys.* **86**, 1035-1046 (1998).

[306] V. E. Zakharov, and A. B. Shabat, *Sov. Phys. JETP* **34**, 62-69 (1972).

[307] Y. Kodama, and A. Hasegawa, "Theoretical Foundation of Optical-Soliton Concept in Fibers", *Prog. Optics* **30**, 205-259 (1992).

[308] Y. Kodama, and K. Nozaki, "Soliton Interaction in Optical Fibers", *Opt. Lett.* **12**, 1038-1040 (1987).

[309] Y. Kodama, and A. Hasegawa, "Nonlinear Pulse-Propagation in a Monomode Dielectric Guide", *IEEE J. Quantum Electron.* **23**, 510-524 (1987).

[310] J. K. Lucek, and K. J. Blow, "Soliton Self-Frequency Shift in Telecommunications Fiber", *Phys. Rev. A* **45**, 6666-6674 (1992).

[311] P. Beaud, W. Hodel, B. Zysset, and H. P. Weber, "Ultrashort Pulse-Propagation, Pulse Breakup, and Fundamental Soliton Formation in a Single-Mode Optical Fiber", *IEEE J. Quantum Electron.* **23**, 1938-1946 (1987).

[312] F. M. Mitschke, and L. F. Mollenauer, "Discovery of the soliton self-frequency shift", *Opt. Lett.* **11**, 659-661 (1986).

[313] J. P. Gordon, "Theory of the soliton self-frequency shift", *Opt. Lett.* **11**, 662-664 (1986).

[314] N. Tzoar, and M. Jain, "Self-phase modulation in long-geometry optical waveguides", *Phys. Rev. A* **23**, 1266-1270 (1981).

[315] N. Akhmediev, and M. Karlsson, "Cherenkov Radiation Emitted by Solitons in Optical Fibers", *Phys. Rev. A* **51**, 2602-2607 (1995).

[316] P. K. A. Wai, H. H. Chen, and Y. C. Lee, "Radiations by Solitons at the Zero Group-Dispersion Wavelength of Single-Mode Optical Fibers", *Phys. Rev. A* **41**, 426-439 (1990).

[317] M. Klauder, E. W. Laedke, K. H. Spatschek, and S. K. Turitsyn, "Pulse-Propagation in Optical Fibers near the Zero Dispersion Point", *Phys. Rev. E* **47**, R3844-R3847 (1993).

[318] X. Liu, C. Xu, W. H. Knox, J. K. Chandalia, B. J. Eggleton, S. G. Kosinski, and R. S. Windeler, "Soliton self-frequency shift in a short tapered air-silica microstructure fiber", *Opt. Lett.* **26**, 358-360 (2001).

[319] V. P. Yanovsky, and F. W. Wise, "Nonlinear Propagation of High-Power, Sub-100-Fs Pulses near the Zero-Dispersion Wavelength of an Optical-Fiber", *Opt. Lett.* **19**, 1547-1549 (1994).

[320] J. K. Ranka, R. S. Windeler, and A. J. Stentz, "Optical properties of high-delta air-silica microstructure optical fibers", *Opt. Lett.* **25**, 796-798 (2000).

[321] A. B. Fedotov, P. Zhou, Y. N. Kondrat'ev, S. N. Bagayev, V. S. Shevandin, K. V. Dukel'skii, A. V. Khokhlov, V. B. Smirnov, A. P. Tarasevitch, D. von der Linde, and A. M. Zheltikov, "Spatial and spectral filtering of supercontinuum emission generated in microstructure fibres", *Quantum Electron.* **32**, 828-832 (2002).

[322] A. B. Fedotov, P. Zhou, Y. N. Kondrat'ev, S. O. Konorov, E. A. Vlasova, D. A. Sidorov-Biryukov, V. S. Shevandin, K. V. Dukel'skii, A. V. Khokhlov, S. N. Bagayev, V. B. Smirnov, A. P. Tarasevitch, D. von der Linde, and A. M. Zheltikov, "Frequency up-conversion of spectrally sliced mode-separable supercontinuum emission from microstructure fibers", *Laser Phys.* **13**, 816-826 (2003).

[323] G. Genty, M. Lebtonen, H. Ludvigsen, and M. Kaivola, "Supercontinuum generation under higher-order mode excitation in a microstructured fiber", *Holey Fibers and Photonic Crystals/Polarization Mode Dispersion/Photonics Time/Frequency Measurement and Control, 2003 Digest of the LEOS Summer Topical Meetings* 60-61 (2003).

[324] D. V. Skryabin, F. Luan, J. C. Knight, and P. S. Russell, "Soliton self-frequency shift cancellation in photonic crystal fibers", *Science* **301**, 1705-1708 (2003).

[325] I. H. Malitson, "Interspecimen comparison of the refractive index of fused silica", *J. Opt. Soc. Am.* **55**, 1205-1209 (1965).

[326] B. E. A. Saleh, and M. C. Teich, *Fundamentals of Photonics, Wiley-Interscience* (1991).

[327] W. Demtröder, *Laser Spectroscopy: Basic Concepts and Instrumentation, Second Edition, Springer, Berlin* (1996).

[328] L. Cohen, and C. Lin, "A universal fiber-optic (UFO) measurement system based on a near-IR fiber Raman laser", *IEEE J. Quantum Electron.* **14**, 855-859 (1978).

[329] B. Costa, D. Mazzoni, M. Puelo, and E. Vezzoni, "Phase-shift technique for the measurement of chromatic dispersion in optical fibers using LED's", *IEEE J. Quantum Electron.* **18**, 1509-1515 (1982).

[330] L. G. Cohen, "Comparison of single-mode fiber dispersion measurement techniques", *J. Lightwave Technol.* **3**, 958-966 (1985).

[331] D. Derickson, *Fiber Optic test and Measurement, Prentice Hall, New Jersey* (1998).

[332] B. Christensen, J. Mark, G. Jacobsen, and E. Bodtker, "Simple Dispersion Measurement Technique with High-Resolution", *Electron. Lett.* **29**, 132-134 (1993).

[333] S. Diddams, and J. C. Diels, "Dispersion measurements with white-light interferometry", *J. Opt. Soc. Am. B-Opt. Phys.* **13**, 1120-1129 (1996).

[334] M. Volanthen, H. Geiger, M. J. Cole, and J. P. Dakin, "Measurement of arbitrary strain profiles within fibre gratings", *Electron. Lett.* **32**, 1028-1029 (1996).

[335] S. D. Dyer, and K. B. Rochford, "Low-coherence interferometric measurements of fibre Bragg grating dispersion", *Electron. Lett.* **35**, 1485-1486 (1999).

[336] T. Niemi, M. Uusimaa, and H. Ludvigsen, "Limitations of phase-shift method in measuring dense group delay ripple of fiber Bragg gratings", *IEEE Photonics Technol. Lett.* **13**, 1334-1336 (2001).

[337] C. Clark, M. Farries, K. Vistanatha, and A. Tager, "Measuring chromatic dispersion of fiber gratings", *Lightwave* **17**, 70-77 (1999).

[338] Y. Li, D. Way, N. Robinson, and S. Liu, "Impact of dispersion compensation gratings on OC192 systems", *Conference on Optical Amplifiers and their Applications OAA'98* TuB5 (1998).

[339] M. Beck, I. A. Walmsley, and J. D. Kafka, "Group Delay Measurements of Optical-Components near 800 Nm", *IEEE J. Quantum Electron.* **27**, 2074-2081 (1991).

[340] G. Lenz, B. J. Eggleton, C. R. Giles, C. K. Madsen, and R. E. Slusher, "Dispersive properties of optical filters for WDM systems", *IEEE J. Quantum Electron* **30**, 1390-1402 (1998).

[341] D. Ouzounov, D. Homoelle, W. Zipfel, W. W. Webb, A. L. Gaeta, J. A. West, J. C. Fajardo, and K. W. Koch, "Dispersion measurements of microstructured fibers using femtosecond laser pulses", *Opt. Commun.* **192**, 219-223 (2001).

[342] M. W. Chbat, P. R. Prucnal, M. N. Islam, C. E. Soccolich, and J. P. Gordon, "Long-Range Interference Effects of Soliton Reshaping in Optical Fibers", *J. Opt. Soc. Am. B-Opt. Phys.* **10**, 1386-1395 (1993).

[343] K. Enneser, M. Ibsen, M. Durkin, M. N. Zervas, and R. I. Laming, "Influence of nonideal chirped fiber gratings characteristics on dispersion cancellation", *IEEE Photonics Technol. Lett.* **10**, 1476-1478 (1998).

[344] R. Fortenberry, "Enhanced wavelength resolution chromatic dispersion measurements using fixed sideband technique", *Conference on Optical Fiber Communication OCF'2000* TuG8 (2000).

[345] R. Fortenberry, W. V. Sorin, and P. Hernday, "Improvement of group delay measurement accuracy using a two-frequency modulation phase-shift method", *IEEE Photonics Technol. Lett.* **15**, 736-738 (2003).

[346] G. P. Agrawal, and N. K. Dutta, "Semiconductor Lasers", Second Edition, *Van Nostrand Reihold New York* (1993).

[347] A. Yariv, "Optical Electronics in Modern Communications", *Oxford University Press New York* (1997).

[348] C. H. Henry, "Theory of the linewidth of semiconductor lasers", *IEEE J. Quantum Electron.* **18**, 259-264 (1982).

[349] L. B. Mercer, "1/F Frequency Noise Effects on Self-Heterodyne Linewidth Measurements", *J. Lightwave Technol.* **9**, 485-493 (1991).

[350] Y. Yamamoto, "AM and FM quantum noise in semiconductor lasers-Part I: Theoretical analysis", *IEEE J. Quantum Electron.* **19**, (1983).

[351] A. L. Schawlow, and C. H. Townes, "Infrared and optical masers", *Phys. Rev.* **112**, 1940-1949 (1958).

[352] M. Lax, "Classical noise V. Noise in self-sustained oscillators", *Phys. Rev.* **160**, 290-307 (1967).

[353] A. Mooradian, "Laser linewidth", *Physics Today* **38**, 43-48 (1985).

[354] C. H. Henry, "Phase Noise in Semiconductor-Lasers", *J. Lightwave Technol.* **4**, 298-311 (1986).

[355] D. Welford, and A. Mooradian, "Output power and temperature dependence of the linewidth of single-frequency cw (GaAl)As diode lasers", *Appl. Phys. Lett.* **40**, 865-867 (1982).

[356] A. Yariv, "Quantum Electronics", Second Edition, *Wiley New York* (1975).

[357] M. Osinski, and J. Buus, "Linewidth Broadening Factor in Semiconductor-Lasers - an Overview", *IEEE J. Quantum Electron.* **23**, 9-29 (1987).

[358] P. Miltenyi, H. Jung, and W. Elsaber, "Temporal and spectral refractive-index dynamics of mode-locked external-cavity semiconductor laser diodes", *J. Opt. Soc. Am. B-Opt. Phys.* **14**, 2701-2704 (1997).

[359] L. Hsu, A. Mooradian, and R. L. Aggarwal, "Spectral linewidth of a free-running continuous-wave single-frequency external-cavity quantum-well InGaAs/AlGaAs diode-laser", *Opt. Lett.* **20**, 1788-1790 (1995).

[360] D. Welford, and A. Mooradian, "Observation of linewidth broadening in (GaAl)As diode lasers due to electron number fluctuations", *Appl. Phys. Lett.* **40**, 560-562 (1982).

[361] K. Kikuchi, "Impact of 1/F-Type Fm Noise on Coherent Optical Communications", *Electron. Lett.* **23**, 885-887 (1987).

[362] K. Kikuchi, "Origin of Residual Semiconductor-Laser Linewidth in High-Power Limit", *Electron. Lett.* **24**, 1001-1002 (1988).

[363] K. Kikuchi, "Effect of 1/F-Type Fm Noise on Semiconductor-Laser Linewidth Residual in High-Power Limit", *IEEE J. Quantum Electron.* **25**, 684-688 (1989).

[364] H. Olesen, B. Tromborg, H. E. Lassen, and X. Pan, "Mode instability and linewidth rebroadening in DFB lasers", *Electron. Lett.* **28**, 444-445 (1992).

[365] J. Buus, "Single frequency semiconductor lasers", *SPIE-The international society for optical engineering, Bellingham, Washington.* 65-66 (1991).

[366] T. Okoshi, K. Kikuchi, and A. Nakayama, "Novel method for high resolution measurement of laser output spectrum", *Electron. Lett.* 630-631 (1980).

[367] L. E. Richter, H. I. Mandelberg, M. S. Kruger, and P. A. McGrath, "Linewidth Determination from Self-Heterodyne Measurements with Subcoherence Delay Times", *IEEE J. Quantum Electron.* **22**, 2070-2074 (1986).

[368] P. B. Gallion, and G. Debarge, "Quantum phase noise and field correlation in single frequency semiconductor laser systems", *IEEE J. Quantum Electron.* **20**, 343-349 (1984).

[369] H. Ludvigsen, and E. Bodtker, "New Method for Self-Homodyne Laser Linewidth Measurements with a Short Delay Fiber", *Opt. Commun.* **110**, 595-598 (1994).

[370] H. Ludvigsen, M. Tossavainen, and M. Kaivola, "Laser linewidth measurements using self-homodyne detection with short delay", *Opt. Commun.* **155**, 180-186 (1998).

[371] B. F. Skipper, and H. Olesen, "Tuning characteristics of an external cavity semiconductor laser", *Sources for Coherent Optical Communication, IEE Colloquium on* 3/1-3/3 (1991).

[372] M. Okai, T. Tsuchiya, A. Takai, and N. Chinone, "Factors Limiting the Spectral Linewidth of Cpm-Mqw-Dfb Lasers", *IEEE Photonics Technol. Lett.* **4**, 526-528 (1992).

[373] N. A. Olsson, and J. P. Vanderziel, "Performance-Characteristics of 1.5-Mu-M External Cavity Semiconductor-Lasers for Coherent Optical Communication", *J. Lightwave Technol.* **5**, 510-515 (1987).

[374] H. Kakiuchida, and J. Ohtsubo, "Characteristics of a semiconductor laser with external feedback", *IEEE J. Quantum Electron.* **30**, 2087-20097 (1994).

[375] W. Jianglin, Z. Hanyi, W. Qun, and Z. Bingkun, "Single-mode characteristics of short coupled-cavity semiconductor lasers", *IEEE J. Quantum Electron.* **23**, 1005-1009 (1987).

[376] W. Fuhrmann, and W. Demtroder, "A Continuously Tunable GaAs Diode-Laser with an External Resonator", *Appl. Phys. B* **49**, 29-32 (1989).

[377] C. Voumard, "External-cavity-controlled 32 MHz narrow-band CW GaAlAs-diode lasers", *Opt. Lett.* **1**, 61-63 (1977).

[378] J. P. Van der Ziel, and R. Mikulyak, "Single-mode operation of 1.3 mm InGaAsP/InP buried crescent lasers using a short external optical cavity", *IEEE J. Quantum Electron.* **20**, 223-229 (1984).

[379] H. Tabuchi, and H. Ishikawa, "External grating tunable MQW laser with wide tuning range of 240 nm", *Electron. Lett.* **26**, 742-743 (1990).

[380] D. Wandt, M. Laschek, A. Tunnermann, and H. Welling, "Continuously tunable external-cavity diode laser with a double-grating arrangement", *Opt. Lett.* **22**, 390-392 (1997).

[381] R. Wyatt, "Spectral linewidth of external cavity semiconductor lasers with strong, frequency-selective feedback", *Electron. Lett.* **21**, 658-659 (1985).

[382] M. G. Littman, "Single-mode operation of grazing-incidence pulsed dye laser", *Opt. Lett.* **3**, 138-140 (1978).

[383] T. W. Hansch, "Repetitively Pulsed Tunable Dye Laser for High Resolution Spectroscopy", *Appl. Optics* **11**, 895-898 (1972).

[384] B. Boggs, C. Greiner, T. Wang, H. Lin, and T. W. Mossberg, "Simple high-coherence rapidly tunable external-cavity diode laser", *Opt. Lett.* **23**, 1906-1908 (1998).

[385] F. Heismann, R. C. Alferness, L. L. Buhl, G. Eisenstein, S. K. Korotky, J. J. Veselka, L. W. Stulz, and C. A. Burrus, "Narrow-Linewidth, Electrooptically Tunable InGaAsP-Ti-LiNbO3 Extended Cavity Laser", *Appl. Phys. Lett.* **51**, 164-166 (1987).

[386] M. Kourogi, K. Imai, B. Widyatmoko, T. Shimizu, and M. Ohtsu, "Continuous tuning of an electrically tunable external-cavity semiconductor laser", *Opt. Lett.* **16**, 1165-1167 (2000).

[387] G. Coquin, K. W. Cheung, and M. M. Choy, "Single- and multiple-wavelength operation of acoustooptically tuned semiconductor laser at 1.3 mm", *IEEE J. Quantum Electron.* **25**, (1989).

[388] J. Struckmeier, A. Euteneuer, B. Smarsly, M. Breede, M. Born, M. Hofmann, L. Hildebrand, and J. Sacher, "Electronically tunable external-cavity laser diode", *Opt. Lett.* **24**, 1573-1574 (1999).

[389] K. Petermann, "External Optical Feedback Phenomena in Semiconductor-Lasers", *IEEE J. Sel. Top. Quantum Electron.* **1**, 480-489 (1995).

[390] Z. M. Chuang, D. A. Cohen, and L. A. Coldren, "Tuning Characteristics of a Tunable-Single-Frequency External-Cavity Laser", *IEEE J. Quantum Electron.* **26**, 1200-1205 (1990).

[391] D. R. Hjelme, A. R. Mickelson, and R. G. Beausoleil, "Semiconductor-Laser Stabilization by External Optical Feedback", *IEEE J. Quantum Electron.* **27**, 352-372 (1991).

[392] I. W. Oh, and H. R. D. Sunak, "Analysis and design of external cavity, strong feedback, semiconductor lasers for use with coherent optical communications systems", *SPIE Progress in Semiconductor Laser Diodes* **723**, 84-91 (1986).

[393] B. Tromborg, J. H. Osmundsen, and H. Olesen, "Stability analysis for a semiconductor laser in an external cavity", *IEEE J. Quantum Electron.* **20**, 1023-1032 (1984).

[394] N. Schunk, and K. Petermann, "Numerical Analysis of the Feedback Regimes for a Single-Mode Semiconductor-Laser with External Feedback", *IEEE J. Quantum Electron.* **24**, 1242-1247 (1988).

[395] P. Zorabedian, W. R. Trutna, and L. S. Cutler, "Bistability in Grating Tuned External Cavity Semiconductor-Lasers", *IEEE J. Quantum Electron.* **23**, 1855-1860 (1987).

[396] H. Li, J. D. Park, D. S. Seo, L. Diego Marin, and J. G. McInerney, "Reduction of spectral linewidth in semiconductor lasers by application of optical feedback", *SPIE Laser Noise* **1376**, 172-177 (1990).

[397] J. H. Osmundsen, and N. Gade, "Influence of optical feedback on laser frequency spectrum and threshold conditions", *IEEE J. Quantum Electron.* **19**, 465-469 (1983).

[398] H. Sato, and J. Ohya, "Theory of Spectral Linewidth of External Cavity Semiconductor-Lasers", *IEEE J. Quantum Electron.* **22**, 1060-1063 (1986).

[399] E. Patzak, A. Sugimura, S. Saito, T. Mukai, and H. Olesen, "Semiconductor laser linewidth in optical feedback configuration", *Electron. Lett.* **19**, 1026-1027 (1983).

[400] B. Tromborg, H. Olesen, X. Pan, and S. Saito, "Transmission-Line Description of Optical Feedback and Injection Locking for Fabry-Perot and Dfb Lasers", *IEEE J. Quantum Electron.* **23**, 1875-1889 (1987).

[401] C. H. Henry, and R. F. Kazarinov, "Instability of semiconductor lasers due to optical feedback from distant reflectors", *IEEE J. Quantum Electron.* **22**, 294-301 (1986).

[402] D. R. Hjelme, and A. R. Mickelson, "On the Theory of External Cavity Operated Single-Mode Semiconductor-Lasers", *IEEE J. Quantum Electron.* **23**, 1000-1004 (1987).

[403] R. Ludeke, and E. P. Harris, "Tunable GaAs laser in an external dispersive cavity", *Appl. Phys. Lett.* **20**, 499-501 (1972).

[404] H. Talvitie, A. Pietilainen, H. Ludvigsen, and E. Ikonen, "Passive frequency and intensity stabilization of extended-cavity diode lasers", *Rev. Sci. Instrum.* **68**, 1-7 (1997).

[405] W. R. Trutna, and L. F. Stokes, "Continuously tuned external cavity semiconductor laser", *J. Lightwave Technol.* **11**, 1279-1286 (1993).

[406] F. Favre, D. Le Guen, J. C. Simon, and B. Landousies, "External-cavity semiconductor laser with 15 nm continuous tuning range", *Electron. Lett.* **22**, 795-796 (1986).

[407] R. W. Tkach, and A. R. Chraplyvy, "Regimes of Feedback-Effects in 1.5-MuM Distributed Feedback Lasers", *J. Lightwave Technol.* **4**, 1655-1661 (1986).

[408] Y. Kitaoka, H. Sato, K. Mizuuchi, K. Yamamoto, and M. Kato, "Intensity noise of laser diodes with optical feedback", *IEEE J. Quantum Electron.* **32**, 822-828 (1996).

[409] R. F. Kazarinov, and C. H. Henry, "The Relation of Line Narrowing and Chirp Reduction Resulting from the Coupling of a Semiconductor-Laser to a Passive Resonator", *IEEE J. Quantum Electron.* **23**, 1401-1409 (1987).

[410] H. Y. Sun, S. Menhart, and A. Adams, "Calculation of Spectral Linewidth Reduction of External-Cavity Strong-Feedback Semiconductor-Lasers", *Appl. Optics* **33**, 4771-& (1994).

[411] G. P. Agrawal, "Line narrowing in a single-mode injection laser due to external optical feedback", *IEEE J. Quantum Electron.* **20**, 468-471 (1984).

[412] J. O. Binder, and G. D. Cormack, "Mode Selection and Stability of a Semiconductor-Laser with Weak Optical Feedback", *IEEE J. Quantum Electron.* **25**, 2255-2259 (1989).

[413] J. Mork, and B. Tromborg, "The mechanism of mode selection for an external cavity laser", *IEEE Photonics Technol. Lett.* **2**, 21-23 (1990).

[414] A. J. Ikushima, and T. Fujiwara, "Silica-based glasses as photonic materials - Second-order nonlinearity induced by UV-poling", *Mol. Cryst. Liquid Cryst.* **353**, 499-511 (2000).

[415] Y. T. Ren, C. J. Marckmann, J. Arentoft, and M. T. Kristensen, "Thermally poled channel waveguides with polarization-independent electrooptic effect", *IEEE Photonics Technol. Lett.* **14**, 639-641 (2002).

[416] P. G. Kazansky, P. S. Russell, and H. Takebe, "Glass fiber poling and applications", *J. Lightwave Technol.* **15**, 1484-1493 (1997).

[417] P. G. Kazansky, L. Dong, and P. S. Russell, "High 2nd-Order Nonlinearities in Poled Silicate Fibers", *Opt. Lett.* **19**, 701-703 (1994).

[418] F. C. Garcia, I. C. S. Carvalho, E. Hering, W. Margulis, and B. Lesche, "Inducing a large second-order optical nonlinearity in soft glasses by poling", *Appl. Phys. Lett.* **72**, 3252-3254 (1998).

[419] W. Margulis, F. C. Garcia, E. N. Hering, L. C. G. Valente, B. Lesche, F. Laurell, and I. C. S. Carvalho, "Poled glasses", *MRS Bull.* **23**, 31-35 (1998).

[420] A. Kameyama, A. Yokotani, and K. Kurosawa, "Generation and erasure of second-order optical nonlinearities in thermally poled silica glasses by control of point defects", *J. Opt. Soc. Am. B-Opt. Phys.* **19**, 2376-2383 (2002).

[421] T. Fujiwara, D. Wong, and S. Fleming, "Large Electrooptic Modulation in a Thermally-Poled Germanosilicate Fiber", *IEEE Photonics Technol. Lett.* **7**, 1177-1179 (1995).

[422] U. Österberg, and W. Margulis, "Dye laser pumped by Nd:YAG laser pulses frequency doubled in a glass optical fiber", *Opt. Lett.* **11**, 516-518 (1986).

[423] M. K. Balakirev, V. A. Smirnov, L. I. Vostrikova, I. V. Kityk, J. Kasperczyk, and W. Gruhn, "Giant increase of the second harmonic radiation's absorption during optical poling of oxide glass", *J. Mod. Opt.* **50**, 1237-1244 (2003).

[424] B. P. Antonyuk, N. N. Novikova, N. V. Didenko, and O. A. Aktsipetrov, "All optical poling and second harmonic generation in glasses: theory and experiment", *Phys. Lett. A* **287**, 161-168 (2001).

[425] B. P. Antonyuk, "All optical poling of glasses", *Opt. Commun.* **181**, 191-195 (2000).

[426] R. H. Stolen, and H. W. K. Tom, "Self-organized phase-matched harmonic generation in optical fibers", *Opt. Lett.* **12**, 585-587 (1987).

[427] B. Valk, E. M. Kim, and M. M. Salour, "Second harmonic generation in Ge-doped fibers with a mode-locked Kr + laser", *Appl. Phys. Lett.* **51**, 722-724 (1987).

[428] I. C. S. Carvalho, W. Margulis, and B. Lesche, "Preparation of frequency-doubling fibers under UV excitation", *Opt. Lett.* **16**, 1487-1489 (1991).

[429] T. Fujiwara, D. Wong, Y. Zhao, S. Fleming, S. Poole, and M. Sceats, "Electrooptic Modulation in Germanosilicate Fiber with Uv-Excited Poling", *Electron. Lett.* **31**, 573-575 (1995).

[430] T. Fujiwara, M. Takahashi, and A. J. Ikushima, "Second-harmonic generation in UV-poled glass", *Jpn. J. Appl. Phys. Part 1 - Regul. Pap. Short Notes Rev. Pap.* **37**, 15-18 (1998).

[431] T. Fujiwara, M. Takahashi, and A. J. Ikushima, "Second-harmonic generation in germanosilicate glass poled with ArF laser irradiation", *Appl. Phys. Lett.* **71**, 1032-1034 (1997).

[432] A. Kameyama, K. Kurosawa, and A. Yokotani, "Erasing process of thermally poled optical nonlinearities in silica glasses with KrF excimer laser pulses", *Jpn. J. Appl. Phys. Part 1 - Regul. Pap. Short Notes Rev. Pap.* **37**, 65-67 (1998).

[433] A. Kameyama, A. Yokotani, and K. Kurosawa, "Identification of defects associated with second-order optical nonlinearity in thermally poled high-purity silica glasses", *J. Appl. Phys.* **89**, 4707-4713 (2001).

[434] P. Blazkiewicz, W. Xu, D. Wong, and S. Fleming, "Mechanism for thermal poling in twin-hole silicate fibers", *J. Opt. Soc. Am. B-Opt. Phys.* **19**, 870-874 (2002).

[435] C. Cabrillo, F. J. Bermejo, J. M. Gibson, J. A. Johnson, D. Faccio, V. Pruneri, and P. G. Kazansky, "Thermally poled silica samples are structurally heterogeneous: Electron diffraction evidence of partial crystallization", *Appl. Phys. Lett.* **78**, 1991-1993 (2001).

[436] X. Cao, and S. L. He, "An electro-optic modulator based on GeO2-doped silica ridge waveguides with thermal poling", *Chin. Phys. Lett.* **20**, 1081-1083 (2003).

[437] H. Chatellus, S. Montant, A. Le Calvez, E. Freysz, and A. Ducasse, "Spatial control of second-order nonlinearity induced by thermal poling in glasses with optical erasing", *J. Phys. IV* **10**, 257-258 (2000).

[438] H. Y. Chen, J. S. Sue, Y. H. Lin, C. S. Tsai, P. T. Wu, and S. Chao, "Thermal poling and ultraviolet erasure characteristics of type-III ultraviolet-grade fused silica and application to periodic poling on planar substrates", *J. Appl. Phys.* **94**, 1531-1538 (2003).

[439] C. Corbari, J. D. Mills, O. Deparis, B. G. Klappauf, and P. G. Kazansky, "Thermal poling of glass modified by femtosecond laser irradiation", *Appl. Phys. Lett.* **81**, 1585-1587 (2002).

[440] M. X. Qiu, T. Mizunami, R. Vilaseca, F. Pi, and G. Orriols, "Bulk and near-surface second-order nonlinearities generated in a BK7 soft glass by thermal poling", *J. Opt. Soc. Am. B-Opt. Phys.* **19**, 37-42 (2002).

[441] N. Tamagawa, Y. Benino, T. Fujiwara, and T. Komatsu, "Thermal poling of transparent TeO2-based nanocrystallized glasses and enhanced second harmonic generation", *Opt. Commun.* **217**, 387-394 (2003).

[442] P. Thamboon, and D. M. Krol, "Second-order optical nonlinearities in thermally poled phosphate glasses", *J. Appl. Phys.* **93**, 32-37 (2003).

[443] W. Xu, P. Blazkiewicz, and S. Fleming, "Silica fiber poling technology", *Adv. Mater.* **13**, 1014-+ (2001).

[444] D. M. Krol, "Fabrication and characterization of glass-based optical waveguide devices", *Glass Sci Technol.-Glastech. Ber.* **74**, 23-38 (2001).

[445] H. G. de Chatellus, and E. Freysz, "Static and dynamic profile of the electric field within the bulk of fused silica glass during and after thermal poling", *Opt. Lett.* **28**, 1624-1626 (2003).

[446] P. Blazkiewicz, W. Xu, D. Wong, S. Fleming, and T. Ryan, "Modification of thermal poling evolution using novel twin-hole fibers", *J. Lightwave Technol.* **19**, 1149-1154 (2001).

[447] A. De Francesco, and G. E. Town, "Modeling of photoinduced charge separation in germanosilicate optical fibers during UV-excited poling", *IEEE J. Quantum Electron.* **36**, 59-69 (2000).

[448] Y. G. Xi, Z. L. Xu, Z. J. Hou, L. Y. Liu, L. Xu, W. C. Wang, M. Affatigato, and S. Feller, "Second-order optical nonlinearity in bulk PbO/B2O3 glass", *Opt. Commun.* **210**, 367-373 (2002).

[449] H. Takebe, P. G. Kazansky, P. S. J. Russell, and K. Morinaga, "Effect of poling conditions on second-harmonic generation in fused silica", *Opt. Lett.* **21**, 468-470 (1996).

[450] P. G. Kazansky, L. Dong, and P. S. Russell, "Vacuum Poling - an Improved Technique for Effective Thermal Poling of Silica Glass and Germanosilicate Optical Fibers", *Electron. Lett.* **30**, 1345-1347 (1994).

[451] P. G. Kazansky, V. Pruneri, and P. S. Russell, "Blue-Light Generation by Quasi-Phase-Matched Frequency-Doubling in Thermally Poled Optical Fibers", *Opt. Lett.* **20**, 843-845 (1995).

[452] J. Arentoft, "Poling of planar silica-based waveguides", *Ph.D. Thesis* (2000).

[453] P. G. Kazansky, and P. S. Russel, "Thermally Poled Glass - Frozen-in Electric-Field or Oriented Dipoles", *Opt. Commun.* **110**, 611-614 (1994).

[454] A. De Francesco, and G. E. Town, "Modeling the electrooptic evolution in thermally poled germanosilicate fibers", *IEEE J. Quantum Electron.* **37**, 1312-1320 (2001).

[455] D. Wong, W. Xu, S. Fleming, M. Janos, and K. M. Lo, "Frozen-in electrical field in thermally poled fibers", *Opt. Fiber Technol.* **5**, 235-241 (1999).

[456] Y. Quiquempois, N. Godbout, and S. Lacroix, "Model of charge migration during thermal poling in silica glasses: Evidence of a voltage threshold for the onset of a second-order nonlinearity", *Phys. Rev. A* **65**, (2002).

[457] T. G. Alley, S. R. J. Brueck, and M. Wiedenbeck, "Secondary ion mass spectrometry study of space-charge formation in thermally poled fused silica", *J. Appl. Phys.* **86**, 6634-6640 (1999).

[458] N. Godbout, and S. Lacroix, "Characterization of thermal poling in silica glasses by current measurements", *J. Non-Cryst. Solids* **316**, 338-348 (2003).

Abstract of publications

[I] **"Spectral broadening of femtosecond pulses into continuum radiation in microstructured fibers"**, *Opt. Express* **10**, 1083-1098 (2002).

The influence of pump wavelength relative to the zero-dispersion wavelength for supercontinuum generation in microstructured fibers is investigated. Different nonlinear mechanisms are observed depending on whether the pump is located in the normal or anomalous dispersion region of the fiber. Raman scattering is found to play a crucial role in the process. The experimentally observed phenomena are explained and confirmed with a numerical model.

[II] **"Supercontinuum generation in a highly birefringent microstructured fiber"**, *Appl. Phys. Lett.* **82**, 2197-2199 (2003).

Supercontinuum generation in a highly birefringent microstructured fiber is presented. It is shown that the use of a highly birefringent fiber offers clear advantages for continuum generation. In particular, the polarization is preserved along the fiber for all the spectral components. Furthermore, the different dispersion characteristics of the two principal axes of polarization of the fiber provide a convenient way for tuning the properties of the generated continuum. Generation of an ultra-broadband continuum extending from 400 nm to 1750 nm is demonstrated.

[III] **"Measurement of anomalous dispersion in microstructured fibers using spectral modulation"**, *Opt. Express*, submitted.

A novel technique to measure the anomalous dispersion of small core microstructured fibers using short optical pulses is presented. The method relies on the spectral modulation resulting from the evolution of the input pulse into soliton. The technique allows for a direct measurement of the dispersion at the desired wavelength within a 10% accuracy.

[IV] **"New method to improve the accuracy of group-delay measurements using the phase-shift technique"**, *Opt. Commun.* **204**, 119-126 (2002).

A new method for improving the accuracy of the phase-shift technique for group delay measurement is demonstrated. The method allows for accurate reconstruction of the actual group delay when a high modulation frequency is employed for a better timing resolution. A deconvolution with the instrument function of the phase-shift technique is performed on the measured data. Illustration of the method are presented for a fiber Bragg grating and narrow-band thin-film filter.

[V] **"Analysis of the linewidth of a grating-feedback GaAlAs laser"**, *IEEE J. Quantum Electron.* **36**, 1193-1198 (2000).

The tuning properties of a GaAlAs external grating cavity laser are investigated. In particular, the relative detuning between the modes of the external cavity and that of the solitary diode laser are shown to strongly affect the linewidth of the laser. A realistic coupled-cavity model, which incorporates the frequency-dependent reflection from the grating, is used to explain the linewidth variations within one external cavity mode.

[VI] **"Measurements of linewidth variations within external cavity modes of a grating-cavity laser"**, *Opt. Commun.* **203**, 295-300 (2002).

Linewidth variations within an external cavity mode of a grating-cavity laser are measured with high accuracy using the modified self-homodyne technique with a short delay line. The linewidth is found to change by a factor of five from 30 kHz to more than 150 kHz when the laser is tuned over a single external-cavity mode. A simple model based on a linear relationship between the chirp reduction factor and the frequency tuning of the laser is used to describe the results.

[VII] **"Strength and symmetry of the third-order nonlinearity during poling of glass waveguides"**, *IEEE Photonics Technol. Lett.* **14**,1294-1296 (2002).

A novel technique for measuring the second-order susceptibility induced by thermal poling in planar waveguides is presented. The method is based on the change of the wavelength reflection peak of Bragg gratings written in the waveguides prior to poling.